Femtosecond Spectroscopy on Vibrational Self-Trapping in Molecular Crystals and α-Helices

---

Dissertation
zur
Erlangung der naturwissenschaftlichen Doktorwürde
(Dr. sc. nat.)

vorgelegt der
Mathematisch-naturwissenschaftlichen Fakultät
der
Universität Zürich

von
Julian Edler
aus
Deutschland

Promotionskomitee
Prof. Dr. Peter Hamm (Vorsitz)
Prof. Dr. Jürg Hutter
Prof. Dr. Stefan Seeger

Zürich, 2005

To my parents

List of publications

The results of this thesis have been published in the following articles:

Journal publications

- J. Edler, R. Pfister, V. Pouthier, C. Falvo, and P. Hamm.
  Direct observation of self-trapped vibrational states in α-helices.
  Phys. Rev. Lett., **93**(10), 106405, (2004).

- J. Edler and P. Hamm.
  Spectral response of crystalline acetanilide and N-methylacetamide: Vibrational self-trapping in hydrogen-bonded crystals.
  Phys. Rev. B, **69**(21), 214301, (2004).

- J. Edler and P. Hamm.
  Two-dimensional vibrational spectroscopy of the amide I band of crystalline acetanilide: Fermi resonance, conformational substates, or vibrational self-trapping ?
  J. Chem. Phys., **119**(5), 2709, (2003).

- J. Edler and P. Hamm.
  Self-trapping of the amide I band in a peptide model crystal.
  J. Chem. Phys., **117**(5), 2415, (2002).

- J. Edler, P. Hamm, and A. C. Scott.
  Femtosecond study of self-trapped excitons in crystalline acetanilide.
  Phys. Rev. Lett., **88**(6), 067403, (2002).

Conference proceedings

- J. Edler, V. Pouthier, C. Falvo, R. Pfister, and P. Hamm.
  Vibrational self-trapping in an α-helix. In T. Kobayashi, T. Okada, T. Kobayashi, K. A. Nelson, and S. De Silvestri, editors, *Ultrafast Phenomena XIV*, volume 79 of *Chemical Physics*. Springer, Berlin (2005).

- J. Edler and P. Hamm.
  Nonlinear spectroscopy study of vibrational self-trapping in hydrogen bonded crystals. In M. M. Martin and J. T. Hynes, editors, *Femtochemistry and Femtobiology: Ultrafast Events in molecular science*. Elsevier, Amsterdam (2004).

- J. Edler and P. Hamm.
  Nonlinear spectroscopy study of vibrational self-trapping in hydrogen bonded crystals. In F. Kh. Abdullaev and V. V. Konotop, editors, *Nonlinear Waves: classical and quantum aspects*, volume 153 of *NATO Science Series II. Mathematics Physics and Chemistry*. Kluwer Academic Publishers, Dordrecht (2004).

- P. Hamm and J. Edler.
  Nonlinear Vibrational Spectroscopy: a method to study vibrational self-trapping. In T. Dauxois and A. Litvak-Hinenzon and R. MacKay and A. Spanoudaki, editors, *Energy Localisation and Transfer*, volume 22 of *Advanced Series in Nonlinear Dynamics*. World Scientific, Singapore (2004).

- J. Edler and P. Hamm.
  Femtosecond study of vibrational self-trapping in crystalline acetanilide.
  In R. D. Miller, M. M. Murnane, N. F. Scherer, and A. M. Weiner, editors, *Ultrafast Phenomena XIII*, volume 71 of *Chemical Physics*. Springer, Berlin (2003).

Contents

Abstract

Interactions between delocalized excitations, e.g. electronic excitations or high frequency molecular vibrations, and low frequency lattice modes can result in an intrinsic energy localization in solids. This nonlinear phenomenon is commonly called self-trapping or self-localization and has been observed in various materials. Vibrational self-trapping in α-helices, a structural motif in proteins, is of particular interest, as it has been suggested to play a role in the energy transport in biomolecules.[1] The basic idea is that the vibrational energy, which is delocalized as a result of dipole-dipole coupling, localizes due to lattice modes and distorts the helical structure. The helix distortion acts in turn as a potential well and prevents energy dispersion. Through this nonlinear mechanism the vibrational energy is stabilized and can propagate along the helix. The aim of this thesis is to use ultrafast nonlinear spectroscopy to establish the nonlinear spectroscopic signature of vibrational self-trapping and to examine whether self-trapping really exists in α-helical polypeptides. To this end, self-trapping is first confirmed in *model* systems before the experiments are extended to *real* α-helical polypeptides.

Acetanilide (CH_3-CONH-C_6H_5, ACN) forms molecular crystal, which consists of chains of hydrogen bonded peptide groups with structural properties similar to α-helices. As self-trapping in α-helices should originate from couplings that exists in hydrogen bonded chains, ACN provides a good model to study self-trapping. It is well established that the vibrational spectrum of ACN exhibits peculiar band structures in the region of the amide I (i.e the C=O stretching) and the NH stretching band, which have been previously attributed to vibrational self-trapping.[2,3] However self-trapping was observed through an indirect effect, namely the temperature dependence of the absorption spectrum. Here, a much more direct approach, infrared pump-probe spectroscopy, is applied. In a pump-probe experiment one excites a vibrational mode with a pump pulse, and subsequently measures the induced changes of absorption with a probe pulse.

In detail, infrared pump-probe experiments on the amide I band of ACN identify two different types of states through their (an)harmonicities: a delocalized free exciton and a self-trapped state. This assignment agrees perfectly with earlier, more indirect studies. Furthermore, the femtosecond pump-probe experiments show how thermal disorder localizes the free exciton (Anderson localization) while it simultaneously destroys the self-trapping mechanism. Finally, two-dimensional infrared spectroscopy is used to ultimately exclude two previous, alternative explanations for the anomalous structure of the amide I

band, demonstrating explicitly how nonlinear infrared spectroscopy can distinguish different nonlinear phenomena in a way that is not possible by absorption spectroscopy. In addition, this thesis provides the first extensive study on the NH mode of ACN, revealing further striking evidence for vibrational self-trapping. Pump-probe experiments on the NH mode exhibit an ultrafast irreversible energy transfer from a delocalized state to self-trapped states and moreover identify, for the first time, the two phonon modes, which mediate self-trapping. Thus the experiments prove unambiguously self-trapping of the amide I and of the NH mode in ACN.

So far compelling evidence for vibrational self-trapping was only found in ACN. However the self-trapping mechanism should occur in any crystals with a similar structure. The present work compares vibrational modes of ACN and NMA (N-methylacetamide, CH_3–CONH–CH_3), as well as of their carbon deuterated derivatives. The pump-probe and absorption spectra of all crystals show striking similarities, indicating that the substructure of the NH band in NMA originates, at least partly, from vibrational self-trapping and not, as often assumed, solely from a Fermi resonance. Consequently one can speculate that vibrational self-trapping is not a unique property of ACN, but a more general phenomena in hydrogen bonded crystals.

After establishing the nonlinear signature of vibrational self-trapping in model systems, one can approach "real" α-helices. To that end femtosecond pump-probe experiments are performed on the NH mode of a stable α-helix in solution. The corresponding spectra reveal two positive signals, which disappear upon unfolding the helix. Most conventional explanations, such as CH stretching vibrations or multiphoton excitations, are ruled out based on various absorption and pump-probe measurements. However, Fermi resonances could in principle result in two positive peaks in the pump-probe spectra. Nevertheless, the most obvious Fermi resonance, the one with the amide II overtone, can not explain the data. On the other hand, a quantitative comparison with self-trapping theory shows that the two positive signals can reflect two types of self-trapped states, that are connected to the trapping of two vibrational excitations at the same peptide site in the helix or, respectively, at nearest neighbor sites. Thus this thesis presents the first striking experimental evidence of vibrational self-trapping in α-helices.

Zusammenfassung

Wechselwirkungen zwischen delokalisierten Anregungen, wie z. B. elektronisch angeregten Zuständen oder hochfrequenten Molekülschwingungen, und niederfrequenten Gitterschwingungen können in Festkörpern zu einer intrinsischen Energielokalisierung führen. Dieses nichtlineare Phänomen, welches oft mit "self-trapping" oder Selbstlokalisierung bezeichnet wird, wurde in verschiedenen Materialien beobachtet. Die Selbstlokalisierung von Schwingungszuständen in α-Helices, einer Tertiärstruktur von Proteinen, ist dabei von besonderem Interessen, da man vermutet, dass solche Zustände eine wichtige Rolle beim Energietransport in Biomolekülen spielen.[1] Die grundlegende Idee besteht darin, dass die Schwingungsenergie, die auf Grund der Dipol-Dipol Wechselwirkung delokalisiert ist, durch die Kopplung an Gittermoden lokalisiert wird und dadurch die helikale Struktur derformiert. Diese Deformation wirkt gleichzeitig wie ein Potentialtopf, der die Energiedispersion verhindert. Durch diesen nichtlinearen Mechanismus wird die Schwingungsenergie stabilisiert und kann sich entlang der Helix ausbreiten. In der vorliegenden Arbeit werden Methoden der nichtlinearen Ultrakurzzeitspektroskopie eingesetzt um nichtlineare spektroskopische Signaturen dieser Schwingungsselbstlokalisierung zu ermitteln und zu untersuchen ob Selbstlokalisierung in α-helikalen Polypetiden tatsächlich auftritt. Zuerst wird die Existenz von Selbstlokalisierung in Modellsystemen nachgewiesen und anschließend werden echten α-Helices untersucht.

Acetanilid (CH_3-CONH-C_6H_5, ACN) bildet Molekülkristalle, die aus Ketten wasserstoffverbrückter Peptidgruppen bestehen und eine ähnliche Struktur wie α-Helices besitzen. Da die Selbstlokalisierung in α-Helices durch Kopplungen in solchen wasserstoffverbrückten Ketten hervorgehen soll, ist ACN ein gutes Modellsystem zur Untersuchung von Selbstlokalisierung. Das Schwingungsspektrum von ACN weist im Bereich der Amid I (die C=O Streckschwingung) und der NH Streckschwingung eigenartige Bandstrukturen auf, welche anhand von Schwingungsselbstlokalisierung erklärt worden sind.[2,3] Allerdings beruhen die bisherigen Studien auf der Temperaturabhängigkeit des Absorptionsspektrums und damit auf einem indirekten Effekt. In der vorliegenden Arbeit wird ein sehr viel direkterer Ansatz, nichtlineare Pump-Probe Infrarotspektroskopie, gewählt um die Banden zu untersuchen. Hierbei regt man eine Schwingungsmode mit einem intensiven Pumppuls an und misst anschließend mit einem Probpuls die hervorgerufenen Änderungen im Absorptionsspektrum.

Mithilfe eines Pump-Probe Experimentes an der Amid I Bande von ACN werden zwei unterschiedliche Zustände durch ihre (An-)Harmonizitäten identifiziert: ein delokalisiertes freies Exziton und ein selbstlokalisierter Zustand. Diese Zuordnung stimmt perfekt mit den älteren indirekteren Studien überein. Zudem zeigen die Femtosekunden Pump-Probe Experimente wie thermische Unordnung das freie Exziton lokalisiert (Anderson Lokalisierung), und gleichzeitig den Selbstlokalisierungsmechanismus zerstört. Darüber hinaus wird zweidimensionale Infrarotspektroskopie eingesetzt um endgültig zwei alternative Erklärungsmöglichkeiten für die anomale Struktur der Amid I Bande auszuschließen. Dabei wird explizit gezeigt wie nichtlineare Infrarotspektroskopie verschiedene nichtlineare Phänomene auf eine Art und Weise unterscheiden kann, die mit herkömmlicher Absorptionsspektroskopie nicht möglich ist. In dieser Arbeit wird ferner zum ersten Mal die NH-Mode von ACN ausführlich untersucht, wobei weitere eindeutige Beweise für Selbstlokalisierung gefunden werden. Die Pump-Probe Experimente an der NH-Mode zeigen einen ultraschnellen irreversiblen Energietransfer von einem delokalisierten zu einem lokalisierten Zustand. Außerdem werden, erstmals, zwei Phononmoden identifiziert, welche Selbstlokalisierung verursachen. So weisen die Experimente eindeutig die Existenz von Selbstlokalisierung in der NH und der Amid I Mode in ACN nach.

Überzeugende Beweise für Schwingungsselbstlokalisierung wurden bisher nur in ACN gefunden. Selbstlokalisierung sollte jedoch in jedem Kristall, der eine ähnliche Struktur besitzt, auftreten. In der vorliegenden Arbeit werden die Schwingungsmoden von ACN und NMA (CH_3–CONH–CH_3), sowie deren C-deuterierten Isotope verglichen. Das Pump-Probe und das Absorptionsspektrum aller vier Kristalle zeigt auffällige Übereinstimmungen, aus denen man schließen kann, dass die Substruktur der NH Bande in NMA, zumindest teilweise, auf Selbstlokalisierung und nicht, wie oft angenommen, ausschließlich auf einer Fermi Resonanz beruht. Schwingungsselbstlokalisierung scheint also keine einzigartige Eigenschaft in ACN zu sein, sondern ein universelleres Phänomen in wasserstoffverbrückten Kristallen.

Nachdem die nichtlineare Signatur von Schwingungsselbstlokalisierung in Modellsystemen ermittelt wurde, kann man "echte" α-Helices untersuchen. Dazu wurde die NH Mode einer stabilen α-Helix in Lösung mit Femtosekunden Pump-Probe Experimenten untersucht. Die entsprechenden Spektren zeigen zwei positive Signale, welche beim Entfalten der Helix verschwinden. Die meisten konventionellen Erklärungen, wie CH Streckschwingungen oder Multiphotonanregungen, können aufgrund verschiedener Pump-Probe und Absorptions Messungen ausgeschlossen werden. Allerdings könnte eine Fermi Resonanz die beiden positiven Signale erklären. Jedoch kann die wahrscheinlichste Fermi Resonanz, die zwischen dem Amid II Oberton und der NH Mode, die Daten nicht erklären. Andererseits zeigt ein quantitativer Vergleich mit der Selbstlokalisierungstheorie, dass die beiden positiven Signale zwei Arten von selbstlokalisierten Zuständen widerspiegeln können. Diese beiden Zustände entsprechen der Lokalisierung von zwei Schwingungsanregungen auf der selben Peptideinheit der Helix oder auf benachbarten Peptideinheiten. Damit wurden im Rahmen dieser Arbeit die ersten deutlichen experimentellen Beweise für Schwingungsselbstlokalisierung in α-Helices erbracht.

1 Introduction

Proteins are remarkable biomachines, which can efficiently convert chemical energy into mechanical energy. One of their interesting, yet not well understood, properties is the capability of storing and transporting small quanta of energy efficiently. In the 1970s Davydov suggested that self localization plays an important role in this process.[1] His theory was based on the idea that a nonlinear mechanism stabilizes vibrational excitations and thus prevents energy from dissipation. Such a localization is due to collectively interacting vibrational modes. In the presented work ultrafast vibrational spectroscopy is used to examine the spectroscopic fingerprints of such a mechanism and to see whether vibrational localization can occur in polypeptides.

The proposed nonlinear localization of vibrational energy is similar to the soliton mechanism, a phenomena which is well established in physics. The very first soliton was discovered by Russell in 1834 in a water canal in Scotland, when he observed how a water wave travelled at high velocity along the canal without any change of shape.[5] This observation was quite surprising since water waves are normally known to physicist as an example of dispersive waves. A single water wave is typically described as a wavepacket, which is a linear superposition of sinusoidal waves. Each of the waves travels with its own velocity and hence the wavepacket becomes normally broader while it propagates, that is it disperses [see Fig. 1.1]. However, for many waves an additional nonlinear effect plays a role. The nonlinearity causes the higher (more intense) parts of the wave to travel at

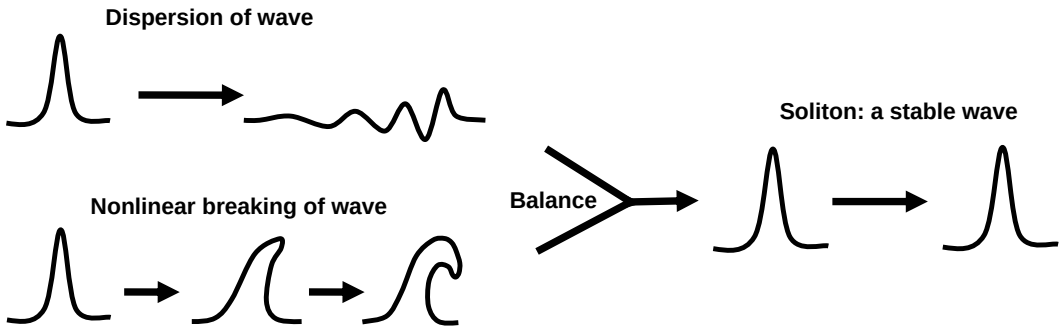

Figure 1.1: Normally a water wave becomes broader while it propagates, that is it disperses. However, a nonlinear term can cause the higher parts of the wave to travel at a higher velocity than the weaker parts, causing eventually a breaking of the wave. Thus dispersion spreads out the energy of the wave, while the nonlinearity draws it together. In case of a soliton these two effects compensate each other, resulting in a stable wavepacket. Figure adapted from Lomdahl.[4]

Figure 1.2: A simple model of a nonlinear lattice consists of a chain of atoms that are connected by slightly nonlinear springs (monoatomic lattice). The arrows illustrate schematically a simple type of discrete breather in such a chain, in which case two neighbors oscillate out of phase with a large amplitude.[11]

a higher velocity than the weaker parts, leading to wave breaking. In case of a soliton, like the one that Russell observed, the effect of dispersion is balanced by the nonlinearity, resulting in the emergence of a stable wavepacket, as illustrated in Fig. 1.1. The correct mathematical description of the solitary wave was found about sixty years after Russell's discovery, when Kortweg and de Vries showed that one can describe the solitary wave by a nonlinear differential equation. This, so-called Kortweg-de Vries equation has besides the usual periodic solutions also localized solutions, which reflect the solitary wave.[6]

In 1955 Fermi, Pasta and Ulam (FPU) showed numerically the existence of solitary waves, when they investigated the flow of energy in solids.[7] To describe the dynamics of crystalline lattice vibrations they used a toy model, which consisted of a chain of equal masses coupled by slightly nonlinear springs [e.g. Fig. 1.2]. After excitation of a normal mode of the chain, the energy did not, as expected, spread out through all normal modes ("thermalization"), but instead returned periodically to the originally excited mode. This discovery remained largely a mystery, until Zabusky and Kruskal described the system with the famous Kortweg-de Vries equation and explained the so-called "FPU recurrence" with pulse-like solitary waves that do not change shape or speed when they collide with each other.[8,9] Due to the particle-like nature they named these waves solitons.[10] For a long time solitary waves were considered an unimportant peculiarity in physics. However, nowadays the soliton concept is well established and solitons have been observed in various fields, such as fluid mechanics, mechanically coupled chains of pendula, electric transmission lines and optics.[8,9]

A natural question that arises is whether such localized waves can be also observed on a molecular scale, like in crystalline solids or biological macromolecules. The major prerequisites for solitary waves are the existence of a nonlinearity and a coupling mechanism. Clearly both conditions are present in molecular systems. The nonlinearity is explicitly exhibited in the models for anharmonic interatomic potentials such as the Morse oscillator or the potentials of hydrogen bonded modes. Couplings between different molecular oscillators are also well known, including for example normal mode coupling and dipole-dipole coupling. Hence one should expect to find localized phenomena in molecular systems.

At the microscopic level crystals as well as some structural motifs in biomolecules (α-helices, β-sheets) are made of discrete atoms or molecules, which typically form periodic structures. Thus one can reduce the complexity of nonlinear excitations in crystals and macromolecules to simple lattice models, based on their periodic structure. Such lattice models have been linked to important problems in physics and can be used to clarify phys-

ical, chemical or biological properties of molecular chains.[12,13] Possibly the most simple model is the monoatomic chain shown in Fig.1.2. This chain describes a one-dimensional array of atoms that are coupled by nonlinear springs, representing nearest neighbor interaction potentials (e.g. the FPU model). In the language of solid state physics this type of array is often referred to as an acoustic chain, since it gives rise to the theory of sound waves in solids. In general the nearest neighbor interaction potential can have the form of a standard atomic potential, such as the Morse or Lennard-Jones potential.

In the last decade there has been a tremendous increase in theoretical studies of nonlinear lattices,[9,8,14–17] which was triggered by the discovery of highly localized nonlinear oscillations in discrete lattices.[18–22] These so-called *intrinsic localized modes* or *discrete breathers* describe an energy localization in real space and oscillate only over a few lattice sites. The two crucial components that make discrete breathers possible are the discreteness of space and the nonlinearity.[16,17] In general discrete breathers are defined as spatially highly localized, time periodic, and stable excitations in extended, periodic, discrete nonlinear systems.[17] For instance, the most simple breather corresponds to two neighbors oscillating out of phase in a monoatomic chain, as illustrated in Fig. 1.2.[11] Discrete breathers are linked to solitons in the framework of the quasicontinuum approximation and can be regarded as an extension of the soliton concept to nonintegrable nonlinear lattice models.[8,23–25] The existence of discrete breathers is quite universal and it was shown that breather solutions exist in finite or infinite systems, independent of the number of degrees of freedom per lattice site, the lattice dimension or other details of the system.[14,16,26] Discrete breathers have been theoretical constructs for more than a decade, until recent experiments have proven their existence in various materials, including Josephson junction arrays,[27,28] micromechanical systems,[29] optical switching waveguides,[30] photonic crystals[31] and magnetic solids.[32,33]

However all of the above mentioned localized phenomena, solitons and discrete breathers, occur in the macroscopic or mesoscopic world, where the laws of classical physics apply. But, when one considers molecular vibrations one has to consider quantum mechanics. Hence the next questions to ask is which type of eigenstates will correspond to "classical" breathers when the corresponding quantum problem is considered. From fundamental quantum mechanical considerations one can not expect spatially localized eigenstates since a translational invariance of the system must be shared by the eigenfunctions of the corresponding quantum system.[9] It was suggested that the eigenfunctions of quantum breathers correspond to Bloch-like superpositions of site functions which have a higher probability of having several quanta of excitation on the same site than of having them on different sites. Thus the particle-like properties of a breather state can be probed by correlation functions.[11,16] However, while numerous papers have been published on classical breathers, only a few studies concern the quantum analogy and thus the current understanding of quantum breathers is rather limited (see Refs. 9,11,16 and 34 for recent reviews). Nevertheless, there have been some interesting experiments, where evidences of quantum breathers were observed in 4-methyl-pyridine crystals,[35,36] in Cu benzoate[37] and in halide bridged transition metal complexes.[38,39]

As a matter of fact, the phenomenon of localized molecular oscillations is not unknown in chemistry. Already in the 1920s physical chemists found evidence that the vibrational energy of the six CH stretching modes in benzene is, for high excitation numbers, localized on a single bond rather than being distributed over the entire molecule.[40] This findings were explained by the local mode theory, which is a quantitative quantum mechanical theory.[41,42] In the 1970s the local mode theory was rediscovered and now the localized modes in benzene are well established in chemistry (see Refs. 9,43 for reviews). In the language of modern nonlinear science, the local modes in benzene correspond to a discrete breather.[9,26]

These observations of localized quantum phenomena let one speculate that other molecular systems support localized excitations. Especially biological macromolecules, such as proteins or DNA provide an interesting system for nonlinear excitations, since they often form quasi crystalline structures with translational symmetry. In fact, localized phenomena in DNA have been discussed in the context of nonlinear science and it was suggested that conformational transitions and transcription mechanisms can be described by soliton-like excitations (see Ref. 13 and references therein).

The prime aim of this thesis is focused on experimental evidence of localized nonlinear excitations in protein model systems. One of the most important structural motifs in proteins are α-helices. An α-helix is essentially a helical chain of amino acids [see Fig.1.3]. Since this structure is translational invariant one can describe it as a one-dimensional lattice. The helical structure is stabilized by hydrogen bonds, which connect the carbonyl (C=O) and the NH group of different amino acid. The hydrogen bonds have the important property to introduce a nonlinear coupling between the vibrational modes (C=O or NH stretching) and low frequency lattice modes (phonons). In addition to this coupling the helical structure allows a strong electrostatic coupling between individual oscillators of each peptide group, i.e. the C=O and NH stretching modes. Thus all necessary prerequisites for soliton-like excitations or for discrete breathers are present in α-helices: nonlinearity, coupling and discreteness.

These observations motivated Davydov in the 1970s to propose a mechanism for energy localization in α-helices.[1] The main idea was that the localization of the C=O vibrational energy distorts, via the hydrogen bonds the lattice. This distortion acts in turn as a potential well onto the vibration, trapping the excitation and preventing its dispersion.[3] In this way the vibrational energy is said to become self-trapped on the helix. It is the balance between lattice distortion and localized vibrational energy that results in the emergence of the self-trapped state. It turned out that the theory behind this so-called "Davydov soliton" is essentially that of a polaron. Polarons are quasi-particles introduced by Landau to describe the motion of an electron through a crystal lattice[45] and are well studied in solid state physics. However, it is important to note that the excitation is vibrational in case of Davydov's self-trapping and not electronic as in Landau's polaron.

Davydov suggested that the vibrational polaron could have a significant relevance for the energy transport in proteins, which is still an unresolved question in biology. The

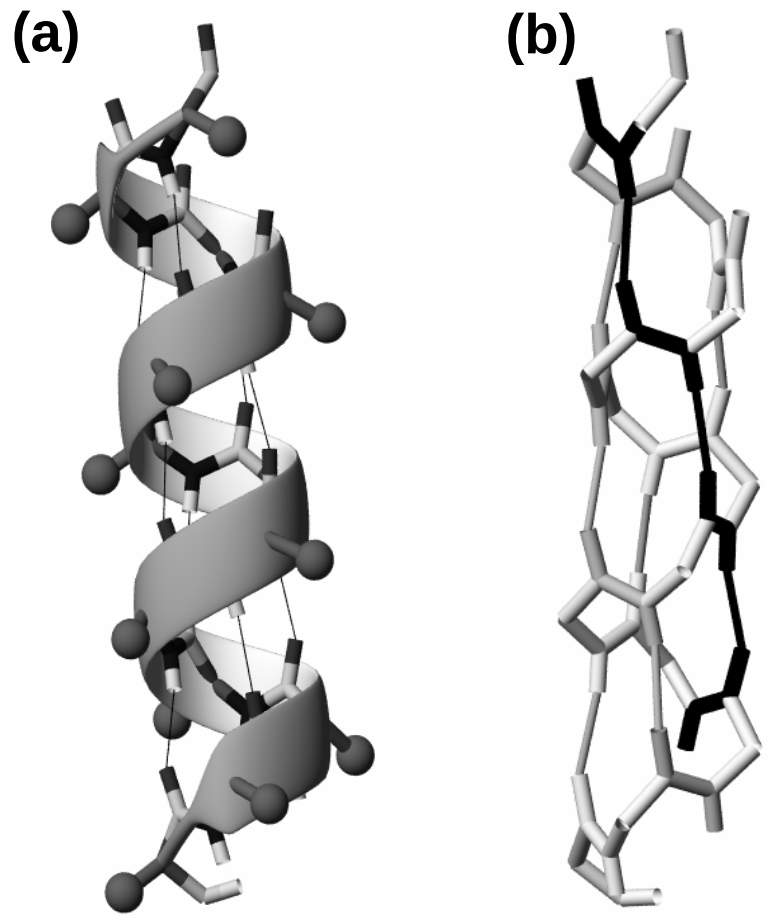

Figure 1.3: The α-helix is the major structural motif in secondary structures of proteins. It is formed by a right handed helical chain, with 3.6 amino acids per turn. All sidegroups are arranged at the outside of the helix. The helical structure is stabilized by hydrogen bonds (thin lines), which connect the NH group of the nth residue with the CO group of the $(n+3)$th residue. (b) The hydrogen bonds form three quasi-one-dimensional chains, one of which is highlighted in black. Figure prepared with MOLMOL.[44]

sites where energy is produced in proteins, e.g. where adenosine triphosphate (ATP) is hydrolyzed, and the site where the energy is needed, e.g. to induce a conformational change, are often separated by several tens of angströms. The energy which is released by this reaction is rather small (about 0.5 eV) and thus only twenty times larger than the average energy of thermal fluctuations.[12] Hence biological systems require some means of energy transport and storage. Davydov suggested that α-helices can act as energy wires in proteins, through vibrational self-trapping.

Although there have been numerous theoretical studies on vibrational self-trapping (see Refs. 3 and 46 for reviews), there has been no clear experimental proof whether such states exist in real α-helices or not. One previous experiment on polyalanine, which was discussed in the context of self-trapping,[47] revealed an anomalous temperature dependence of the NH spectrum. In addition recent pump-probe experiments on myoglobin, a protein which consists almost solely of α-helices, revealed an unusual long lifetime of the C=O

mode.[48,49] The authors suggest that this long lifetime indicates the existence of self-trapped states. However, both of these experiments a rather indirect and the conclusions were quite speculative. In fact the experimental detection of such a vibrational polaron is difficult. Most α-helices are found in large proteins and the vibrational modes that are specific for the helical amino acids are covered by modes that belong to other non-helical parts of the protein. Isolated α-helical polypeptides on the other hand are very flexible structures and parts of the helix open, resulting in defects, that might destroy the self-trapping mechanism. Thus when one wants to find experimental evidence for vibrational self-trapping, one seems to be forced to turn to model systems.

Crystalline acetanilide (ACN) provides such a model, as it consists of hydrogen bonded peptide units with similar structural properties as α-helices [Fig. 1.4].[2] The Italian physicist Careri studied in the 1970s the carbonyl stretching mode of ACN to examine the vibrational dynamics in polypeptides, when he discovered an anomalous splitting of the corresponding absorption band in the infrared spectrum.[50] After a decade of unsuccessful attempts to assign the splitting in a conventional manner he turned to Davydov's self-trapping theory, which explained perfectly the temperature dependence of the carbonyl mode.[2] This suggestion of self-trapped states in ACN was discussed controversially and a considerable amount of experiments, most of which supported the polaronic assignment, were performed to test self-trapping theory.

In this thesis self-trapping is confirmed in peptide model crystals, such as ACN, in a first step and then it is tested whether such states exist also in real α-helical polypeptides. To that end ultrafast nonlinear pump-probe spectroscopy is performed on molecular crystals and on α-helical polypeptides. In previous studies self-trapping in ACN was observed through an indirect effect, namely the temperature dependence of the infrared absorption spectrum, which is considered to report on underlying nonlinearities. Pump-probe spectroscopy offers an alternative, more direct approach, since it is exclusively sensitive

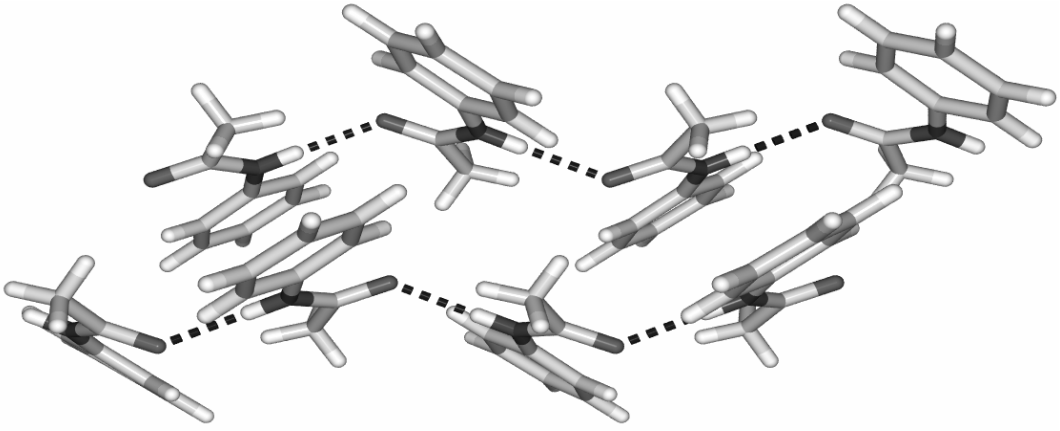

Figure 1.4: Three dimensional structure crystalline acetanilide (CH_3-CONH-C_6H_5, ACN). View down the crystalline a-axis. The NH and C=O groups of individual peptide units are connected by hydrogen bonded chains, which are comparable to those in α-helices.

to anharmonic effects and eliminates all harmonic contributions. Anharmonicity at the same time give rise to nonlinear dynamics. Thus nonlinear (pump-probe) spectroscopy is ideal for the study of self-trapping phenomena. A further advantage of ultrafast nonlinear spectroscopy is the high time resolution, which enables one to extract detailed information about underlying dynamical processes. Thus one can examine the real time dynamics of energy relaxation and transfer processes of vibrationally excited states. In addition, the ultrashort pump pulse can impulsively excite, through the laser bandwidth, low frequency modes of the hydrogen bond. Thereby pump-probe experiments can yield detailed information about a coupling between vibrational modes and lattice distortions, which is the underlying mechanism of self-trapping. Thus ultrafast pump-probe spectroscopy is an extremely powerful tool to study vibrational self-trapping.

The text is organized as follows. After this introduction the basic theoretical concepts are presented. Chapter 2 gives a short introduction to the nonlinear response function which is needed to interpret the results of pump-probe spectroscopy. Chapter 3 is devoted to the theory of nonlinear phenomena in molecular systems. Different anharmonic contributions to the potential energy surface, namely intrinsic anharmonicity, excitonic coupling, coupling to low frequency modes and Fermi resonances, are discussed with respect to their effect on the nonlinear spectrum. It is shown how the combination of two coupling mechanisms, that is excitonic coupling and coupling to low frequency modes, gives rise to vibrational self-trapping. Chapters 4.1 and 4.2 correspond to the materials and methods section and describe in detail the experimental setup and the sample preparation. The experiments are presented in Chapters 5 to 7. In a first step vibrational self-trapping is studied in peptide model crystals, and in a second step a real α-helix is considered. In Chapters 5 self-trapping of the carbonyl mode in ACN is confirmed by nonlinear spectroscopy. In addition previous alternative explanations are firmly excluded. Subsequently self-trapping of the NH mode in ACN is discussed and explicit evidence for a coupling to low frequency modes is revealed. In chapter 6 the study is extended from ACN to a different but structurally similar molecular crystal: N-methylacetamide. The results show that certain nonlinear spectroscopic fingerprints appear in both molecules, indicating that vibrational self-trapping is not restricted to ACN. Finally in Chapter 7 a real α-helix, in contrast to the previous model crystals, is examined. The experiments reveal two bound states, which correspond to quantum breathers. In this way Davydov's self-rapping mechanism in α-helices is confirmed for first time. At the end, the major results are summarized in Chapter 8 and the final conclusions are drawn.

2 Theory of nonlinear optical spectroscopy

Nonlinear molecular phenomena, such as anharmonic vibrational excitons, vibrational polarons and Fermi resonances originate from different anharmonic contributions to the potential energy surface. As nonlinear optical spectroscopy is exclusively sensitive to anharmonicities, it offers a direct approach to study these different phenomena. In the present chapter the basic concepts of the theory of nonlinear spectroscopy are introduced, while the different anharmonic phenomena are discussed in the following Chapter.

The nonlinear response function

In optical measurements nuclear motions and relaxation processes show up only through their effect on the optical polarization, which is the only material quantity that appears in the Maxwell equations. Hence a complete knowledge of the polarization is required for the interpretation of optical spectroscopy.[51] In this chapter, which is based to a large extent on References 51–54, a brief introduction into the theory of nonlinear spectroscopy is given.

In the dipole approximation the interaction between a molecule and a light field $E(t)$ is described by the Hamiltonian

$$\hat{H} = \hat{H}_{mol} + E(t)\hat{\mu} \tag{2.1}$$

where $\hat{H}_{mol}$ is the Hamiltonian of the molecular system and $\hat{\mu}$ the dipole moment operator. One can treat the dynamics of the system with the Liouville-Von Neumann equation:

$$\frac{d}{dt}\hat{\rho} = \frac{-i}{\hbar}\left[\hat{H}, \hat{\rho}\right] \tag{2.2}$$

Here the state of the system is represented by the density operator $\hat{\rho}$,which takes statistical averaging over an ensemble into account. In general, the interaction with the electric field $E(t)\hat{\mu}$ is much weaker than the internal fields of the molecule and can hence be treated perturbatively. In the interaction picture the density operator can be expressed by the

perturbative expansion:[51]

$$\begin{aligned}\hat{\rho}(t) =& \sum_{n=0}^{\infty} \rho^{(n)} \\ =& \rho^{(o)}(-\infty) + \sum_{n=1}^{\infty} \left(-\frac{i}{\hbar}\right)^n \int_{-\infty}^{t} d\tau_n \int_{-\infty}^{\tau_n} d\tau_{n-1} \ldots \int_{-\infty}^{\tau_2} d\tau_1 E(\tau_n) \cdot E(\tau_{n-1}) \cdot \ldots \\ & \cdot E(\tau_1) \cdot \hat{U}_{mol}(t, t_0) \cdot [\hat{\mu}(\tau_n), [\hat{\mu}(\tau_{n-1}), \ldots [\hat{\mu}(\tau_1), \hat{\rho}(-\infty)] \ldots]] \cdot \hat{U}^{\dagger}_{mol}(t, t_0) \end{aligned} \tag{2.3}$$

using the time evolution operator $\hat{U}_{mol}(t, t_0)$ of the system Hamiltonian. The optical polarization P is given by the expectation value of the dipole operator $\hat{\mu}$:

$$P = Tr\left(\hat{\mu}\hat{\rho}(t)\right) = \langle \hat{\mu}\hat{\rho}(t) \rangle \tag{2.4}$$

where $\langle \ldots \rangle$ denotes the trace. Combining Equ. 2.3 and 2.4 gives the n$^{\text{th}}$ order polarization $P^{(n)}$, which is the observable in a nonlinear experiment:

$$\begin{aligned} P^{(n)}(t) =& \langle \hat{\mu}\hat{\rho}^{(n)} \rangle \\ =& \int_0^{\infty} dt_n \int_0^{\infty} dt_{n-1} \ldots \int_0^{\infty} dt_1 E(t - t_n) E(t - t_n - t_{n-1}) \cdot \ldots \\ & \cdot E(t - t_n - t_{n-1} - \ldots - t_1) \cdot S^{(n)}(t_n, t_{n-1}, \ldots, t_1) \end{aligned} \tag{2.5}$$

with the n$^{\text{th}}$ order nonlinear response function $S^{(n)}$. The n$^{\text{th}}$ order polarization consists

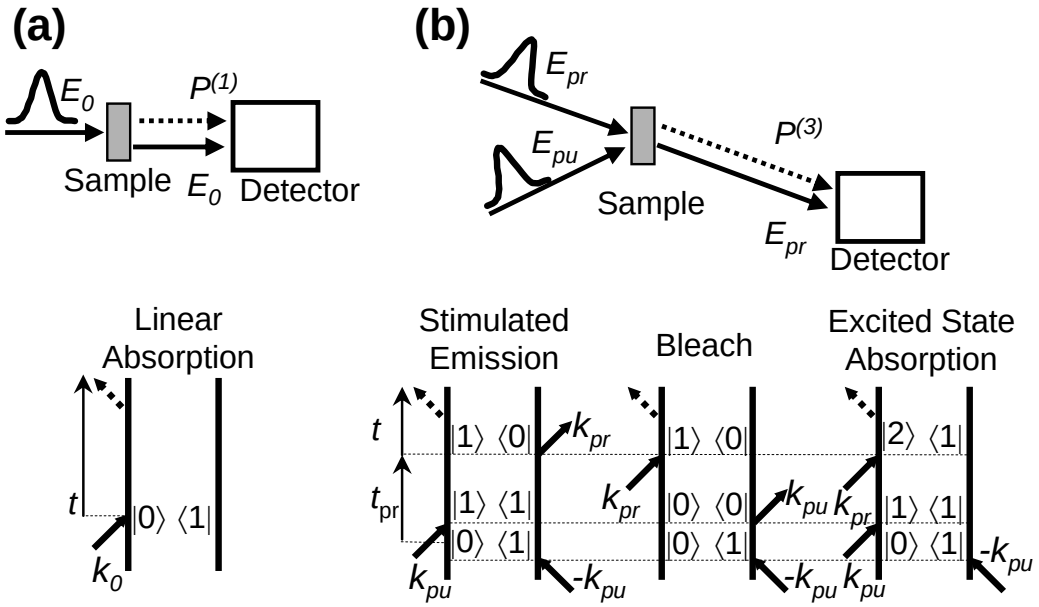

Figure 2.1: Principle of the experimental setup (top) and double sided Feynman diagrams (bottom) for (a) absorption spectroscopy and (b) pump-probe spectroscopy. The pump-probe signal consists of three contributions: stimulated emission, bleach and excited state absorption.[54]

of a convolution of electric fields that interact at different times with the system. The response function $S^{(n)}$, which represents the molecular properties that we can measure in nonlinear spectroscopy is given by

$$S^{(n)}(t_n, t_{n-1}, \ldots, t_1) = \left(-\frac{i}{\hbar}\right)^n \Theta(t_n) \cdot \Theta(t_{n-1}) \cdot \ldots \cdot \Theta(t_1) \cdot \\ \cdot \langle \hat{\mu}(t_n + t_{n-1} + \ldots, t_1)[\hat{\mu}(t_{n-1} + \ldots + t_1), \ldots [\hat{\mu}(0), \hat{\rho}(-\infty)] \ldots] \rangle \quad . \tag{2.6}$$

Here the time coordinate transformation $\tau_1 = 0$, $t_1 = \tau_2 - \tau_1$, $t_2 = \tau_3 - \tau_2, \ldots, t_n = t - \tau_n$ has been applied. $\Theta(t)$ is the Heaviside step function. In media with inversion symmetry, such as isotropic media, the even-order polarization terms vanish and the 3$^{\text{rd}}$ order term is the lowest nonlinear contribution. Evaluation of the commutators in the brackets $\langle \ldots \rangle$ yields for the 3$^{\text{rd}}$ order contribution the following eight terms:

$$\begin{aligned}
&\langle \mu(t_3 + t_2 + t_1)\mu(t_2 + t_1)\mu(t_1)\mu(0)\rho(-\infty) \rangle \\
-&\langle \mu(t_3 + t_2 + t_1)\mu(t_2 + t_1)\mu(t_1)\rho(-\infty)\mu(0) \rangle \\
-&\langle \mu(t_3 + t_2 + t_1)\mu(t_2 + t_1)\mu(0)\rho(-\infty)\mu(t_1) \rangle \\
+&\langle \mu(t_3 + t_2 + t_1)\mu(t_2 + t_1)\rho(-\infty)\mu(0)\mu(t_1) \rangle \\
-&\langle \mu(t_3 + t_2 + t_1)\mu(t_1)\mu(0)\rho(-\infty)\mu(t_2 + t_1) \rangle \\
+&\langle \mu(t_3 + t_2 + t_1)\mu(t_1)\rho(-\infty)\mu(0)\mu(t_2 + t_1) \rangle \\
+&\langle \mu(t_3 + t_2 + t_1)\mu(0)\rho(-\infty)\mu(t_1)\mu(t_2 + t_1) \rangle \\
-&\langle \mu(t_3 + t_2 + t_1)\rho(-\infty)\mu(0)\mu(t_1)\mu(t_2 + t_1) \rangle
\end{aligned} \tag{2.7}$$

Each term represents a possible interaction between the light fields and the density matrix of the molecular system, i.e. the state of the system. Double-sided Feynman diagrams, (see for example Fig. 2.1) are a useful tool to keep track of the various contributions to the response function, described by Equ. 2.7, and give a graphical picture of the molecule field interactions.[51] In such diagrams, the vertical lines represent, from bottom to top, the time evolution of the molecular density matrix. The *ket* and *bra* pairs between the lines indicate which matrix element of the density matrix is occupied. Arrows pointing in- or outwards represent interactions between the system and the light field, in other words the acting of the dipole operator onto the density matrix. The last arrow illustrates the emission of a light field, i.e. the polarization, and points always outwards. In practice one can use the diagrams to calculate the third order polarization by considering only the contributions of those diagrams that correspond to the phase matching conditions of the experiment. The phase matching condition, giving momentum conservation, depends on the geometry of the experiment. When each light field caries a wave vector k_i, the wave vector $k^{(3)}$ of the 3$^{\text{rd}}$ order polarization $P^{(3)}$ is given by

$$k^{(3)} = \pm k_1 \pm k_2 \pm k_3. \tag{2.8}$$

Absorption and pump-probe spectroscopy

Figure 2.1(a) shows the diagram for linear absorption spectroscopy. One starts with the system in the ground state with a density matrix element $\hat{\rho} = |0\rangle\langle 0|$. In absorption spectroscopy the light field interacts once with the system and generates a $|1\rangle\langle 0|$ coherence, which then irradiates the first order polarization $P^{(1)}$. In third order nonlinear spectroscopy, such as pump-probe, the system interacts three times with a laser pulse, generating either a $|1\rangle\langle 0|$ or a $|2\rangle\langle 1|$ coherence, which irradiates the third order polarization $P^{(3)}$. In contrast to linear spectroscopy there are many ways in nonlinear spectroscopy for the light fields to interact with the system, resulting in many contributions to the 3$^{\text{rd}}$ order polarization. The number of terms can be reduced by the rotating wave approximation, which assumes near resonance conditions and by the semi impulsive limit, when the light fields are short, time-ordered laser pulses. The envelopes of the light fields are then approximated by δ-functions and the integrals in Equ. 2.5 disappear. In this case the n$^{\text{th}}$ order polarization $P^{(n)}$ is the same as the n$^{\text{th}}$ response function $S^{(n)}$. If one further assumes purely homogeneously broadened lines, one obtains for the linear polarization:

$$P^{(1)}(t) = \frac{-i}{\hbar} E_o \mu_{01}^2 e^{-i\omega_{01}t} e^{-\gamma t} \tag{2.9}$$

where γ is the homogeneous dephasing rate, ω_{01} is the transition frequency between the ground state and the first excited state and μ_{01} the transition dipole matrix element of the dipole operator $\hat{\mu}$. In pump-probe spectroscopy the first two interactions between the system and the light field come from the intense pump pulse, which excites the system from the ground state $\nu = 0$ to the first excited state $\nu = 1$, and the time between these two interactions is $t_1 = 0$. The subsequent probe pulse measures the resulting change in absorption, i.e. an absorption spectrum in the excited state. The probe pulse can reach the first and second excited state and hence a three level system is needed to discuss the optical response. When one considers the phase matching conditions, that apply for pump-probe experiments, one obtains a 3$^{\text{rd}}$ order polarization, which consists of three terms [see Fig. 2.1] representing (i) the $\nu = 1 \rightarrow 0$ stimulated emission (SE), (ii) the bleach (Bl), reflecting the decrease of the $\nu = 0 \rightarrow 1$ transition due to the depletion of the ground state and (iii) the $\nu = 1 \rightarrow 2$ excited state absorption (ESA):

$$P^{(3)}(t, t_{pu,pr}) = P^{(3)}_{SE}(t, t_{pu,pr}) + P^{(3)}_{Bl}(t, t_{pu,pr}) + P^{(3)}_{ESA}(t, t_{pu,pr}) \tag{2.10}$$

with

$$P^{(3)}_{SE}(t, t_{pu,pr}) = \frac{i}{\hbar^3} |E_{pu}|^2 E_{pr} \mu_{01}^4 e^{-i\omega_{01}t} e^{-\gamma t} e^{t_{pu,pr}/T} \tag{2.11}$$

$$P^{(3)}_{Bl}(t, t_{pu,pr}) = \frac{i}{\hbar^3} |E_{pu}|^2 E_{pr} \mu_{01}^4 e^{-i\omega_{01}t} e^{-\gamma t} e^{t_{pu,pr}/T} \tag{2.12}$$

$$P^{(3)}_{ESA}(t, t_{pu,pr}) = \frac{-i}{\hbar^3} |E_{pu}|^2 E_{pr} \mu_{01}^2 \mu_{12}^2 e^{-i\omega_{12}t} e^{-\gamma t} e^{t_{pu,pr}/T} \tag{2.13}$$

where $t_{pu,pr}$ is the delay time between pump and probe pulse, T the vibrational relaxation time, E_{pu} the electric field of the pump pulse, E_{pr} the one of the probe pulse and ω_{12} is

the transition frequency between the first and second excited state with transition dipole moment μ_{12}.

In pump-probe spectroscopy, a square law detector measure the generated nth order polarization by heterodyning it with the original probe field:

$$I_{pu,pr}(t, t_{pu,pr}) \propto |E_{pr} - iP^{(3)(t,t_{pu,pr})}|^2 = |E_{pr}|^2 + 2Im(E_{pr} \cdot P^{(3)}(t, t_{pu,pr})) + |P^{(3)(t,t_{pu,pr})}|^2 \tag{2.14}$$

where the third term is generally neglected. For small signals the absorbance change is given by:

$$\Delta A_{pu,pr}(t, t_{pu,pr}) = -\log \frac{I_{pu,pr}}{I_{pr}} \approx 2Im(E_{pr} P^{(3)}(t, t_{pu,pr})) \tag{2.15}$$

If the signal is recorded after transmitting the light through a spectrometer one obtains the absorbance change as a function of the delay time and the frequencies of the broadband probe pulse:

$$\Delta A(\omega_{pr}, t_{pu,pr}) \approx 2Im \int_0^\infty dt E_{pr} P^{(3)}(t, t_{pu,pr}) e^{i\omega_{pr} t} \tag{2.16}$$

The excited state absorption appears in a pump-probe spectrum as a positive signal (increase in detected light intensity) at probe frequency $\omega_{pr} = \omega_{12}$ with intensity I_{ESA} proportional to $\mu_{01}^2 \mu_{12}^2$, whereas bleach and stimulated emission are both negative each at probe frequency $\omega_{pr} = \omega_{01}$ with intensities I_{Bl} and I_{SE} both proportional to μ_{01}^4. For an harmonic oscillator $\omega_{01} = \omega_{12}$ and $2\mu_{01}^2 = \mu_{12}^2$. Hence the three contributions vanish identically and the nonlinear response is zero. In general one can show that the nonlinear response of any system of harmonic normal modes always vanishes exactly.[51] Therefore nonlinear spectroscopy is exclusively sensitive to anharmonicities.

Quantum beats

In hydrogen bonded molecules the vibrational states are anharmonically coupled to low frequency modes, that introduce a substructure for the vibrational states [see Chapter 3.4 for details]. In the most simple case, the substructure consists of a splitting of the first excited vibrational state and the system can be described by three energy levels $|0\rangle$, $|1\rangle$ and $|1'\rangle$. The two substates $|1\rangle$ and $|1'\rangle$ are close together and both can be simultaneously excited by a spectrally broad laser pulse, resulting in a coherent superposition $|1\rangle\langle 1'|$ of the two states.

Using the rotating wave approximation, the semi impulsive limit and the pump-probe phase matching conditions one obtains the Feynman diagrams shown in figure 2.2. These diagrams represent the terms for stimulated emission and bleach of each resonance as well as two additional quantum beat contributions. The corresponding 3rd order polarization

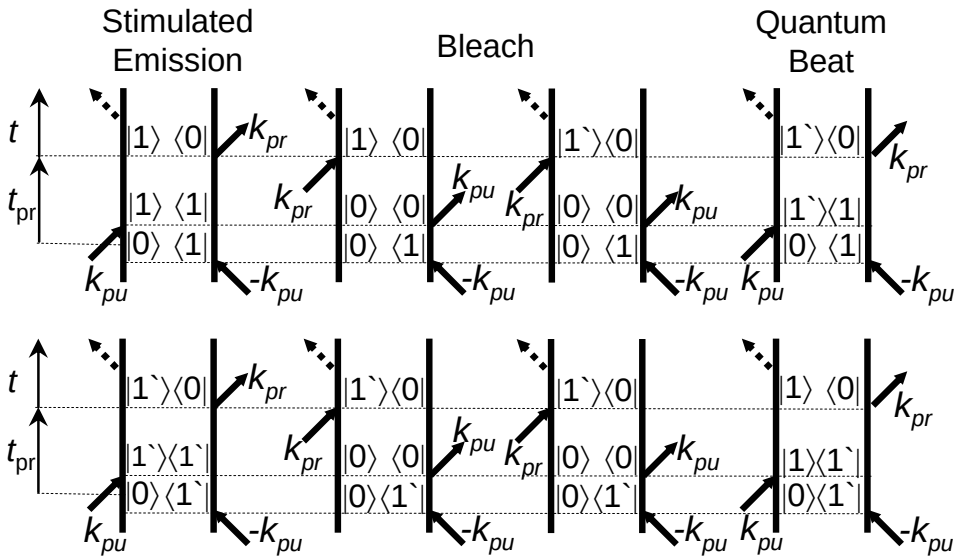

Figure 2.2: To model a quantum beat experiment one has to taken eight Feynman diagrams into account. The Bleach and Stimulated Emission diagrams correspond to those in Fig. 2.1. The pump pulse can create a $|1'\rangle\langle 1|$ or $|1'\rangle\langle 1|$ coherence, that results in additional quantum beat contributions.

is:

$$\begin{aligned} P^{(3)}(t, t_{pu,pr}) =& \frac{2i}{\hbar^3}|E_{pu}|^2 E_{pr}\mu_{01}^4 e^{-i\omega_{01}t}e^{-\gamma t}e^{t_{pu,pr}/T} + \frac{2i}{\hbar^3}|E_{pu}|^2 E_{pr}\mu_{01'}^4 e^{-i\omega_{01'}t}e^{-\gamma t}e^{t_{pu,pr}/T} \\ &+ \frac{i}{\hbar^3}|E_{pu}|^2 E_{pr}\mu_{01}^2\mu_{01'}^2 \left(e^{-i\omega_{11'}t_{pu,pr}}e^{-i\omega_{10}t} + e^{-i\omega_{1'1}t_{pu,pr}}e^{-i\omega_{10}t}\right) e^{-\gamma t}e^{t_{pu,pr}/T} \end{aligned} \tag{2.17}$$

The new quantum beat contributions contain an oscillating term that depends on the delay time $t_{pu,pr}$ and oscillates with a frequency $\omega_{11'} = \omega_1 - \omega_{1'}$. When one scans the delay time $t_{pu,pr}$ one observes in the absorbance change signal $\Delta A_{pupr}(t, t_{pu,pr})$ intensity oscillations with frequency $\omega_{11'}$, which correspond to the splitting between the two substates. Such oscillations are also called quantum beats.

3 Nonlinear phenomena in hydrogen bonded systems

In this chapter the capability of nonlinear spectroscopy to study different molecular anharmonicities is reviewed. First the harmonic molecular potential energy surface [Section 3.1] and the intrinsic anharmonicity [Section 3.2] are introduced. In the following sections two coupling mechanisms, that can exist in hydrogen bonded systems, are discussed, namely excitonic coupling [Section 3.3] and coupling between high frequency vibrational modes and hydrogen bond modes [Section 3.4]. The combination of the two coupling mechanisms can give rise to vibrational self-trapping, as shown in Section 3.5. Finally Fermi resonances are discussed in Section 3.6. The chapter is in part based on References 54–56.

3.1 Molecular potential energy surface

The electronic energy of a molecule as a function of the nuclear coordinates is determined by the molecular potential energy surface. This potential energy surface can always be Taylor expanded about the equilibrium configuration along certain nuclear coordinates:

$$V(x_1, x_2) = V_0 + \frac{\partial V}{\partial x_1}x_1 + \frac{\partial V}{\partial x_2}x_2 + \frac{1}{2}\frac{\partial^2 V}{\partial x_1^2}x_1^2 + \frac{\partial^2 V}{\partial x_1 x_2}x_1 x_2 + \frac{1}{2}\frac{\partial^2 V}{\partial x_2^2}x_2^2 + \dots \tag{3.1}$$

For simplicity the expansion is here restricted to two coordinates, x_1 and x_2. In general there are of course $3N-6$ coordinates, where N is the number of atoms in the molecule. Here the Taylor expansion is truncated to second order, which is the *harmonic approximation*. Equation 3.1 can be simplified, without loss of generality, by choosing the arbitrary zero energy point so that $V_0 = 0$ and by choosing a local minimum for the origin of the coordinate system so that $\frac{\partial V}{\partial x_1} = 0$ and $\frac{\partial V}{\partial x_2} = 0$. Furthermore one can perform a coordinate transformation to get rid of the mixed (bilinear) term $\frac{\partial^2 V}{\partial x_1 x_2}x_1 x_2$. Hence Equ. 3.1 can be expressed in new coordinates $\tilde{q}_1$ and $\tilde{q}_2$ as[54]:

$$V(\tilde{q}_1, \tilde{q}_2) = \frac{1}{2}\frac{\partial^2 V}{\partial \tilde{q}_2^2}\tilde{q}_1^2 + \frac{1}{2}\frac{\partial^2 V}{\partial \tilde{q}_2^2}\tilde{q}_2^2 + \dots \tag{3.2}$$

As a consequence of the harmonic approximation the so-called normal modes $\tilde{q}_1$ and $\tilde{q}_2$ decouple completely. In the following dimensionless coordinates

$$q_i = \sqrt{\frac{m_i\Omega_i}{\hbar}}\tilde{q}_i \qquad p_i = \frac{1}{\sqrt{\hbar m_i \Omega_i}}\tilde{p}_i \tag{3.3}$$

are used, where Ω_i are the frequencies of the normal modes and m_i the reduced masses. The quantum mechanical Hamiltonian can be written, using the corresponding operators $\hat{q}_i$ and $\hat{p}_i$, as:

$$\hat{H} = \frac{\hbar\Omega_1}{2}\left(\hat{p}_1^2 + \hat{q}_1^2\right) + \frac{\hbar\Omega_2}{2}\left(\hat{p}_2^2 + \hat{q}_2^2\right) + \dots \tag{3.4}$$

$$= \hbar\Omega_1\left(\hat{B}_1^\dagger\hat{B}_1 + \frac{1}{2}\right) + \hbar\Omega_2\left(\hat{B}_2^\dagger\hat{B}_2 + \frac{1}{2}\right) + \dots \tag{3.5}$$

where $\hat{B}_n^\dagger$ and $\hat{B}_n$ are the creation and annihilation operators of the harmonic oscillators:

$$\hat{B}_n = \frac{1}{\sqrt{2}}\left(\hat{q}_n + i\hat{p}_n\right) \qquad \hat{B}_n^\dagger = \frac{1}{\sqrt{2}}\left(\hat{q}_n - i\hat{p}_n\right) \tag{3.6}$$

with the commutation relations

$$\left[\hat{B}_n, \hat{B}_m^\dagger\right] = \delta_{nm} \qquad \left[\hat{B}_n, \hat{B}_m\right] = \left[\hat{B}_n^\dagger, \hat{B}_m^\dagger\right] = 0. \tag{3.7}$$

In the previous Chapter it was shown that the pump-probe signal of a harmonic system is zero and that nonlinear (e.g. pump-probe) spectroscopy is only sensitive to anharmonic contributions of the potential energy surface.[51] Hence a pump-probe spectrum of a molecular system, whose potential energy surface is determined by Equ. 3.2, is zero. In the following sections different anharmonic contributions and their effects on the pump-probe signal are discussed in detail.

3.2 Intrinsic anharmonicity

Typical molecular vibrations are not perfectly harmonic. As a criteria for the accuracy of the harmonic approximation one can define the parameter[54]

$$\gamma = \frac{\omega_{01} - \omega_{12}}{\omega_{01}}, \tag{3.8}$$

where ω_{01} and ω_{21} are the transition frequencies between ground and first excited state and between first and second excited state, respectively. A typical value in an isolated peptide unit is $\gamma = 1\%$ for the amide I mode, i.e. the CO stretching mode, and $\gamma = 4\%$ for the NH mode. The intrinsic anharmonicity of an oscillator has its origin in terms of order q^3 and q^4 or higher in the potential energy expansion (Equ. 3.2) and the Hamiltonian of an oscillator with intrinsic anharmonicity is

$$\hat{H} = \frac{1}{2}\hbar\Omega(\hat{p}^2 + \hat{q}^2) + \frac{1}{6}\frac{\partial^3 V}{\partial q^3}\hat{q}^3 + \frac{1}{24}\frac{\partial^4 V}{\partial q^4}\hat{q}^4 + \dots \tag{3.9}$$

$$= \hbar\Omega\left(\hat{B}^\dagger\hat{B} + \frac{1}{2}\right) + \Delta^{(3)}\left(\hat{B} + \hat{B}^\dagger\right)^3 + \Delta^{(4)}\left(\hat{B} + \hat{B}^\dagger\right)^4 + \dots \tag{3.10}$$

with the anharmonic parameters $\Delta^{(3)}$ and $\Delta^{(4)}$:

$$\Delta^{(3)} = \frac{1}{12\sqrt{2}}\frac{\partial^3 V}{\partial q^3} \qquad \Delta^{(4)} = \frac{1}{96}\frac{\partial^4 V}{\partial q^4} \tag{3.11}$$

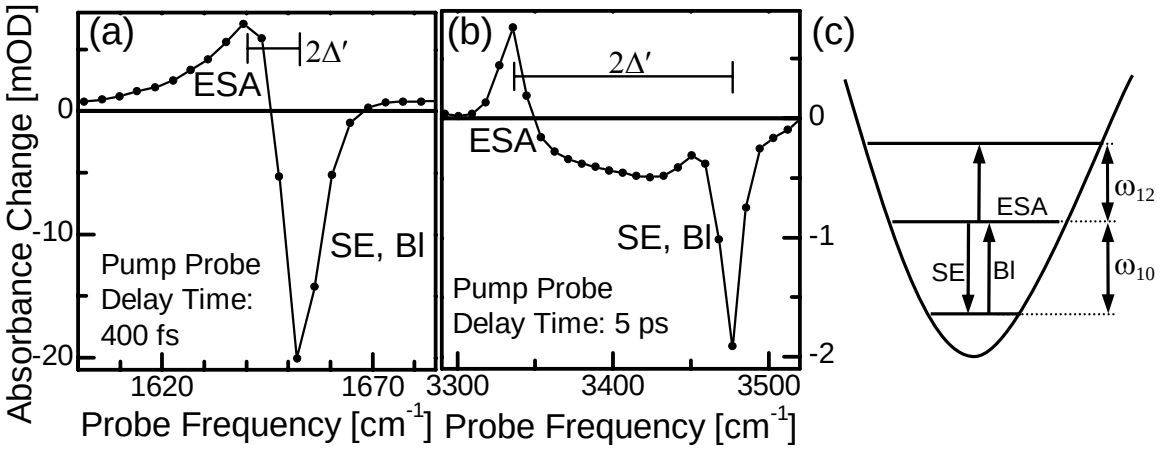

Figure 3.1: Typical pump-probe spectrum of an anharmonic oscillator: (a) the amide I mode of a poly-γ-benzyl-L-glutamate (PBLG) film and (b) the NH stretching mode of isolated N-methylacetamide (NMA) in chloroform. Stimulated emission (SE) and bleach (Bl) appear as a negative signal, whereas the excited state absorption (ESA) appears as a positive signal. The shift 2Δ between positive and negative contributions reflects the intrinsic anharmonicity. (c) The corresponding scheme of energy levels in an anharmonic oscillator. The arrows depict ESA, SE and Bl transitions.

If one restricts Equ. 3.10 to terms that conserve the number of excitations, i.e. terms with the same number of annihilation and creation operators, and performs a normal mode transformation, one obtains the Hamiltonian

$$\hat{H} = \hbar\Omega \left(\hat{B}^\dagger \hat{B} + \frac{1}{2} \right) + \Delta' \hat{B}^\dagger \hat{B}^\dagger \hat{B} \hat{B}, \tag{3.12}$$

here Δ' is the new anharmonicity parameter. This Hamiltonian can be used to describe the intrinsic anharmonicity of vibrational excitations.[54,57] It is important to note that the intrinsic anharmonicity does not lead to a coupling between two normal modes q_1 and q_2, as a system of two anharmonic oscillators is described by

$$\hat{H} = \hbar\Omega_1 \left(\hat{B_1}^\dagger \hat{B_1} + \frac{1}{2} \right) + \Delta_1' \hat{B_1}^\dagger \hat{B_1}^\dagger \hat{B_1} \hat{B_1} + \hbar\Omega_2 \left(\hat{B_2}^\dagger \hat{B_2} + \frac{1}{2} \right) + \Delta_2' \hat{B_2}^\dagger \hat{B_2}^\dagger \hat{B_2} \hat{B_2}. \tag{3.13}$$

However bleach, stimulated emission and excited state absorption do no longer cancel exactly for an anharmonic oscillator, since the transition frequencies ω_{01} and ω_{12} are unequal. Figure 3.1 shows two typical examples for pump-probe spectra of anharmonic vibrations. Bleach and stimulated emission appear as a negative signal at transition frequency ω_{01}, whereas the excited state absorption appears as a positive signal at a lower frequency ω_{12}. The shift between the two peaks corresponds directly to the anharmonicity parameter Δ' in Equ. 3.12.

3.3 Vibrational exciton

3.3.1 Vibrational exciton Hamiltonian

Figure 3.2 shows the molecular structure of an α-helix, one of the most common structural motifs in proteins. The arrows illustrate the orientation of the dipole moments of the amide I modes in the individual peptide units. As all dipoles are aligned in a similar direction, they can couple strongly through dipole-dipole interaction, giving rise to a delocalized state. Following the terminology used in electronic spectroscopy, the various amide I modes are said to form a vibrational exciton. In a truly one dimensional chain of harmonic oscillators such an excitation is described by the Frenkel Hamiltonian[58]

$$\hat{H}^{(0)} = \sum_n \hbar\Omega \left(\hat{B}_n^\dagger \hat{B}_n + \frac{1}{2} \right) + \sum_n \beta \left(\hat{B}_n^\dagger \hat{B}_{n+1} + \hat{B}_n \hat{B}_{n+1}^\dagger \right), \tag{3.14}$$

where n runs over all sites in the chain, Ω is the vibrational frequency of the amide I mode and β the excitonic coupling (which decays very quickly with distance, so that we consider in general only nearest neighbor interaction). Depending on distance and relative orientation, the coupling β can be of the order of about 10 cm^{-1} and hence, can lead to appreciable exciton delocalization. The expression 3.14 is not restricted to an α-helix and can be applied to other chains of peptide units.[57,59]

In the context of nonlinear spectroscopy the Hamiltonian 3.14 is often written in the basis of localized site states for 0, 1 and 2 vibrational quanta:[57,60,61]

$$\begin{aligned} |0\rangle & \\ |n\rangle &= \hat{B}_n^\dagger |0\rangle \\ |nm\rangle &= a_{nm} \hat{B}_n^\dagger \hat{B}_m^\dagger |0\rangle, \quad n \leq m \end{aligned} \tag{3.15}$$

Here $a_{nn} = 1/\sqrt{2}$ for $n = m$ and $a_{nm} = 1$ for $n \neq m$ are the appropriate normalization factors. In the ground state $|0\rangle$ no vibrational quantum is excited. The $|n\rangle$ have one vibrational quanta on the nth site, the $|nm\rangle$ have one quanta on each site n and m and the $|nn\rangle$ correspond to two quanta on site n. For example, the Hamiltonian of a system

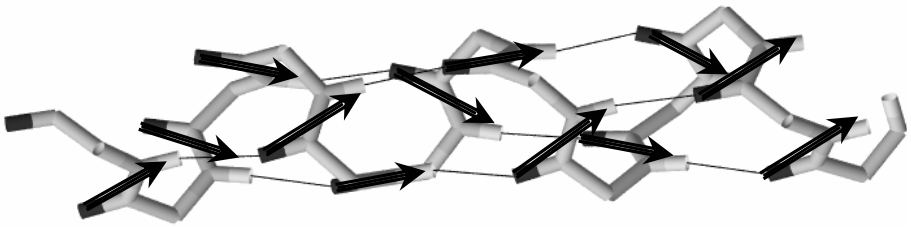

Figure 3.2: The α-helix is one of the most common structures in proteins. The thin lines illustrate the hydrogen bonds between the C=O and NH groups. The arrows depict the transition dipoles of the amide I mode. Figure prepared with MOLMOL.[44]

of two coupled oscillators is written in this site basis as

$$\hat{H}^{(0)} = \left(\begin{array}{c|cc|ccc} 0 & & & & & \\ \hline & \hbar\Omega_1 & \beta & & & \\ & \beta & \hbar\Omega_2 & & & \\ \hline & & & 2\hbar\Omega_1 & 0 & \sqrt{2}\beta \\ & & & 0 & 2\hbar\Omega_2 & \sqrt{2}\beta \\ & & & \sqrt{2}\beta & \sqrt{2}\beta & \hbar(\Omega_1+\Omega_2) \end{array}\right). \tag{3.16}$$

Since Equ. 3.14 conserves the number of excitations the 0, 1 and 2 quanta manifolds, which are separated by lines in the Hamiltonian Equ. 3.16, decouple and the Hamiltonian is block diagonal.

Since the coupling term in Equ. 3.14 is linear in both coordinates (bilinear) the Hamiltonian is actually harmonic and one could, in principle, perform a normal mode transformation and reformulate the problem in a harmonic eigenstate basis. However the nonlinear response of a harmonic system vanishes completely [see Chapter 2], and therefore Equ. 3.14 is not sufficient to describe nonlinear spectroscopy. One can include the intrinsic anharmonicity by lowering the site energies of only the double-excited states $|nn\rangle$ by a factor Δ [see Fig. 3.3(a)].[60] The resulting perturbed Hamiltonian $\hat{H} = \hat{H}^{(0)} + \hat{V}$ consists of an harmonic part $\hat{H}^{(0)}$ (Frenkel Hamiltonian, Equ. 3.14) and an additional anharmonicity term $\hat{V}$. The anharmonicity term $\hat{V}$ is diagonal in the site basis $\{|nm\rangle\}$, $n \leq m$, and its matrix elements are:

$$V_{nm,n'm'} = -\Delta \cdot \delta_{nm}\delta_{nn'}\delta_{mm'} \tag{3.17}$$

The spectroscopic states observed experimentally are the excitonic states, rather than the site states, and one has to formulate the problem in the exciton basis set in order to describe linear and nonlinear spectroscopy. The diagonalization of the harmonic Hamiltonian 3.14 is readily accomplished and one obtains the delocalized one-excitonic states $|k\rangle$, that are observed in absorption spectroscopy, as linear combinations of the single site states $|n\rangle$:[60]

$$|k\rangle = \sum_k q_{kn} |n\rangle \tag{3.18}$$

with expansion coefficients q_{kn} and eigenenergies ϵ_k. Throughout this chapter the indices k and l label excitonic states whereas n and m label site states. In pump-probe spectroscopy the system interacts with two photons and two-excitonic states $\{|kl\rangle\}$, $k \leq l$ have to be considered as well.[51] In case of the harmonic Hamiltonian 3.14 the excitonic states are also harmonic and we know without explicit diagonalization of the Hamiltonian that the two-excitonic states are product states of the one-excitonic states,[60]

$$|kl\rangle = a_{kl}(|k\rangle|l\rangle + |l\rangle|k\rangle), \tag{3.19}$$

with eigenenergies $\epsilon_k + \epsilon_l$. The expansion of the two-excitonic states $|kl\rangle$ in the site basis $\{|nm\rangle\}$ reads:

$$|kl\rangle = \sum_{n\leq m} Q_{kl,nm} |nm\rangle \tag{3.20}$$

with the expansion coefficients:

$$Q_{kl,nm} = \frac{a_{kl}}{a_{nm}} q_{kn} q_{lm} \tag{3.21}$$

However, one has to use the perturbed Hamiltonian $\hat{H}$ that includes the anharmonicity term $\hat{V}$ to describe nonlinear spectroscopy (Equ. 3.17). In the basis of the excitonic states $\{|kl\rangle\}$ the matrix elements of the anharmonicity term $\hat{V}$ are obtained through a unitary transformation:[60]

$$V_{kl,k'l'} = \sum_{nmn'm'} Q_{kl,nm} V_{nm,n'm'} Q^{-1}_{n'm',k'l'} = -\Delta \sum_{n} Q_{kl,nn} Q_{k'l',nn} \tag{3.22}$$

Up to this point, the expression is exact. However, since $\hat{V}$ is not diagonal in the two-excitonic basis, the product states $\{|kl\rangle\}$ are not the eigenstates of the anharmonic Hamiltonian $\hat{H} = \hat{H}^{(0)} + \hat{V}$ and anharmonicity mixes into all two-excitonic states [see Fig. 3.3(a)]. The eigenenergies of $\hat{H}$ can be evaluated perturbatively in the small anharmonicity limit, where the anharmonic shift $\Delta\epsilon_{kl}$ of the two-excitonic states is small compared to the level separation in the two-exciton band.[62] In this limit, the two-excitonic states can still be identified as product states of the one-excitonic states, lowered in energy by the so called diagonal and off-diagonal anharmonicities, which in lowest order of $\hat{V}$ are:[55]

$$\Delta\varepsilon_{kl} = V_{kl,kl} = -2\Delta \cdot a_{kl}^2 \sum_{n} q_{kn}^2 q_{ln}^2 \tag{3.23}$$

If the coupling β is weak the one excitonic states are predominately localized on one individual site:

$$q_{nm} = \delta_{nm} + q'_{nm} = \delta_{nm} + \frac{\beta_{nm}}{\epsilon_m - \epsilon_n} \quad \text{with} \quad |\frac{\beta_{nm}}{\epsilon_m - \epsilon_n}| < 1 \tag{3.24}$$

Then one obtains in first order of $\hat{V}$ and lowest order of β_{nm} the diagonal anharmonicities:[60,62]

$$\Delta\epsilon_{kk} = -\Delta \tag{3.25}$$

and the off-diagonal anharmonicities:

$$\Delta\epsilon_{kl} = -4\Delta \frac{\beta_{kl}^2}{(\epsilon_k - \epsilon_l)^2} \tag{3.26}$$

3.3.2 Nonlinear spectroscopy of vibrational excitons

A recently introduced new type of nonlinear spectroscopy, two-dimensional infrared (2D-IR) spectroscopy, allows a direct observation of the exciton coupling parameter β.[59,60] In 2D-IR spectroscopy individual one-exciton states are excited by a spectrally narrow pump pulse and subsequently probed by a broadband pulse, which measures the transitions up to the two-exciton state or down to the ground state. One typically observes excited state absorption, stimulated emission and bleach [see Chapter 2]. The response is plotted as a function of the pump and probe frequency. Figure 3.3(b) shows a prototype 2D-IR spectrum for a system, which consists of two coupled amide-I oscillators. In order to construct such a spectrum one first calculates the population probabilities of states $|k\rangle$, where k depends on the pump frequency, and subsequently the up- and downward transitions seen by the probe-pulse. The transitions are weighted by their transition strength and by the population probability of the state $|k\rangle$ prepared by the pump pulse. Each peak in the 2D spectrum corresponds to one of the transitions shown in the level scheme in Fig. 3.3(a). The various signals are generally classified into diagonal and cross peaks, each consisting

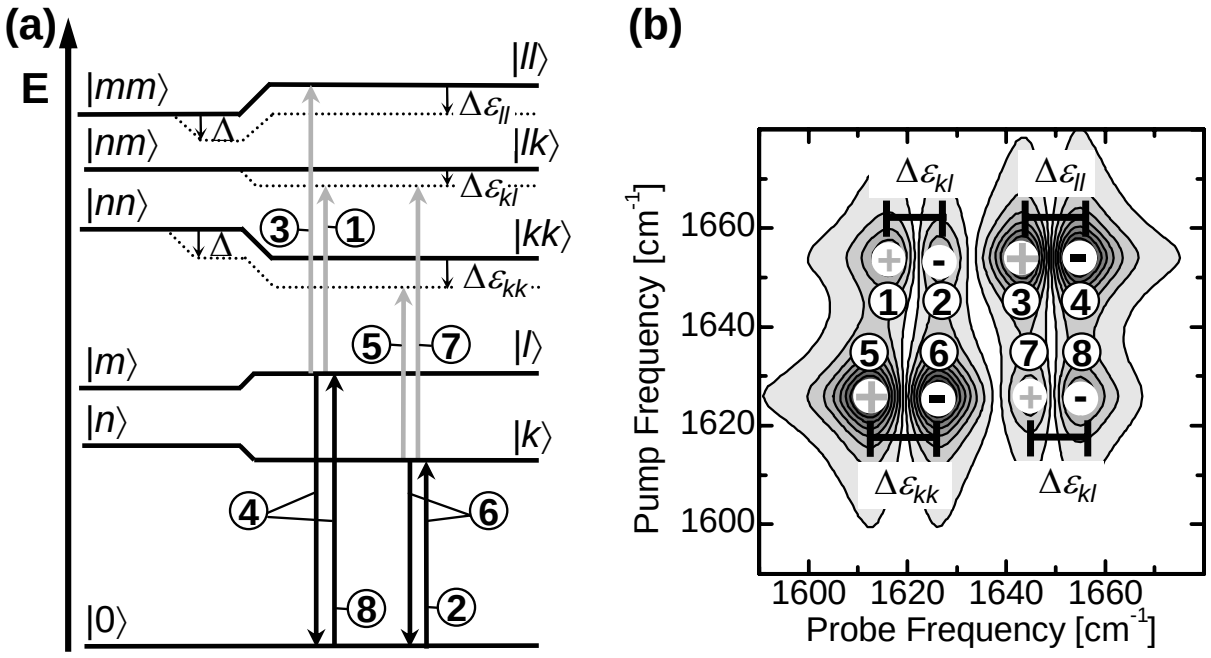

Figure 3.3: (a) System of excitonically coupled vibrational states. The site states $|n\rangle$ and $|m\rangle$ couple and form the excitonic states $|k\rangle$ and $|l\rangle$. In the harmonic limit ($\Delta = 0$), the two excitonic states are product states of the one-excitonic states (solid lines). Anharmonicity lowers the site energy of the double-excited states $|nn\rangle$ by Δ. Due to the excitonic coupling, site-anharmonicity mixes into all two-excitonic states, yielding diagonal $\Delta\epsilon_{kk}$ and off diagonal $\Delta\epsilon_{kl}$ anharmonicity (dotted lines). The arrows, corresponding to the peaks in the 2D spectrum, depict all harmonically allowed transitions. (b) A schematic 2D-IR spectrum of a system consisting of two coupled anharmonic oscillators. The positive peaks correspond to the grey arrows in (b) while the negative peaks correspond to the black arrows.

of a negative and a positive band. When pump and probe pulse are resonant one obtains diagonal peaks, in which case the positive peak represents the excited state absorption and the negative peak the stimulated emission and bleach. The shift between the positive and negative peaks corresponds directly to the intrinsic anharmonicity Δ (Equ. 3.25). Cross peaks appear in the 2D plot at the intersection, where pump and probe frequencies of the two coupled modes cross each other. They originate from the off-diagonal anharmonicity $\Delta\epsilon_{kl}$ and are thus a direct indication of the exciton coupling β (Equ. 3.26) between the two amide-I modes.

3.3.3 Delocalization of vibrational exciton

A commonly used measure for the delocalization of excitonic systems is the participation ratio P_k:[63–65]

$$P_k = \sum_n q_{kn}^4 \tag{3.27}$$

Interestingly, diagonal anharmonicity

$$\Delta\varepsilon_{kk} = -\Delta \sum_n q_{kn}^4, \tag{3.28}$$

which is the quantity we observe when pumping and probing the same transition (Equ. 3.23), scales like the participation ratio P_k:[63–65]

$$P_k = -\frac{\Delta\varepsilon_{kk}}{\Delta} = \sum_n q_{kn}^4 \tag{3.29}$$

The participation ratio is $P_k = 1$ for a perfectly localized state and $P_k = 1/N$ for a perfectly delocalized state, where N is the size of the aggregate. Diagonal anharmonicity therefore is a direct measure of delocalization of vibrational excitons.

Strictly speaking, this conclusion is only correct in the small anharmonicity limit, in which the anharmonic shift of the two-excitonic states, which is of the order of $\Delta\epsilon_{kl} = \Delta/N$, is smaller than the level separation in the two-excitonic band, which is of the order of $16|\beta_{n,n+1}|/N^2$ (the total width of the two-exciton band is $8|\beta_{n,n+1}|$, assuming a linear aggregate with only nearest neighbor coupling). Hence, strictly speaking, the picture of almost-harmonic states breaks down when the aggregates become larger than $N > 16|\beta_{n,n+1}|/\Delta$. When the level density in the two-excitonic band becomes denser, the oscillator strength of harmonically allowed transitions,$|k\rangle \rightarrow |kn\rangle$, is distributed among harmonically forbidden transitions $|k\rangle \rightarrow |lm\rangle$ with $k \neq l, m$. However, direct numerical diagonalization of the two-exciton Hamiltonian $\hat{H} = \hat{H}^{(0)} + \hat{V}$ shows that this redistribution of oscillator strength involves only transitions which are very close in resonance and moreover shows that this redistribution preserves the center of mass of the excited state absorption band. The picture of almost-harmonic states is still approximately valid when the bandwidth of the spectroscopic states is much broader than the spectral region which contributes to that mixing process, that is whenever the anharmonic shift of the excitonic states is small compared to the level separation in the one-excitonic band, which is of the order of $4|\beta_{n,n+1}|/N$.

3.4 Hydrogen bonds and coupling to low frequency modes

In a hydrogen bond two molecules or two sidegroups of one molecule are connected via a hydrogen atom. Figure 3.4(a) shows a typical hydrogen bond between the NH and the C=O group in a polypeptide. In general, the formation of a X−H$\cdots$Y hydrogen bond leads to a distortion of the potential energy surface, which determines the nuclei position, resulting in very anharmonic or even double well potentials and an overall weakening of the covalent X−H bond. This phenomenon leads to characteristic signatures in the vibrational spectrum of the X−H stretching mode and has been extensively studied by vibrational spectroscopy. The most pronounced effect is a strong red shift of the center frequency, which scales approximately linearly with the hydrogen bond length. The shift is accompanied by an intensity increase, a line broadening and frequently a peculiar line shape with a rich substructure.[66–70] These effects are explained by an anharmonic coupling between the high frequency stretching motion of the X−H group and low frequency modes, which modulate the hydrogen bond length X$\cdots$Y.[66,71] A Taylor expansion of the corresponding potential energy surface yields[66,67]:

$$V(Q,q) = \frac{1}{2}\hbar\Omega Q^2 + \frac{1}{2}\hbar\omega q^2 + \frac{\chi}{2}Q^2 q + \ldots \tag{3.30}$$

The first two terms represent the harmonic oscillations of the high frequency mode Q with frequency Ω and of the low frequency mode q with frequency ω, respectively. The third term introduces the anharmonic coupling χ between the two modes, that leads to the distinct nonlinear behavior of hydrogen bonded systems. Both the hydrogen bonded NH and CO mode can be described by Equ. 3.30 and in the following both modes are referred to as the high frequency mode. Nevertheless it is important to note that the nonlinear coupling χ of the N−H mode to the low frequency mode is $\approx 5-10$ times larger than

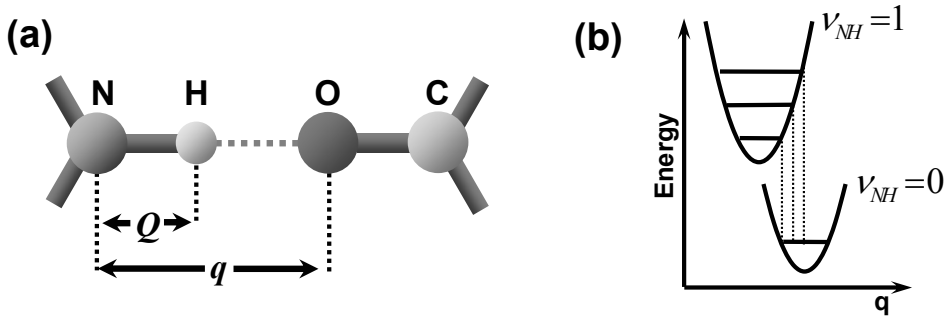

Figure 3.4: (a) A prototype N-H$\cdots$O=C hydrogen bond. Q represents the high frequency oscillator and q the hydrogen bond length. (b) Potential energy surface for the vibrational energy levels $\nu_{NH} = 0$ and $\nu_{NH} = 1$. In the excited state the hydrogen bonds are stronger and one obtains a Franck Condon progression.

that of the C=O mode. Upon quantization (see Equ. 3.6), Equ. 3.30 translates into:

$$\hat{H} = \hbar\Omega\left(\hat{B}^\dagger\hat{B} + \frac{1}{2}\right) + \hbar\omega\left(\hat{b}^\dagger\hat{b} + \frac{1}{2}\right) + \frac{\chi}{2\sqrt{2}}\hat{B}^\dagger\hat{B}\left(\hat{b}^\dagger + \hat{b}\right) + \ldots \tag{3.31}$$

where $\hat{B}^\dagger$ and $\hat{B}$ are the creation and annihilation operators of the high frequency mode, while $\hat{b}^\dagger$ and $\hat{b}$ are those of the low frequency mode. Terms that do not conserve the number of high frequency excitations (i.e. non resonant terms) have been discarded. Hamiltonian Equ. 3.31 can be diagonalized analytically.[3] However the problem simplifies significantly when one considers the one order of magnitude difference between the frequencies of the phonon modes and the high frequency vibrational mode, allowing an adiabatic separation of time scales.[71] In this approximation, the high frequency vibration adopts adiabatically to the position of the phonon coordinates, in the same way as the electron adopts to the position of the nucleus in the Born Oppenheimer approximation. When the coordinate q is fixed one can transform the first three terms in Equ. 3.30 to:

$$V(Q,q) = \frac{1}{2}\hbar\Omega_{\mathit{eff}}Q^2 + \frac{1}{2}\hbar\omega q^2 \tag{3.32}$$

with

$$\hbar\Omega_{\mathit{eff}} = \hbar\Omega + \chi q \tag{3.33}$$

Equation 3.33 implies that the high frequency Ω_{eff} varies linearly with the hydrogen bond distance, which is described by the phonon coordinate q. This dependence has been observed experimentally for various hydrogen bonded crystals,[68] allowing one to estimate the coupling constant χ. Starting from Equ. 3.32 and 3.33 one obtains the potential energy surface for each excitation level ν of the high frequency mode as a function of phonon coordinate q:

$$E_\nu(q) = \hbar\Omega_{eff}\left(\nu + \frac{1}{2}\right) + \frac{1}{2}\hbar\omega q^2 \tag{3.34}$$

Figure 3.4(b) illustrates schematically the potential energy surfaces for $\nu = 0$ and $\nu = 1$. It should be noted that this is the displaced oscillator picture that one knows from electronic Franck Condon transitions. The nonlinear coupling χ gives rise to a displacement of the potential energy surface in the excited state. The minimum of that potential energy surface is shifted towards smaller intermolecular distances, giving rise to a stronger hydrogen bond in the excited state. Consequently, a "Franck-Condon-like" progression is obtained for the absorption spectrum, consisting of one vibrational excitation plus several quanta of phonon excitation.

Recently the nonlinear response of hydrogen bonded vibrations has been studied extensively.[69,70,72,73] Figure 3.5 shows the pump-probe signal of the OD stretching mode of hydroxy-deuterated 2-(2'-hydroxyphenyl)benzothiazole (HBT-D), a molecule with an intramolecular OD$\cdots$N hydrogen bond.[70] The striking feature is a pattern of pronounced oscillations, which is superimposed on the signal. These oscillations have been attributed to a ground state wave packet motion. After excitation of the OD stretching vibration

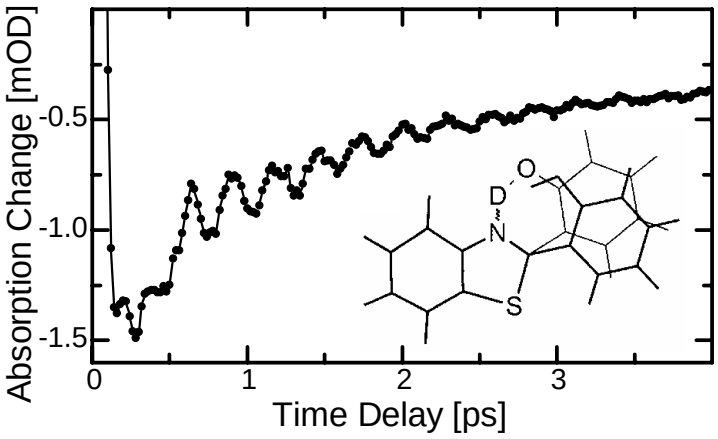

Figure 3.5: pump-probe response of hydroxydeuterated 2-(2'-hydroxyphenyl)benzothiazole (HBT-D), after impulsive excitation of the OD stretching mode. The inset illustrates the ring deformation mode in HBT-D (thick line: equilibrium position). Adapted from Madsen *et al.*[70]

by a ultrashort pump pulse (100 fs) the hydrogen bond gets stronger and is contracted. As a consequence a vibrational wavepacket in a low frequency hydrogen bond mode is impulsively excited.[70] The observation of the beatings is a direct consequence of a displacement of the excited state potential energy surface and thus a consequence of the nonlinear coupling between the high frequency stretching vibration and a low frequency hydrogen bond mode (Hamiltonian 3.31). In case of HBT-D the low frequency mode corresponds to the ring deformation mode shown in the inset of Fig 3.5). Similar examples of nuclear coherent motion following hydrogen bond excitation have been found in other molecules with intramolecular hydrogen bonds.[69,72,73]

3.5 Vibrational polaron

3.5.1 One-dimensional hydrogen bonded systems

In the previous chapters two coupling mechanisms were introduced: excitonic coupling between vibrational modes [Chapter 3.3] and nonlinear coupling between vibrational and low frequency modes [Chapter 3.4]. In the present chapter these two couplings are combined to describe vibrational excitations in hydrogen bonded molecular crystals and α-helices. In a hydrogen bonded molecular crystals the individual molecules, e.g. peptides such as acetanilide (ACN) or N-methylacetamide (NMA), are connected by quasi-one-dimensional (1D) chains of hydrogen bonds [Fig. 3.6], that run through the crystal [see also Fig. 5.1 and Fig. 6.1]. An α-helix consists of a chain of peptides that is held in a helical shape by three 1D chains of hydrogen bonds, that run along the outside of the helix [see Fig. 3.2 or Fig. 1.3].

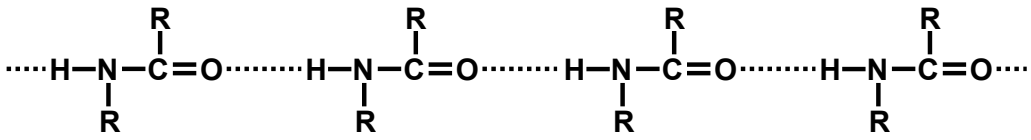

Figure 3.6: One dimensional hydrogen bonded peptide chain. Such chains are found in molecular crystals or along the outside of α helices. The hydrogen bonds (thin lines) connect the NH with the C=O groups.

In such hydrogen bonded chains the N-H (or C=O) stretching vibrations of each peptide unit, couple to form delocalized states (vibrational excitons), as described in Chapter 3.3. However, each oscillator is further coupled via the hydrogen bonds to low frequency modes, that alter the hydrogen bond length [see Chapter 3.4]. Since the hydrogen bonded chains are translational invariant along the direction of the hydrogen bonds, one can describe a collective motion of a low frequency mode as a phonon mode. Thus the hydrogen bonds mediate an exciton-phonon coupling. Phonons, which are the normal modes of a lattice structure, are generally classified into two types: acoustic and optical phonons.[74,75] Acoustic phonons reflect vibrations between individual units cells, while optical phonons correspond to vibrations between molecules inside a unit cell [see Fig. 3.7].[a] Optical phonons appear only in systems where the unit cell contains more than one molecule, such as crystalline ACN (eight molecules) or NMA (four molecules).[76,77] Hence in ACN and NMA vibrational excitons can couple to both, acoustic and optical phonons. On the other hand, in hydrogen bonded chains in α-helices, the unit cell corresponds to just one peptide unit and exciton-phonon coupling is only possible with acoustic phonons.

3.5.2 The Davydov theory

In the 1970s Davydov proposed that vibrational excitations in α-helices can self-trap (self localize) along the helix due to the combination of excitonic and exciton-phonon coupling.[1] The basic idea is that of a polaron, i.e. a vibrational excitation that maintains a persistent and nontrivial correlation with lattice phonons. In simple words, the vibrational exciton distorts through phonon coupling the lattice structure of the helix, which reacts, in turn through phonon coupling, to trap the exciton. As a result one obtains a bound exciton-phonon state (a polaron). This phenomenon is generally called self-trapping and it was assumed that the self-trapped state can propagate along the helix in a soliton-like form. Self-trapping is described by a Fröhlich-like Hamiltonian, which is essentially a combination of Equ. 3.14 and 3.31.[78] The Hamiltonian consists of three components, $\hat{H}_{ex}$, $\hat{H}_{ph}$ and $\hat{H}_{int}$, which describe respectively, excitonic coupling, harmonic phonon modes

[a] Here, the term phonon is used to describe the "external" dynamics of the peptide units, while vibrational excitons describe the "internal" dynamics. However, strictly speaking, vibrational excitons are also phonons ("internal phonons").

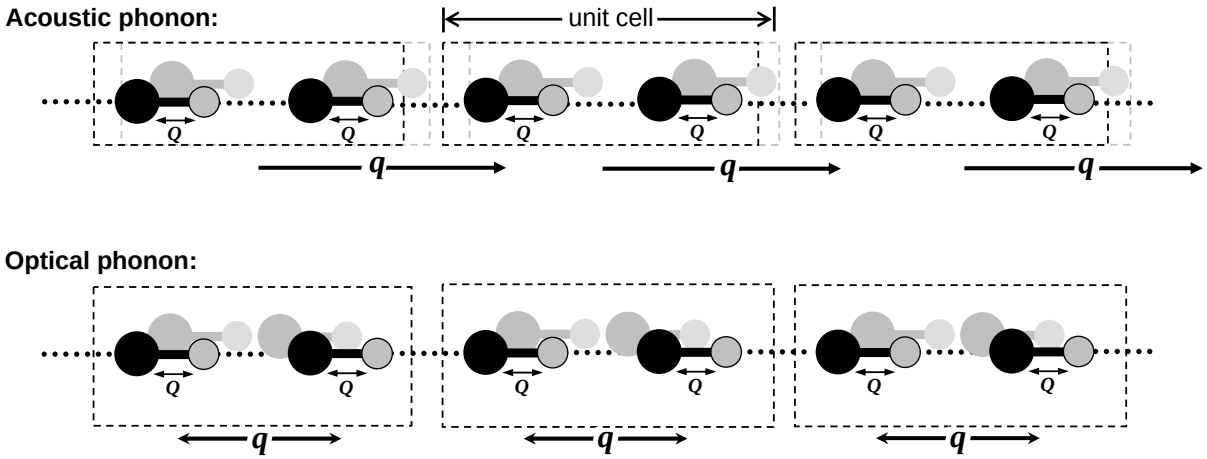

Figure 3.7: Illustration of acoustic and optical phonon modes in a molecular crystal. q is the coordinate of the low frequency phonon mode and Q the one of the high frequency molecular vibration. Acoustic phonons describe oscillations between individual unit cells, while optical phonons correspond to vibrations between the molecules inside one unit cells.

and exciton-phonon coupling in a 1D molecular chain. In the most general form the Hamiltonian reads

$$\begin{aligned}
\hat{H} &= \hat{H}_{ex} + \hat{H}_{ph} + \hat{H}_{int} \\
\hat{H}_{ex} &= \sum_n \hbar\Omega \left(\hat{B}_n^\dagger \hat{B}_n + \frac{1}{2} \right) + \sum_n \beta \left(\hat{B}_n^\dagger \hat{B}_{n+1} + \hat{B}_n \hat{B}_{n+1}^\dagger \right) \\
\hat{H}_{ph} &= \sum_q \hbar\omega_q \left(\hat{b}_q^\dagger \hat{b}_q + \frac{1}{2} \right) \\
\hat{H}_{int} &= \sum_{n,q} \chi_n^q \left(\hat{b}_q^\dagger + \hat{b}_q \right) \hat{B}_n^\dagger \hat{B}_n \quad ,
\end{aligned} \tag{3.35}$$

where $\hat{B}_n^\dagger$ ($\hat{B}_n$) create (destroy) a vibrational excitation on peptide unit n with frequency Ω, β is the excitonic coupling strength and $\hat{b}_n^\dagger$ ($\hat{b}_n$) create (destroy) one quantum of phonon energy of wave vector q with frequency ω_q. Finally, the exciton-phonon coupling strength χ_n^q indicates how strongly localized vibrational energy will distort the lattice and how strongly a lattice distortion will trap the localized vibrational energy. By choosing specific phonon dispersion relations ω_q and coupling functions χ_n^q different coupling geometries and phonon band structures can be accommodated. In case of a coupling to acoustic modes the exciton-phonon coupling χ_n^q and the dispersion relation ω_q are[79–82]

$$\chi_n^q = 2i\chi \sin qa \sqrt{\frac{\hbar}{2NM\omega_q}} e^{-iqna}, \tag{3.36}$$

$$\omega_q = \omega \sin\left(1/2\,|qa|\right), \tag{3.37}$$

where N is the total number of peptides in the chain, M the mass of each peptide unit and a the lattice spacing between them. In this case $\hat{H}_{ph}$ and $\hat{H}_{int}$ in Equ. 3.35 are expressed

as

$$\hat{H}_{ph} = \sum_n \left(\frac{\hat{p}_n^2}{2M} + \frac{1}{2}\kappa \left(\hat{u}_{n+1} - \hat{u}_n \right)^2 \right) \tag{3.38}$$

$$\hat{H}_{int} = \sum_n \chi \left(\hat{u}_{n+1} - \hat{u}_{n-1} \right) \hat{B}_n^\dagger \hat{B}_n \quad , \tag{3.39}$$

where $\hat{p}_n$ and $\hat{u}_n$ are the momentum and displacement operators of the peptide unit, κ is the spring constant of the hydrogen bond and χ the exciton-phonon coupling. The two forms of $\hat{H}$ are related by[83]

$$\hat{b}_q = \frac{1}{\sqrt{N}} \sum_n e^{iqna} \left(\sqrt{\frac{M\omega_q}{2\hbar}} \hat{u}_n + i \sqrt{\frac{1}{2\hbar M\omega_q}} \hat{p}_n \right) \tag{3.40}$$

$$\hat{b}_q^\dagger = \frac{1}{\sqrt{N}} \sum_n e^{-iqna} \left(\sqrt{\frac{M\omega_q}{2\hbar}} \hat{u}_n - i \sqrt{\frac{1}{2\hbar M\omega_q}} \hat{p}_n \right) . \tag{3.41}$$

Since the quantum polaron system (Equ. 3.35) cannot be exactly solved,[84] Davydov derived from the Hamiltonian classical-like equations of motion, which are supposed to reflect the quantum evolution of a collective excitation.[3,12] The method was based on a trial wave function, which described a state vector as a functional of generalized coordinates. The equations of motion (evolution equations) of these generalized coordinates were taken to be the classical Hamiltonian equations, where the expectation value of the quantum Hamiltonian is used as the Hamiltonian function.[85] Davydov showed that under certain approximation the equations of motion reduce to the nonlinear Schrödinger equation that arises in the study of solitons.[86] Based on this theory a localization and a soliton-like transport of vibrational energy along an α-helix was proposed.

Davydov's theory has been discussed extensively during the last twenty years and alternative formulations and derivations of the trial wave function, the equations of motion and the nonlinear Schrödinger equation were presented (see Refs. 3 and 46 for reviews). In the following two aspects of vibrational self-trapping theory are discussed in more detail, since they are used to describe the experiments in the following chapters. The first section addresses coupling to optical, instead of acoustic, phonons while the second section introduces a slightly modified Davyodv model, which emphasizes the intrinsic anharmonicity and strong exciton-phonon coupling.

3.5.3 Coupling to optical phonons

The unit cells of hydrogen bonded crystals can contain several molecules and hence a coupling between excitons and both optical and acoustic phonons is possible. In the studies of vibrational self-trapping in ACN coupling to optical phonons is considered more likely, since one observes strong changes in the IR spectra, which can not be explained with a coupling to acoustic phonons (see Chapter 5, Ref. 3 and Ref. 87 for more details). For

dispersionless optical phonons the exciton-phonon coupling χ_n^q and the phonon frequency ω_q are[3]

$$\chi_n^q = \chi^q = \chi\sqrt{\frac{\hbar}{2m\omega_q}} \tag{3.42}$$

$$\omega_q = \omega_\circ = const. \tag{3.43}$$

Thus the theoretical model corresponds to a linear chain, where each site consists of a vibrational oscillator that is coupled to a low frequency mode. In this case the Hamiltonian Equ. 3.35 becomes

$$\begin{aligned}
\hat{H} &= \hat{H}_{ex} + \hat{H}_{ph} + \hat{H}_{int} \\
\hat{H}_{ex} &= \sum_n \hbar\Omega \left(\hat{B}_n^\dagger \hat{B}_n + \frac{1}{2}\right) + \sum_n \beta \left(\hat{B}_n^\dagger \hat{B}_{n+1} + \hat{B}_n \hat{B}_{n+1}^\dagger\right) \\
\hat{H}_{ph} &= \sum_n \hbar\omega_\circ \left(\hat{b}_n^\dagger \hat{b}_n + \frac{1}{2}\right) \\
\hat{H}_{int} &= \sum_n \chi \hat{B}_n^\dagger \hat{B}_n \left(\hat{b}_n^\dagger + \hat{b}_n\right).
\end{aligned} \tag{3.44}$$

One commonly refers to this form of the Hamiltonian as the Holstein polaron Hamiltonian.[88] In analogy to the Davydov theory the equations of motion, giving rise to the nonlinear Schrödinger equation, can be derived from a trial wave function and self-trapped (soliton) solutions are obtained.[3,89]

The Hamiltonian 3.44 (and 3.35) can be diagonalized analytically, if the nonlinear coupling χ (χ_n^q) or the excitonic coupling β are neglected.[3] In the first case the problem reduces to the vibrational exciton Hamiltonian discussed in Chapter 3.3. In the second case the individual sites in the chain are decoupled and one obtains the Hamiltonian of a hydrogen-bonded molecule, which corresponds to the problem of a displaced oscillator [Chapter 3.4]. When both couplings are included one has to solve the Hamiltonian numerically, which is possible with high accuracy.[90] In analytical treatments of vibrational self-trapping the nearest neighbor coupling β is commonly neglected in a first step, since it is smaller than the exciton-phonon coupling χ and is included only afterwards in a perturbative manner.[3,87] The resulting problem simplifies significantly when one considers the one order of magnitude difference between the frequencies Ω and $\omega_\circ$. After the adiabatic separation of time scales, outlined in Chapter 3.4, one obtains a potential energy surface for each excitation level of the exciton as a function of phonon coordinates (see Equ. 3.34). The energy surfaces correspond to those depicted in Fig. 3.4(b). Exciton phonon coupling is responsible for the displacement of the potential energy surfaces in the excited state (the so-called self-trapped states) for which a "Franck-Condon" progression is obtained consisting of one vibrational excitation plus several quanta of phonon excitations. The spectral signatures of self-trapping in nonlinear spectroscopy are the major topic of this dissertation and are discussed in detail in Chapters 5 and 6.

3.5.4 Polaron bound states

It has been pointed out that many problems in the Davydov theory have their origin in polaron theory and that different parameter regions require different theoretical approaches.[80,91,92] The three relevant parameters of the problem are the excitonic coupling strength β, the phonon cutoff frequency ω_q and the polaron binding energy, which depends on the exciton-phonon coupling χ_n^q. Depending on the parameters one is either in the small polaron regime or in the large polaron regime. Small polaron usually describes the non-adiabatic limit, where the phonon frequency ω_q is large compared to the excitonic coupling β. Such a small polaron, or more precisely non-adiabatic small polaron, occupies a minimum number of lattice sites, usually one. On the contrary a large polaron generally refers to the adiabatic limit, where the typical phonon frequency is small relative to the excitonic coupling, and the polaron extends over a large number of lattice sites usually justifying a continuum approximation.[81,91,92] The so-called Davydov soliton corresponds to a large polaron in the adiabatic limit[80] an entity which has been studied extensively in the literature.[45,88,93,94]

Brown and Ivić have devised a unified theory that interpolates between small and large polaron regimes, by combining time dependent variational techniques with partial "dressing" methods.[91] In the non-adiabatic limit, i.e. when the exciton bandwidth is less than the phonon cutoff frequency, the polaron states are dominated by the quantum nature of the phonons, which can result in a "phonon dressing" of the exciton. Here, a dressed exciton corresponds to an exciton that is surrounded by a cloud of virtual phonons. The phonon cloud yields a local distortion of the lattice, which follows the exciton instantaneously.[88,93,95] This dressing effect modifies the exciton frequency Ω, reduces the exciton bandwidth, and allows an additional attractive exciton-exciton interaction. Such an interaction between different excitons, can result in bound states of two or more vibrational quanta.[95]

However the exciton-phonon coupling is not the only source of nonlinearity in hydrogen bonded molecular chains. Also the intrinsic anharmonicity of the vibrational modes can break the independence of the excitons and hence can give rise to nonlinear dynamics. In fact, in theory the intrinsic anharmonicity itself can cause in 1D classical lattices intrinsic localized modes, often referred to as discrete breathers [see Chapter 1].[14,16,17] These modes, which have been studied extensively in classical lattices, favor a local energy accumulation that might be pinned to the lattice or may travel through it. In a quantum lattice the intrinsic anharmonicity favors the formation of two-exciton bound states.[11,16,96] The bound states correspond to a trapping of two quanta of vibrational energy over a few neighboring sites with an energy that is lower than the energy of two quanta lying far apart. Lateral interaction can result in a motion of such states from one lattice site to another, leading to a delocalized wavepacket. Bound states are viewed as the quantum mechanical counterpart of discrete breathers.[11,96]

In conclusion both nonlinearities, intrinsic anharmonicity and strong exciton-phonon coupling, can have a similar effect on the exciton dynamics, resulting in bound exciton states. In a recent work Pouthier and coworkers studied vibrational excitations in α-helices[97,98] with special emphasize on the intrinsic anharmonicity and strong exciton-phonon coupling. This theory is used in Chapter 7 to discuss the nonlinear response signal of an α-helix and is briefly reviewed in the following. Pouthier's work is based on a modification of the Hamiltonian Equ. 3.35, which considers coupling to acoustic phonons and includes the intrinsic anharmonicity of the vibrational modes (Equ. 3.10) as well as additional terms to describe the exciton-exciton interaction:

$$\begin{aligned}
\hat{H} &= \hat{H}_{ex} + \hat{H}_{ph} + \hat{H}_{int} \\
\hat{H}_{ex} &= \sum_n \hbar\Omega \left(\hat{B}_n^\dagger \hat{B}_n + \frac{1}{2} \right) + \sum_n \beta \left(\hat{B}_n^\dagger \hat{B}_{n+1} + \hat{B}_n \hat{B}_{n+1}^\dagger + \hat{B}_n^\dagger \hat{B}_{n+1}^\dagger + \hat{B}_n \hat{B}_{n+1} \right) \\
&\quad + \Delta^{(3)} (\hat{B}_n^\dagger + \hat{B}_n)^3 + \Delta^{(4)} (\hat{B}_n^\dagger + \hat{B}_n)^4 \\
\hat{H}_{ph} &= \sum_q \hbar\omega_q \left(\hat{b}_q^\dagger \hat{b}_q + \frac{1}{2} \right) \\
\hat{H}_{int} &= \sum_{n,q} \chi_n^q \left(\hat{b}_q^\dagger + \hat{b}_q \right) \left(\hat{B}_n^\dagger + \hat{B}_n \right)^2
\end{aligned} \tag{3.45}$$

The Davydov polaron Hamiltonian is recovered by restricting equation 3.45 to terms that conserve the number of excitations and by neglecting the intrinsic anharmonicity. In the discussion of the Davydov theory, the non-conserving additional terms $\hat{B}_n^\dagger \hat{B}_{n+1}^\dagger$ and $\hat{B}_n \hat{B}_{n+1}$ in $\hat{H}_{ex}$ have been previously used by Takeno, who referred to the corresponding excitation as a vibron.[99] The Hamiltonian 3.45 can be simplified by unitary transformations to obtain an effective Hamiltonian $\hat{H}_{\mathit{eff}}$ that describes the dynamics of the anharmonic vibrons dressed by a virtual cloud of phonons, i.e. anharmonic small polarons.[97]

The effective Hamiltonian $\hat{H}_{\mathit{eff}}$ conserves the polaron number and the eigenstates can be expanded by the number state method.[96] Using this method, the two-polaron wave function, which describes states with two vibrational quanta, is expressed as

$$|\Psi\rangle = \sum_{n_1, n_2 \geq n_1} \Psi(n_1, n_2) |n_1, n_2\rangle, \tag{3.46}$$

where the basis vector $|n_1, n_2\rangle$ characterizes two polarons located at site n_1 and n_2, respectively.[97,100] By taking advantage of the lattice periodicity one can expand the two-polaron wave function as a Bloch wave

$$\Psi(n_1, n_2 = n_1 + m) = \frac{1}{\sqrt{N}} \sum_{n_1} e^{ik(n_1 + m/2)} \Psi_k(m). \tag{3.47}$$

Here m characterizes the distance between the two polarons and k is the wave vector, that is associated with the center of mass of the two polarons. The momentum k is a good quantum number and the corresponding Schrödinger equation can be solved numerically for each k value to obtain the two-polaron eigenstates and to determine the

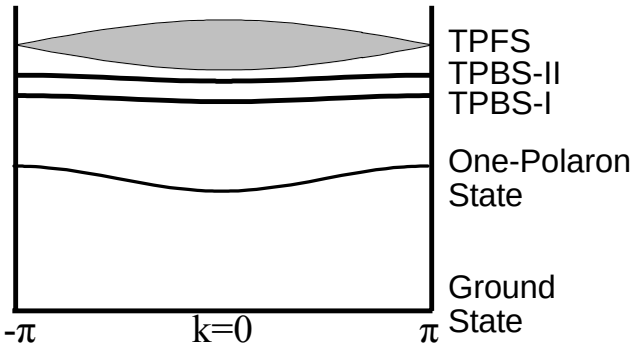

Figure 3.8: Schematic of the energy levels in the case of self-trapped anharmonic excitations[97] (not on scale). The two polaron eigenstate energy spectrum exhibits three bands: The two-polaron free state (TPFS) continuum and the two two-polaron bound states (TPBS-I and TPBS-II).

two-polaron energy spectrum.[97] Pouthier uses in his original work the word vibron for the dressed states. Here polaron is used to clearly distinguish dressed vibrons (polaron) from undressed vibrons (vibron or vibrational exciton).

The two-polaron energy spectrum exhibits three types of states [see Fig. 3.8]: (i) two-polaron free states (TPFS) belonging to an energy continuum which corresponds to two non-interacting polarons (ii) two-polaron bound states I (TPBS-I) which refer to the trapping of the polarons at the same site, and (iii) two-polaron bound states II (TPBS-II) which characterize polarons trapped at nearest neighbor sites. The occurrence of TPBS-II, which originates from an overlap between the virtual cloud of phonons of each vibron, appears as a signature of the acoustic nature of the phonons, that are responsible for correlations between adjacent sites. In case of an undressed state, i.e. $\chi_n^q = 0$, one obtains, besides the two-vibron free state just one two-vibron bound state. The dressing effect itself causes the formation of two bound states, which are therefore also observed when the intrinsic anharmonicity is zero ($\Delta^{(3)}$=$\Delta^{(4)}$=0). However, when the intrinsic anharmonicity is nonzero the dressing effect is enhanced by the additional anharmonicity, resulting in lower energies and smaller bandwidths of the bound states. Depending on the intrinsic anharmonicity and the polaron binding energy, the TPBS-II are either located inside or below the TPFS continuum, while the TPBS-I are located over the entire Brillouin zone below the TPFS continuum. Based one this model one can now calculate a pump-probe spectrum. Since infrared wavelengths are much longer than a unit cell, one only needs to consider $k = 0$ transitions. The pump-probe spectrum of the NH mode of an α-helix is discussed in detail in Chapter 7. The data shows the spectral signature of two-polaron bound states.

3.6 Fermi resonances

In the Davydov theory the vibrational excitations in hydrogen bonded crystals or α-helices are described by a 1D chain model. Each site in the chain consists of a single vibrational oscillator. However, a real hydrogen bonded crystal consists of a chain of molecules, instead of single oscillators, where each molecule contains several atoms and hence many vibrational modes. When a fundamental normal mode is accidentally resonant with an overtone or a combination of lower frequency modes and when an anharmonic term of the potential energy surface couples them, the overtone (or the combination) mode gains oscillator strength.[101] This phenomenon, called Fermi resonance, can give rise to a double peak in the linear absorption spectrum. Since vibrational self-trapping can also result in a double peak signature in the absorption spectrum,[2,56,102,103] one has to be careful not to misinterpret a Fermi resonance with a vibrational polaron. Fermi resonances and vibrational self-trapping originate from two different anharmonic contributions to the potential energy surface. Since these anharmonicities can give rise to completely different 2D-IR spectra [see Chapter 5.1.3], one can use 2D-IR spectroscopy to distinguish the two phenomena. In the following section the 2D-IR spectrum of an elementary Fermi resonance is constructed. A Fermi resonance between a fundamental mode q_1 and an overtone of mode q_2 is described by an additional $q_1 q_2^2$ term in the potential energy surface:

$$V(q_1, q_2) = \frac{\partial^2 V}{2\partial q_1^2} q_1^2 + \frac{\partial^2 V}{2\partial q_2^2} q_2^2 + \frac{\partial^3 V}{2\partial q_1 \partial q_2^2} q_1 q_2^2 \tag{3.48}$$

If one considers only resonant terms ($\Omega_1 \approx 2\Omega_2$) one can write the Fermi resonance Hamiltonian as

$$\hat{H} = \hbar\Omega_1 \hat{B}_1^\dagger \hat{B}_1 + \hbar\Omega_2 \hat{B}_2^\dagger \hat{B}_2 + \frac{\delta}{2\sqrt{2}} \left(\hat{B}_1 \hat{B}_2^{\dagger 2} + \hat{B}_1^\dagger \hat{B}_2^2 \right), \tag{3.49}$$

where $\hat{B}_1^\dagger$ and $\hat{B}_1$ are the creation and annihilation operators of the high frequency mode and $\hat{B}_2^\dagger$ and $\hat{B}_2$ those of the lower frequency mode. The zero-point energy has been subtracted and the Fermi coupling δ is defined as

$$\delta = \frac{\partial^3 V}{2\partial q_1 \partial q_2^2}. \tag{3.50}$$

In linear absorption spectroscopy, only the $|\hat{B}_1, \hat{B}_2\rangle$ states $|1,0\rangle$ and $|0,2\rangle$ are reached, where the first digit labels the excitation of the fundamental mode and the second digit that of the coupled lower frequency mode. When diagonalizing the Hamiltonian 3.49 in the reduced basis, $\{|1,0\rangle|0,2\rangle\}$, we obtain the well known results for the eigenenergies (for a perfect Fermi resonance, $\Omega_1 = 2\Omega_2$):[101]

$$\begin{aligned} E_{1_1} &= \hbar\Omega_1 - \frac{\delta}{2}, \\ E_{1_2} &= \hbar\Omega_1 + \frac{\delta}{2}, \end{aligned} \tag{3.51}$$

and the eigenstates:

$$|1_1\rangle = -\frac{1}{\sqrt{2}}|1,0\rangle + \frac{1}{\sqrt{2}}|0,2\rangle\,,$$
$$|1_2\rangle = +\frac{1}{\sqrt{2}}|1,0\rangle + \frac{1}{\sqrt{2}}|0,2\rangle\,. \tag{3.52}$$

Both states mix and split and the otherwise dark overtone gains oscillator strength from the high frequency mode. This model can be extended in a straightforward manner to also account for 3rd-order nonlinear spectroscopy.[56] The essential difference is that the probe pulse will now also be resonant with states $|2,0\rangle$, $|1,2\rangle$ and $|0,4\rangle$. Hence, we have to extend the basis to:

$$\{|1,0\rangle\,,|0,2\rangle\,,|2,0\rangle\,,|1,2\rangle\,,|0,4\rangle\} \tag{3.53}$$

in which the Hamiltonian Equ. 3.49 reads

$$\hat{H} = \left(\begin{array}{cc|ccc} \hbar\Omega_1 & \frac{1}{2}\delta & & 0 & \\ \frac{1}{2}\delta & 2\hbar\Omega_2 & & & \\ \hline & & 2\hbar\Omega_1 & \sqrt{\frac{1}{2}}\delta & 0 \\ 0 & & \sqrt{\frac{1}{2}}\delta & \hbar(\Omega_1+2\Omega_2) & \sqrt{\frac{3}{2}}\delta \\ & & 0 & \sqrt{\frac{3}{2}}\delta & 4\hbar\Omega_2 \end{array}\right). \tag{3.54}$$

The Hamiltonian is block-diagonal so that the manifolds $\{|1,0\rangle\,,|0,2\rangle\}$ and $\{|2,0\rangle\,,|1,2\rangle\,,|0,4\rangle\}$ decouple. Thus it is sufficient to expand the Hamiltonian in the restricted basis $\{|1,0\rangle\,,|0,2\rangle\}$ when discussing linear spectroscopy. For each order of non-linear spectroscopy, an additional block appears in the Hamiltonian, which however decouples from the remainder. Diagonalization of the second block yields (for $\Omega_1 = 2\Omega_2$)

$$E_{2_1} = 2\hbar\Omega_1 - \sqrt{2}\delta,$$
$$E_{2_2} = 2\hbar\Omega_1,$$
$$E_{2_3} = 2\hbar\Omega_1 + \sqrt{2}\delta, \tag{3.55}$$

and

$$|2_1\rangle = \frac{1}{2\sqrt{2}}|2,0\rangle - \frac{1}{\sqrt{2}}|1,2\rangle + \sqrt{\frac{3}{8}}|0,4\rangle\,,$$
$$|2_2\rangle = -\frac{\sqrt{3}}{2}|2,0\rangle + \frac{1}{2}|0,4\rangle\,,$$
$$|2_3\rangle = \frac{1}{2\sqrt{2}}|2,0\rangle + \frac{1}{\sqrt{2}}|1,2\rangle + \sqrt{\frac{3}{8}}|0,4\rangle\,. \tag{3.56}$$

The transitions strengths between the various eigenstates can be obtained from the elements of the transition dipole matrix $\mu\langle 0|\,\hat{B}_1+\hat{B}_1^\dagger\,|1_i\rangle$ and $\mu\,\langle 1_i|\,\hat{B}_1+\hat{B}_1^\dagger\,|2_j\rangle$, respectively, where μ is the transition dipole of the fundamental normal mode and the notation $|i_j\rangle$ is

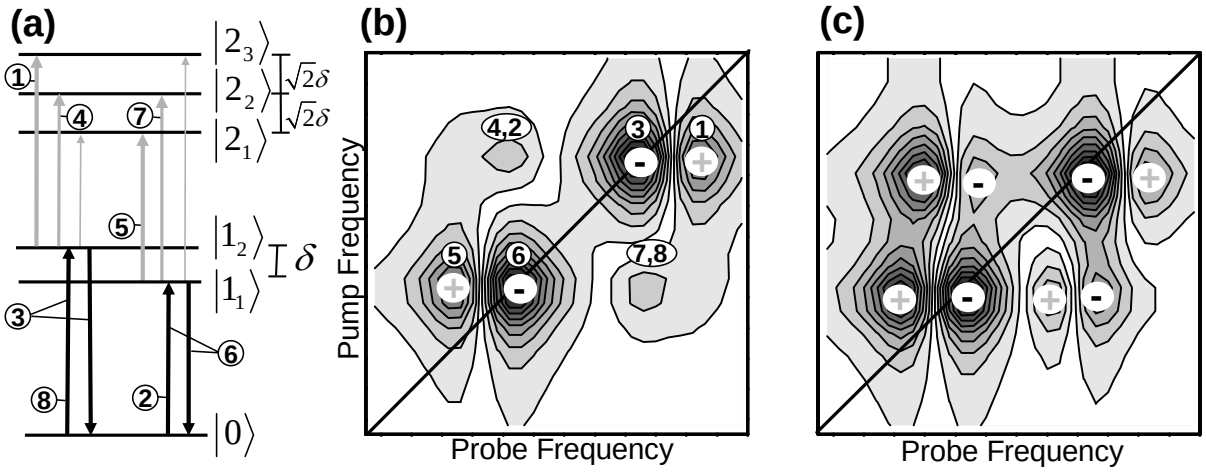

Figure 3.9: (a) Vibrational energy levels and (b) calculated 2D IR spectrum of a harmonic Fermi resonance. Upgoing grey arrows correspond to a positive excited state absorption. Up and down going black arrows symbolize the negative bleach and stimulated emission signal, respectively. (c) calculated 2D IR spectrum of an anharmonic Fermi resonance. A Lorentzian line shape with bandwidth 11 cm^{-1} is assumed for all transitions. The Fermi coupling δ, the anharmonicity Δ_1 and the frequencies Ω_i, are chosen to correspond to the Fermi resonance of the C=O mode in benzoylchloride [see Chapter 5.1.3]

defined by equations 3.52 and 3.56. The transition strength is equally distributed among the $|0\rangle \rightarrow |1_1\rangle$ and $|0\rangle \rightarrow |1_2\rangle$ transitions, as expected for a symmetric Fermi resonance. Of the excited state transitions, the $|1_1\rangle \rightarrow |2_1\rangle$, $|1_1\rangle \rightarrow |2_2\rangle$, $|1_2\rangle \rightarrow |2_2\rangle$ and $|1_2\rangle \rightarrow |2_3\rangle$ transitions are about equally strong, while the two other possibilities, $|1_1\rangle \rightarrow |2_3\rangle$ and $|1_2\rangle \rightarrow |2_1\rangle$, carry only negligible oscillator strength. With these ingredients, the 2D-IR spectrum of a Fermi resonance, which is shown in Fig. 3.9(b), can readily be constructed: we first calculate the population probabilities of states $|1_1\rangle$ or $|1_2\rangle$ depending on the pump frequency, and subsequently calculate the up- and downward transitions seen by the probe-pulse according to the level scheme in Figure 3.9(a). The spectrum shows two negative and four positive peaks. Two of the positive peaks have a significantly lower intensity than the other two peaks since the corresponding positive excited state absorption signals ($|1_1\rangle \rightarrow |2_2\rangle$ and $|1_2\rangle \rightarrow |2_2\rangle$) are reduced by negative bleach signals, which appear for harmonic modes at the same position in the 2D spectrum.

Hamiltonian Equ. 3.49 does not include the intrinsic anharmonicity of the vibrational modes. However, nonlinear spectroscopy is specifically sensitive to anharmonicities and hence one should use anharmonic, instead of harmonic oscillators to describe a Fermi resonance. The eigenenergies of an anharmonic oscillator scale like $E_n = n\Omega - n^2\Delta$,[101] a result which is taken into account by including the terms $\Delta_i B^\dagger B^\dagger BB$ (Equ. 3.13) into Hamiltonian Equ. 3.49. Thus one obtains additional terms $n^2\Delta_i$ on the diagonal of the Hamiltonian matrix. A Fermi resonance between two anharmonic oscillators is hence

described by

$$H = \left(\begin{array}{cc|ccc} \hbar\Omega_1 - \Delta_1 & \frac{1}{2}\delta & & 0 & \\ \frac{1}{2}\delta & 2\hbar\Omega_2 - \Delta_2 & & & \\ \hline & & 2\hbar\Omega_1 - 4\Delta_1 & \sqrt{\frac{1}{2}}\delta & 0 \\ 0 & & \sqrt{\frac{1}{2}}\delta & \hbar(\Omega_1 + 2\Omega_2) - \Delta_1 - 4\Delta_2 & \sqrt{\frac{3}{2}}\delta \\ & & 0 & \sqrt{\frac{3}{2}}\delta & 4\hbar\Omega_2 - 16\Delta_2 \end{array}\right). \tag{3.57}$$

The analytic solution of Hamiltonian 3.57 is in contrast to the harmonic case (Equ. 3.55 and 3.56) no longer instructive. Nevertheless, the Hamiltonian 3.57 is easily diagonalized numerically. After diagonalization one can construct, in the same way as in the harmonic case, a 2D-IR spectrum. Figure 3.9(c) shows such a 2D-IR spectrum for a perfect Fermi resonance ($\Omega_1 = 2\Omega_2$) between an anharmonic fundamental mode and an overtone of a harmonic ($\Delta_2 = 0$) mode. Including the anharmonicity Δ_1 results in dramatic changes in the 2D-IR spectrum, which reflect the high sensitivity of nonlinear spectroscopy to anharmonicities. In the anharmonic case one observes a pattern of four positive and four negative peaks. The two additional negative peaks appear in the anharmonic spectrum, since negative bleach and positive excited state absorption signals are no longer at the same spectral positions.

In general, a Fermi resonance depends on the splitting $\Omega_1 - 2\Omega_2$ (which is zero for a perfect resonance), the Fermi coupling δ as well as the two anharmonicities Δ_1 and Δ_2, and thus the 2D-IR spectrum can be quiet different from the ones shown in Figs. 3.9 (b) or (c). Nevertheless one can still use the method outlined above to calculate the expected pump-probe and absorption spectra [see e.g. Chapter 7.3].

3.7 Summary

This introduction shows how pump-probe spectroscopy can help to resolve nonlinear couplings, as it directly reveals the underlying anharmonicities of the potential energy surface. In the harmonic approximation (i.e. the normal mode picture) one expands the potential energy surface up to second order of the nuclear coordinates. One can show very generally that a perfectly harmonic system yields a pump-probe spectrum that vanishes exactly, since the negative contributions, bleach and stimulated emission, and the positive one, excited state absorption, cancel completely. Hence, pump-probe spectroscopy is particularly sensitive to higher order terms in the potential energy surface expansion. The linear absorption spectrum is, of course, non-zero even in the harmonic approximation. The higher order, or anharmonic, terms give rise to different nonlinear phenomena, which are briefly summarized in the following. For simplicity only two normal modes, q_1 and q_2 are regarded.

In the case of two completely uncoupled modes the only anharmonicities are the intrinsic anharmonicities of the vibrational modes. They are of the order q_1^3 and q_1^4 (q_2^3 and q_2^4)

and higher, but do not contain any mixed terms, such as $q_1^x q_2^y$. Intrinsic anharmonicity gives rise to a non-zero pump-probe signal, but it does not couple individual modes. Mixed terms of the order $q_1 q_2$, where q_1 and q_2 are for example the amide I modes of individual peptide units translate upon quantization to a coupling term $(B_1^\dagger B_2 + B_2^\dagger B_1)$ and can lead to the formation of vibrational excitons. In general, a bilinear term $q_1 q_2$ vanishes as a result of the normal mode coordinate transformation. Hence the pump-probe spectrum of a system, that contains besides the harmonic terms only $q_1 q_2$ terms, is zero. However, if there are additional cubic and quartic terms, that is if the modes are intrinsically anharmonic, the pump-probe spectrum is nonzero. In this case, the bilinear and the higher order terms lead to so-called diagonal and off-diagonal anharmonicities in the nonlinear spectra (Equ. 3.25 and 3.26 and Fig. 3.3).

Couplings between a high frequency vibrational coordinate q_1 and a low frequency phonon coordinate q_2 are described by terms of the order $q_1^2 q_2$. These terms can give rise to a displacement of the potential energy surface in the excited state, which can result in a progression in the absorption spectrum and in oscillation in the time dependent pump-probe signal. In combination with a bilinear coupling such a term can lead to self-trapping of the high frequency mode, as it translates under quantization to a $(\hat{b}_q^\dagger + \hat{b}_q)\hat{B}_n^\dagger \hat{B}_n$ term in the polaron Hamiltonian Equ. 3.35. The details of the self-trapping mechanism depend further on the coupling strength, the nature of the phonons and the anharmonicity of the high frequency mode.

Terms of the order $q_1 q_2^2$, where q_1 is again the high frequency coordinate and q_2 is now a coupled lower frequency mode, can lead to a Fermi resonance when the additional resonance condition $\Omega_1 \approx 2\Omega_2$ is fulfilled. In this case the corresponding term in the Hamiltonian (Equ. 3.49) is $(\hat{B}_1 \hat{B}_2^{\dagger 2} + \hat{B}_1 \hat{B}_2^2)$ and the pump-probe spectra are non-zero for both, intrinsically anharmonic or harmonic modes (Fig. 3.9).

As shown explicitly in this thesis, the various anharmonic contributions can give rise to completely different pump-probe spectra, although the corresponding absorption spectra are almost identical. Thus nonlinear vibrational spectroscopy can distinguish between different anharmonicities in a way that is not possible with linear absorption spectroscopy.

4 Materials and methods

4.1 Experimental setup

Intensive and sufficiently short light pulses are required to perform vibrational pump-probe experiments. In the present work a commercial Ti:sapphire laser system was used to generate intense femtosecond laser pulses at 800 nm, which were converted subsequently by parametric amplification and difference frequency mixing to the mid-infrared pulses, that were used in the pump-probe experiment. Figure 4.1 shows an overview of the experimental set-up, which is described in detail in the following sections.

4.1.1 Laser system

A Ti:sapphire laser oscillator generates the femtosecond pulses, that are necessary to seed a subsequent regenerative amplifier. The oscillator is based on titanium-doped aluminum oxide (Ti:Al_2O_3, Ti:sapphire) as a gain medium, which, in our setup, is pumped by a frequency doubled, Nd:YVO_4, continuous wave laser. Ultrashort pulses are generated based on self-mode-locking (Kerr lens mode-locking) and dispersion compensation.[104–106] The oscillator produces 80 fs pulses centered at 800 nm with a repetition rate of 82 MHz and a pulse energy of ≈ 8 nJ. Intensive pulses, which are needed for the subsequent, parametric amplification are obtained in a regenerative amplifier, using chirped pulse amplification (CPA). Briefly, the idea is first to stretch the pulse duration, thus reducing the peak power, then to amplify the pulse in a Ti:sapphire laser cavity, pumped by

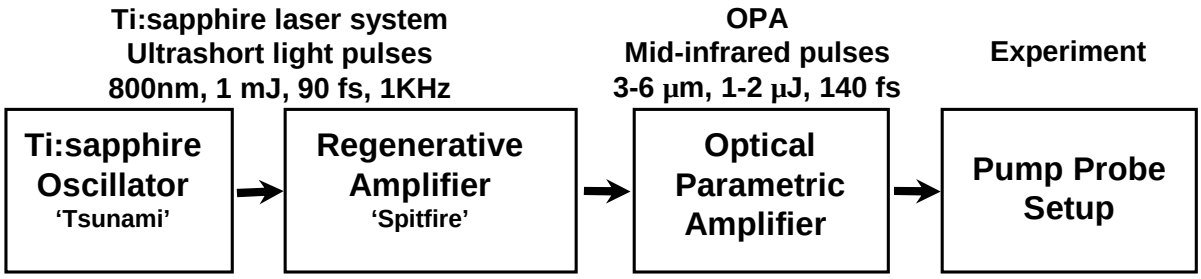

Figure 4.1: Overview of the experimental setup. A commercial Ti:sapphire system produces pulses at 800 nm, which are converted in an optical parametric amplifier (OPA) to mid-infrared pulses. The nonlinear response of the sample is measured in a pump-probe setup.

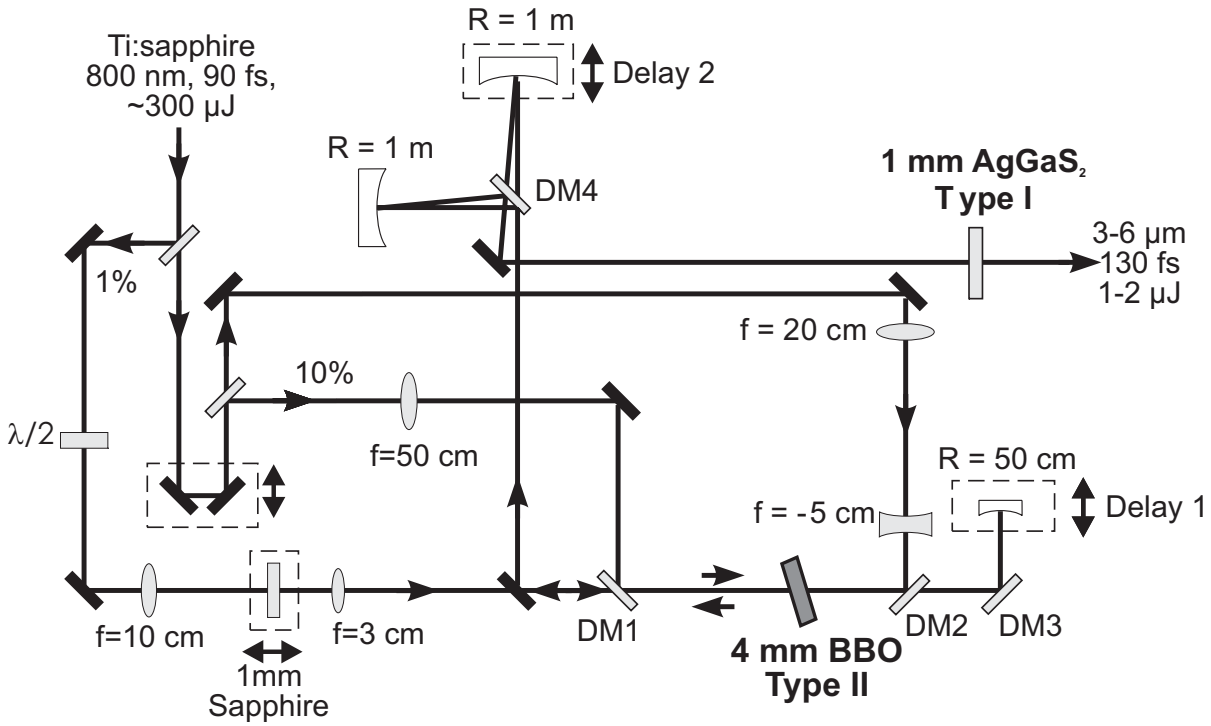

Figure 4.2: Optical parametric amplification in BBO and subsequent difference frequency mixing in $AgGaS_2$ (Fig. taken from Stenger[53]).

a frequency doubled, Nd:YLF laser, and finally to recompress the amplified pulse to nearly the original duration.[104,107] The setup used in this study is commercially available (Spectra-Physics Lasers) and consists of a *Tsunami* oscillator, pumped by a *Millennia* laser and a *Spitfire* amplifier in combination with an *Evolution* pump laser. The system produces 90 fs (FWHM) laser pulses at 800 nm with a pulse energy of 1 mJ at a repetition rate of 1 kHz. The pulse energy is reduced by beam splitters and neutral density filters to ≈300 μJ before the pulses are sent to the optical parametric amplifier.

4.1.2 Optical parametric amplifier

A two stage optical parametric amplifier (OPA), based on β-barium borate (BBO), is used in combination with difference frequency mixing to generate intense, stable and widely tunable mid-infrared pulses [Fig. 4.2].[53,108] In a 1 mm sapphire window a single filament white-light continuum is generated, which is focused as a seed for the parametric amplification into a type II BBO crystal (cut angle $\vartheta = 27°$, $\varphi = 30°$) in spatial overlap with a small portion (15 μJ) of the 800 nm pump pulse. The 800 nm light is focused very tightly and acts as a spatial filter for the seed light, which has a larger beam waist and a poorer mode quality. The generated idler pulse is removed by a dichroic mirror (DM3), while the signal pulse is used as a seed for a second amplification stage in the same BBO crystal. A 200 μJ fraction of the 800 nm light, adjusted by a 1:4 telescope to match the size of the seed pulse, serves as the pump light. The combined energy of the generated signal

and idler pulses is ≈ 40-70 μJ/pulse, which corresponds to a conversion of ≈ 25%. Signal and idler pulses are separated by another dichroic mirror (DM4) and the idler passes over a variable delay line to adjust the temporal delay between the two pulses. Both pulses are then focused into a type I $AgGaS_2$ crystal (cut angle $\vartheta = 32.6°,\ \varphi = 45°$), where the difference frequency, with respect to the frequencies of signal and idler, is generated. Mid-infrared pulses are obtained which are tunable between 3 and 6 μm (1400-3500 cm^{-1}). The typical pulse energy is 1-2 μJ and the pulse duration is about 130 fs. An outstanding feature of the setup is its unusual low intensity fluctuation of only 0.2% (rms), which is much smaller than the 1-2% shot to shot (rms) noise of the Ti:sapphire amplifier.[108]

4.1.3 Pump-probe setup

Figure 4.3 shows the pump-probe setup used to measure the third order nonlinear response. The pulses from the OPA pass first through a long pass filter, which transmits only mid-infrared light and blocks signal and idler. Two weak reflections of a BaF_2 wedge are used as a probe and a reference pulse, while the remaining pulse is sent over a variable delay line and serves as the pump pulse. All three pulses are focused by a 30° off axis parabolic mirror into the sample. Before passing the mirror the beam diameters of probe and reference pulses are enlarged by a telescope, in order to reduce their focus spot size in the sample (90 μm) with respect to that of the pump pulse (140 μm). Pump and probe beam overlap spatially in the sample, while the reference beam passes through a region, which is not excited by the pump pulse. After the interaction with the sample the light is collimated by a second parabolic mirror and the pump pulse is blocked. Probe and reference are spectrally dispersed in a grating spectrometer and focused onto a double array of MCT (Mercury Cadmium Telluride, HgCdTe) detectors (2×31). Two BaF_2 wedges are placed before the spectrometer to correct an inclination of the focal planes on the detector arrays. Typical spectral resolutions are 8 cm^{-1} for a wavelength of $\lambda = 3\mu$m and 4 cm^{-1} for $\lambda = 6\mu$m. In order to increase the overall sensitivity of the setup the long term drifts are eliminated by chopping the pump beam at half the repetition rate of the laser system. One then obtains the absorbance change signal by comparing the probe beam to the reference beam with pump beam (chopper open) and without pump beam (chopper closed). Hence the absorbance change ΔA is given by:

$$\Delta A = log\left[\left(\frac{I_{probe}}{I_{refrence}}\right)_{pump\ \ on} \times \left(\frac{I_{refrence}}{I_{probe}}\right)_{pump\ \ off}\right] \tag{4.1}$$

In this way intensity fluctuations of the laser pulse are correlated and an overall sensitivity of the order of 0.005 mOD can be achieved.

For two dimensional infrared (2D-IR) spectroscopy and frequency-selective experiments narrowband pump pulses are used to excite the sample. For this purpose the pump pulse is filtered by a Fabry-Perot etalon (Fabry-Perot interferometer), which consists of two parallel partial reflectors (R ≈ 80-90%) on a piezo-controlled mirror mount. The resulting pump pulse has an asymmetric temporal pulse shape with a fast rising edge limited

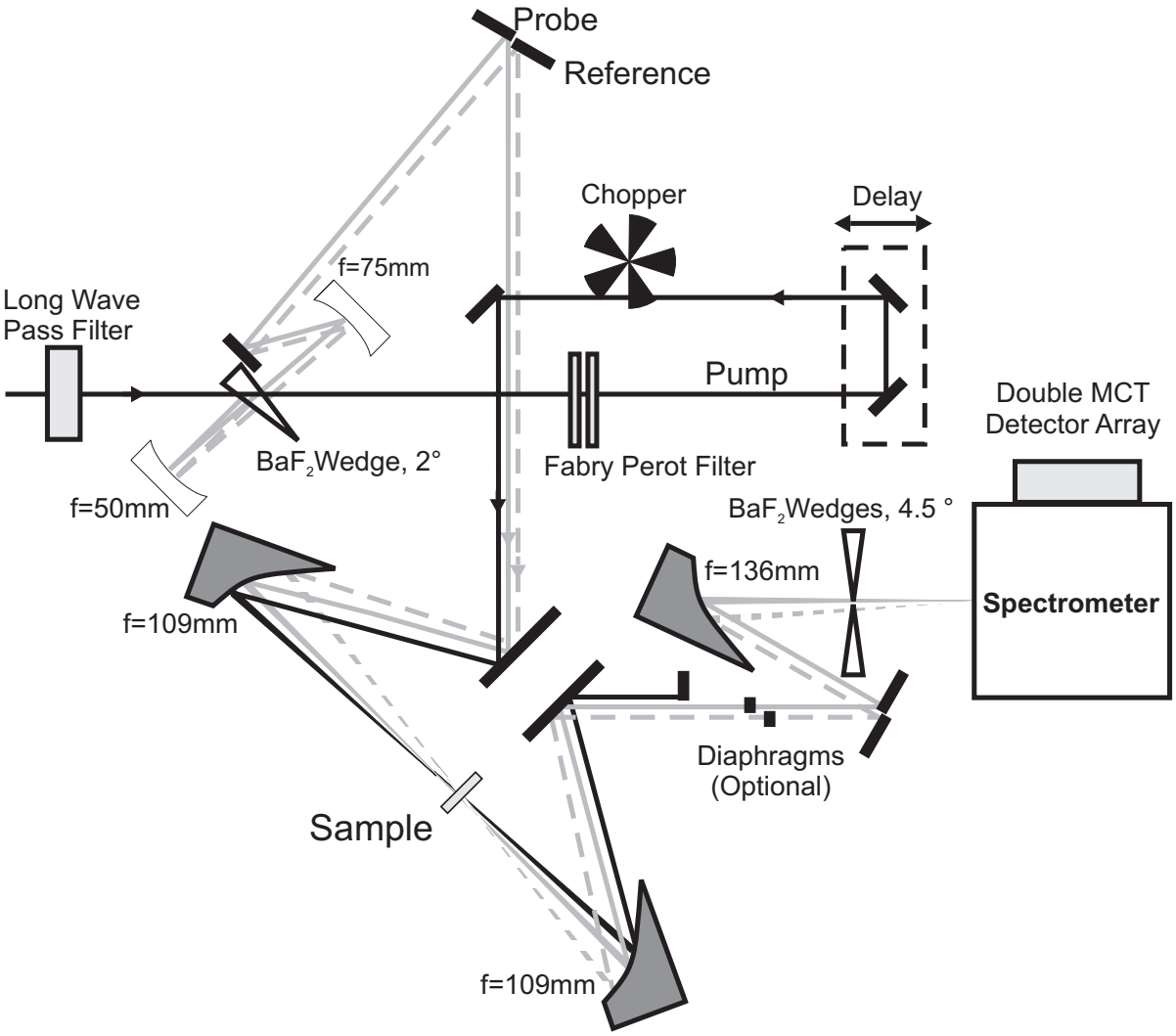

Figure 4.3: pump-probe setup used to measure the third order response function. The light pulse is split into a pump (black), a probe (grey) and a reference (dashed grey) pulse. Pump and probe pulses overlap in the sample, while the reference pulse passes through a region which is not excited. The absorbance change spectra is recorded by a double detector array at the end of the spectrometer (Fig. adapted from Stenger[53]).

by the pulse duration of the original pulse and a falling slope which decays exponentially with 250 fs for $\lambda = 3\ \mu m$ and 750 fs for $\lambda = 6\ \mu m$.[57,109] A spectral width of $\approx 30\ \mathrm{cm}^{-1}$ (3 μm) and $\approx 14\ \mathrm{cm}^{-1}$ (6 μm) is achieved. The center frequency of the pulse is tuned by adjusting the Fabry-Perot filter with the help of a computer controlled feedback loop. For this purpose the pump instead of the probe pulse is sent to the detector. In this way one obtains two frequencies that are used to construct a 2D-IR spectrum: the center frequency of the pump pulse and the frequency of the spectrally dispersed probe pulse.[57,59]

In some experiments the detected signal shows a pattern of interference fringes which are superimposed on the absorbance change spectrum. The oscillation frequency of the fringes increases with increasing pump-probe delay time. These fringes are caused by a

small fraction of the pump pulse, which is scattered in the direction of the probe pulse and hence into the spectrometer. The scattering is either due to sample impurities, crystal defects in the sample or scratches on the windows of the sample holder. The spectrometer performs a Fourier transformation of the pulses, which can then interfere in the frequency domain on the detector array. Since the pulses are spectrally dispersed by the grating they become temporally stretched and can interfere at delay times that are much longer than the original pulse duration. When the delay time is varied by half an optical cycle of the IR light the fringes shift by half an oscillation period. Hence the contribution from the interferences can be reduced by averaging over delay times varied over one optical cycle of the IR light. As a result, each measuring point is an average of up to 32 slightly shifted pump-probe delay times. For most samples this method yields absorbance change spectra without scattering artifacts. However, in some experiments additional diaphragms are placed in the path of the probe and reference pulse [see Fig.4.3] to further reduce the contributions from scattered pump light.

In case of crystalline samples (e.g. crystalline acetanilide, ACN) the scattering seems to originate mainly from crystal defects [see Fig. 4.5(b)] which occur along the direction of the crystal axis. For ACN very strong interferences, which cover the absorbance change spectra completely, are observed when the crystal b-axis (hydrogen bonded chain) is orientated perpendicular to the detector array. In this case a large fraction of the pump light is scattered directly onto the detector array. However, when the b-axis is orientated parallel to the detector array, the pump light is scattered away from the array and the interferences are significantly reduced, enabling the observation of pump-probe spectra. Since the orientation of the (crystalline) sample is then determined by the orientation of the detector array, one has to use a half wave plate, placed between OPA and pump-probe setup, to align the E-vector of the laser pulse with the vibrational dipole moments of the sample molecules. In case of ACN samples it was crucial for the observation of a pump-probe signal that all three pulses (pump, probe and reference) were passing through an essentially defect-free area of the crystal [see Fig. 4.5(b)]. Therefore the reference pulse was placed as close as possible to the pump pulse. In order to find a defect free position of the sample and to align the overlap between pump and probe pulses, the absorbance change signal was monitored at long delay times (>8 ps), where interferences between pump and probe pulses are not resolved.

4.2 Sample preparation

4.2.1 Crystalline acetanilide and N-methylacetamide

Acetanilide (ACN) was purchased from Aldrich, Germany (zone refined, purity: 99.95 %) and deuterated ACN (ACN-D_8) from Cambridge Isotope Laboratories, USA (purity: 98 %). Monocrystalline ACN was prepared by cooling a thin layer of the molten substance between two CaF_2 windows.[110] To this end, a few milligrams of ACN were placed on a

CaF_2 window, which was mounted in a brass sample holder. The sample holder was either placed on a hot plate or connected to four resistors (R=33 Ω), which were used to heat the sample. By controlling the heat current one could adjust accurately the temperature of the sample holder. After melting the ACN (mp=115 °C) a second (hot!) window was carefully placed on top of the liquid ACN film and a hot cover plate was mounted on the sample holder [see Fig. 4.4]. Afterwards the temperature was lowered by about 10 °C/h until crystals formed from the supercooled liquid (at 60-70 °C). Some control of the crystal thickness was obtained by tightening the cover plate during the cooling process to apply some pressure. The quality of the crystals was examined under a microscope. Most of the crystals contained numerous shrinkage cracks and air/gas inclusions, which formed during the crystallization process [see Fig. 4.5(a)]. In these cases the sample was rejected and the process was repeated. Only crystals with a large uniform monocrystalline area, as the one shown in Fig. 4.5(b), were selected for the experiments. In general, thinner crystals contained fewer defects and most of the shrinkage cracks occurred along the crystalline b-axis, which runs parallel to the hydrogen bonds [see Fig. 5.1]. The crystalline orientation of the sample was determined by measuring the polarized IR spectrum.[110] The normal orientation of crystalline ACN is tabular with the *bc* face of the unit cell parallel to the surface of the CaF_2 substrate [a *100* orientation, see Fig. 1.4]. However some samples contained areas with a *001* orientation (the *ab* face parallel to the substrate surface). Such samples were not used in the experiments.

In case of ACN-D_8 the cooling method did not result in any monocrystalline samples, which was most likely a consequence of the lower purity of the substance. Hence monocrystalline ACN-D_8 was grown out of a concentrated solution of Ethanol/Chloroform (20/80). To this end a droplet of the solution was placed on a CaF_2 window. After a few hours the solvent was completely evaporated and crystalline areas were formed. This alternative crystallization method resulted in lower quality samples, which showed strong scattering of the laser pulses in the pump-probe experiment.

N-methylacetamide (NMA) was obtained from Aldrich, Switzerland (purity: 99+%) and NMA-D_6 from C/D/N Isotopes, Canada (purity: 98.3 %). Monocrystalline samples

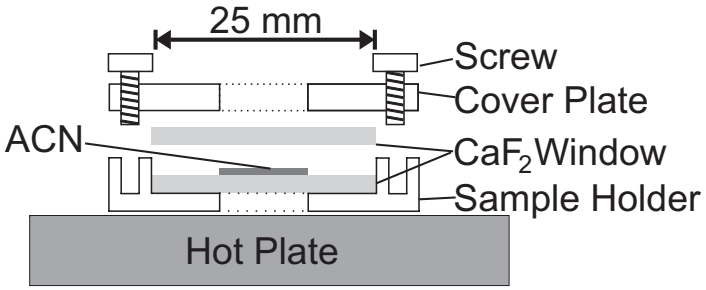

Figure 4.4: Sample Holder used for experiments and sample preparation. The sample holder is placed on a hot plate (or alternatively connected to four resistors) to melt the ACN, which is spread onto a CaF_2 window. After melting, a second CaF_2 window is mounted on top of the ACN film. Then a cover plate is tightened onto the sample holder.

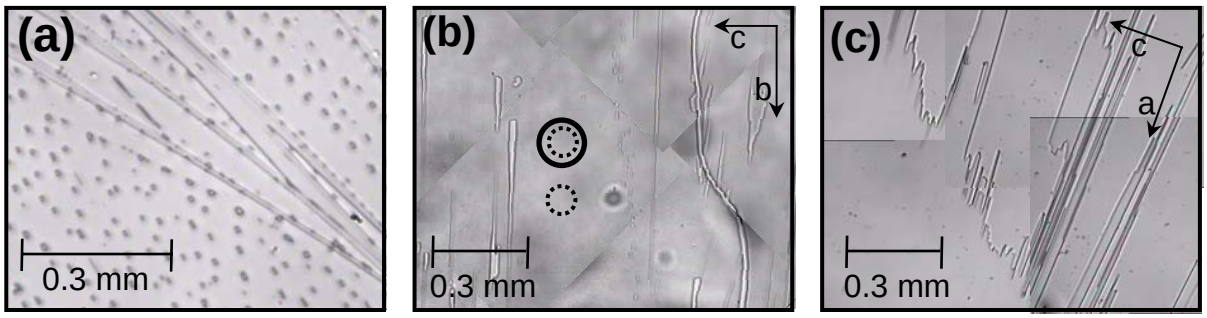

Figure 4.5: (a) Crystalline ACN sample with air inclusions and shrinkage cracks (b) Monocrystalline ACN. The circles depict the pump pulse (full line) and probe and reference pulses (dotted lines). Shrinkage cracks occur along the direction of the b-axis. (c) Monocrystalline NMA-D_6

were prepared by the cooling method described in the previous paragraph. Beforehand NMA or NMA-D_6 (5-10 μl) was heated on a CaF_2 window to $\approx$ 100 °C for about 15 minutes in order to remove any possible water contaminations of the highly hygroscopic substance. To prevent a water contamination of the supply container the whole process was performed in a nitrogen flushed glove box. In case of NMA and NMA-D_6 the cooling method resulted almost always in samples with monocrystalline *010* orientations [see Fig. 4.5(c)]. IR absorption spectroscopy was used to verify that the samples did not contain any water traces. All NMA spectra were measured at temperatures below the solid phase transition, which is found either at 0 °C[111] or 10 °C.[77]

For both, FTIR and pump-probe experiments, a small sample area, which showed only one crystalline orientation, was selected. The other areas of the sample were covered by a piece of paper, which was carefully glued onto the CaF_2 window. The FTIR spectra were obtained with the E vector parallel and perpendicular to the hydrogen bond chain (the b and c axis in ACN and the a and c axis in NMA, see Fig. 5.1 and Fig. 6.1). The comparison between polarized absorption spectra [see e.g. Fig. 6.2] and the literature data[2,110,112] confirmed that our samples were in a monocrystalline phase. In case of ACN and NMA-D_6 the crystals in the sample were perfectly aligned in one direction, while the ACN-D_8 and NMA samples showed some disorder. The thickness of the crystals was estimated to 5-10 μm from the absorption spectra.[110] All pump-probe spectra were obtained with the E vector parallel to the hydrogen bond chain. For temperature dependent FTIR experiments the samples were placed in a helium closed cycle cryostat (Air Products, Displex 202A) and measurements were performed between 18 K and 293 K ($\pm$2 K). The temperature dependent pump-probe measurements on ACN were performed in a liquid nitrogen cooled open cycle cryostat (Janis Research Company, ST-100) at temperatures between 77 K and 293 K ($\pm$2 K).

4.2.2 Poly-γ-benzyl-L-glutamate

The polymer poly-γ-benzyl-L-glutamate (PBLG) forms extremely stable and long α-helices in both, helicogenic solvents and films grown from these solvents.[113] The monomeric unit of PBLG, shown in Fig. 4.6(a), is a non-natural amino acid with a long side chain that stabilizes the helix. A sample of PBLG with a chain length of ≈90 monomers (molecular weight of 17400-22000 g/mol) was purchased from Aldrich, Switzerland. Fully C-deuterated PBLG (PBLG-D_{11}) was prepared in our laboratory by the method of Blout and Karlson.[114] First, deuterated γ-benzyl-L-glutamate was prepared from L-glutamic-D_5 acid and benzyl-D_7 alcohol, which were both obtained from C/D/N Isotopes, Canada (yield: 28%).[115] In the next step N-carboxy-γ-benzyl-L-glutamate anhydride was synthesized from triphosgene and deuterated γ-benzyl-L-glutamate in a tetrahydrofurane suspension under nitrogen at 50 °C (yield 81%).[116] For the recrystallization of the anhydride the reaction mixture was partly evaporated, poured into hexane and stored in a refrigerator (T = 5 °C). After the beginning of the crystallization process the reaction mixture was stored up to two days in a freezer (T = −30 °C) to allow completion of the crystallization process. Then the sample was filtered, washed with hexane and dried in a vacuum desiccator. The polymerization of the anhydride was started in very clean dioxane (Fluka, puriss. abs.) at a temperature of 15 °C with sodium methoxide as initiator and an anhydrid:initiator ratio of 50:1. After 12 hours the temperature was increased to 20 °C and then after 24 hours to 25 °C. To isolate the polypeptide the polymer-dioxane mixture was poured under stirring into methanol (with 1 mM HCl). The precipitate was filtered, washed (methanol, ether) and dried in vacuum at 50 °C (yield: 90%). A molecular weight of 6500-15300 g/mol was estimated from viscosity experiments, corresponding to a chain length ≈50 monomers. For the viscosity measurement non deuterated PBLG, synthesized by exactly the same process, was used.

Since the first investigations on PBLG it has been reported that the molecule exists in different molecular configurations, depending on the molecular weight and the solvent.[117] High molecular weight samples in weakly interacting solvents adopt an α-helical configuration, while very low molecular weight samples exist also in a so-called β-configuration or in a solvated form (σ-form).[117–120] The different configurations can be identified by the frequency of the amide I mode in the IR spectrum [α: 1655 cm^{-1}, β: 1630 cm^{-1}, σ: ≈1670 cm^{-1}, see Fig. 4.6(b)].[118] Since only the low molecular weight samples are soluble in formic acid one can easily separate the different species.[118] All PBLG samples that were produced in our laboratory were treated with formic acid to remove low molecular weight species. The α helical configuration of the samples was verified by IR and by nuclear magnetic resonance (NMR) spectroscopy. In the NMR measurements the chemical shifts of the NH and the α-CH protons were measured and compared to the literature.[121]

PBLG is normally a styrofoam- or powder-like white substance, which can be transformed easily into a thin, transparent gel-like film, suitable for FTIR and pump-probe spectroscopy.[122,123] PBLG films were grown from concentrated chloroform solutions by

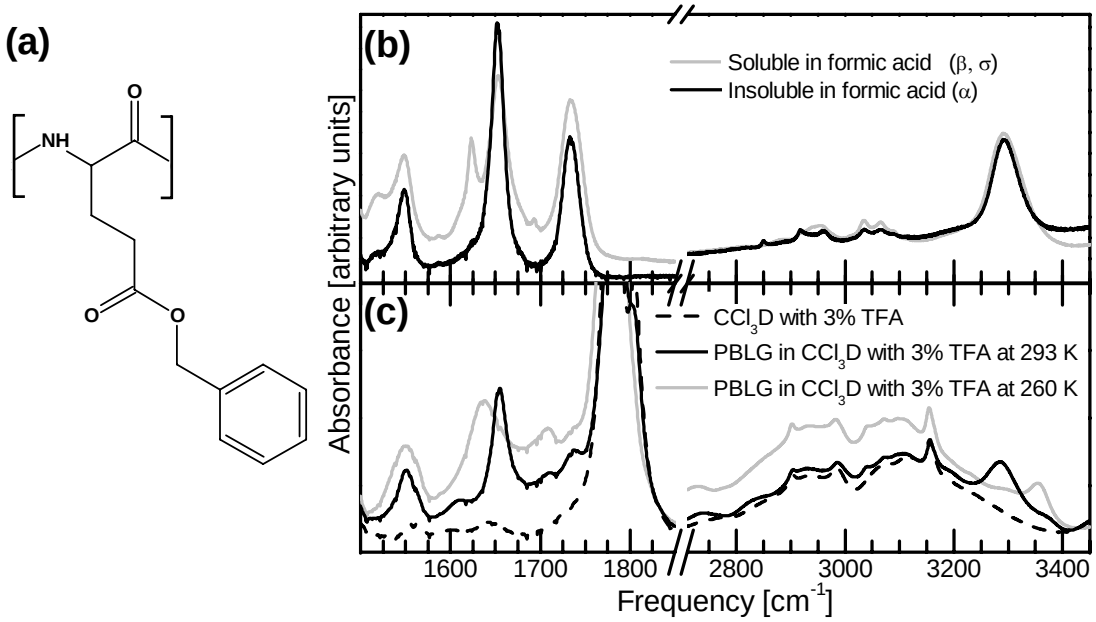

Figure 4.6: (a) Monomer unit of Poly-γ-benzyl-L-glutamate (PBLG). (b) IR spectra of PBLG films grown from the fraction that is soluble in formic acid (low molecular weight) and the one that is insoluble (high molecular weight). The different fractions can be clearly distinguished by the frequency of the amide I mode (1630-1670 cm^{-1}). (c) IR spectra of deuterated Chloroform (CCl_3D) with 3% TFA (dashed line) and PBLG dissolved therein. At this TFA concentration PBLG forms at room temperature a helix (black line) and unfolds below 268 K into a random coil (grey line). The amide I (1654 cm^{-1} at 293 K), amide II (1550 cm^{-1}) and NH (3290 cm^{-1} at 293 K) stretching bands are not yet completely covered by the solvent bands.

evaporation of the solvent. For this purpose a droplet of the solution (10-50 μl) was placed on a clean CaF_2 window. The droplet was spread over the window with a razor blade. After a few minutes the solvent evaporated and a clear thin film was formed. Control of the sample thickness was obtained by varying the droplet size. Oriented PBLG samples were prepared by allowing the solution to concentrate to a gel and then spreading it out by a single stroke of a razor blade.[122] This method only resulted in a partial orientation of very thin films with an absorbance $\leq$7 mOD for the NH stretching mode. Due to the low absorbance and very strong scattering the oriented films were not suitable for pump-probe experiments.

A wide variety of liquids, such as benzene, dioxane, chloroform, ethylene dichloride, dimethylformamide, m-cresol and pyridine serve as helicogenic solvents for PBLG.[113] For the present work deuterated chloroform was chosen as a solvent, since it does not contain absorption bands in the spectral regions of the amide I and the NH mode. Measurements were performed in 50 and 100 mM solutions between two CaF_2 windows, separated by a 100 μm teflon spacer.

When PBLG is dissolved in strong acids, such as trifluoroacetic acid (TFA) or dichloroacetic acid (DCA) it forms a random coil structure.[113] In mixtures of acids and

helicogenic solvents PBLG forms, depending on the mixing ratio, either a random coil or an α-helix with a sharp phase transition between the two configurations.[121,124] The phase transition can also be induced by a temperature change,[124–126] since the helix, which is stable at high temperatures, unfolds at low temperatures to a random coil and vice versa (cold denaturation, see Chapter 7.1 for more details). The transition temperature depends on the mixing ratio between the acid and the helicogenic solvent. Measurements on the two different PBLG conformations were performed in a chloroform solution with 3% TFA. At this concentration, PBLG changes from an α-helix to a random coil at $\approx$ 268 K. At higher TFA concentrations the PBLG absorption bands in the IR spectrum are covered by the more intense TFA bands [Fig. 4.6(c)]. At lower concentrations (1% TFA) PBLG stays in the helical conformation for temperatures as low as to 253 K.[a] The phase transition can be monitored by IR spectroscopy. Upon unfolding, the frequency of the amide I mode decreases from 1654 cm^{-1} to 1630 cm^{-1}, while the frequency of the NH stretching mode increases from 3290 cm^{-1} to 3355 cm^{-1} [see Fig. 4.6(c)]. The temperature of the sample was controlled by a thermoelectric cooling system, consisting of four peltier elements, each with a cooling power of 27 W, which were cooled down to $\approx$ 263 K by a mini chiller (Kühne Kältemaschinenbau GmbH; coolant: 50% glycol, 50% water). Measurements were performed between 253 K and 293 K ($\pm$ 2 K). Since chloroform is very volatile it partly evaporated during the assembly of our standard sample holder [Fig. 4.4], making it impossible to control exactly the concentration of TFA. Therefore a flow cell with a 50 μm spacer was used for the temperature dependent measurements.[127] Use of the flow cell allowed an exact control of the TFA concentration and furthermore assured that different samples had exactly the same thickness, thus allowing a background substraction.

[a] 253K was the lower limit of the employed cooling system.

5 Self-trapped states in acetanilide*

Since the early 1970s crystalline acetanilide (CH_3-CONH-C_6H_5, ACN) has been regarded as a model system to study the nature of vibrational excitations in secondary structures of polypeptides and proteins. ACN forms molecular crystals, which consist of quasi one-dimensional chains of hydrogen bonded peptide groups (-CO-NH-) with structural properties similar to α-helices, one of the most common secondary structure motif in proteins [see Fig. 5.1]. It has been speculated that self-localization of vibrational excitations (i.e. the C=O and NH stretching modes) in α-helices plays an important role in the energy transport in proteins.[1] This self-trapping phenomena is, as outlined in Chapter 3, based on coupling mechanisms that exist in one-dimensional hydrogen bonded chains. Thus ACN is commonly used as a model system to study vibrational self-trapping in α-helices. It is well established that the IR and Raman spectra of the amide I (i.e. the C=O stretching) and the NH stretching band of crystalline ACN exhibit so-called "anomalies" [see Fig. 5.2]:[2,3,110] The amide I mode, which is observed at 1666 cm^{-1} at room temperature, splits into two bands at low temperatures with an additional "anomalous" band at 1650 cm^{-1}. The NH stretching mode is weakly temperature dependent and exhibits a main peak at 3295 cm^{-1} accompanied by an almost-regular sequence of satellite peaks towards lower frequencies. It has been suggested that both anomalies can be explained by self-trapping of vibrational excitations.[2,3,87,89,128–130]

In the present chapter self-trapping theory in ACN is tested in detail utilizing various forms of nonlinear time resolved spectroscopy, including frequency selective and impulsive pump-probe spectroscopy and two-dimensional infrared (2D-IR) spectroscopy. In Section 5.1 the nonlinear response of the amide I mode is discussed, which unambiguously proves that the anomalous double peak corresponds to a delocalized free exciton state and a self-trapped state. Section 5.2 treats the signal of the NH mode, revealing the spectral signatures of ultrafast self-trapping and nonlinear exciton-phonon coupling.

*The work presented in this chapter has been published in:

J. Edler, P. Hamm, and A. C. Scott. *Femtosecond study of self-trapped excitons in crystalline acetanilide.* Phys. Rev. Lett. **88**(6), 067403, (2002).

J. Edler and P. Hamm. *Self-trapping of the amide I band in a peptide model crystal.* J. Chem. Phys. **117**(5), 2415, (2002).

J. Edler and P. Hamm. *Two-dimensional vibrational spectroscopy of the amide I band of crystalline acetanilide: Fermi resonance, conformational substates or vibrational self-trapping ?* J. Chem. Phys. **119**(5), 2709, (2003).

J. Edler and P. Hamm, *Spectral response of crystalline acetanilide and N-methylacetamide: Vibrational self-trapping in hydrogen-bonded crystals*, Phys. Rev. B, **69**(21), 214301, (2004).

5.1 The amide I band

5.1.1 The anomalous peak in the amide I band

Figure 5.2(a) shows the amide I mode of ACN, i.e. the peak at 1666 cm^{-1} and the anomalous temperature dependent peak at 1650 cm^{-1}. The origin of the splitting has been the topic of many theoretical and experimental studies, including IR absorption, X-ray scattering, Raman scattering and neutron scattering.[2,3,46,50,87,89,102,103,128,130,132–141] Careri, Scott and coworkers attributed the anomalous band to vibrational self-trapping[2,3,89] after carefully examining more conventional explanations. Measurements on polycrystalline, amorphous and dissolved ACN samples demonstrated that the hydrogen bond network of the crystal is essential for the appearance of the anomalous band.[128] Investigations of the temperature dependence of the specific heat, the dielectric constant and the volume expansion excluded the occurrence of rotational isomerism or polymorphic transitions,[128] while Davydov splitting was ruled out due to the polarization behavior of the two bands.[2]

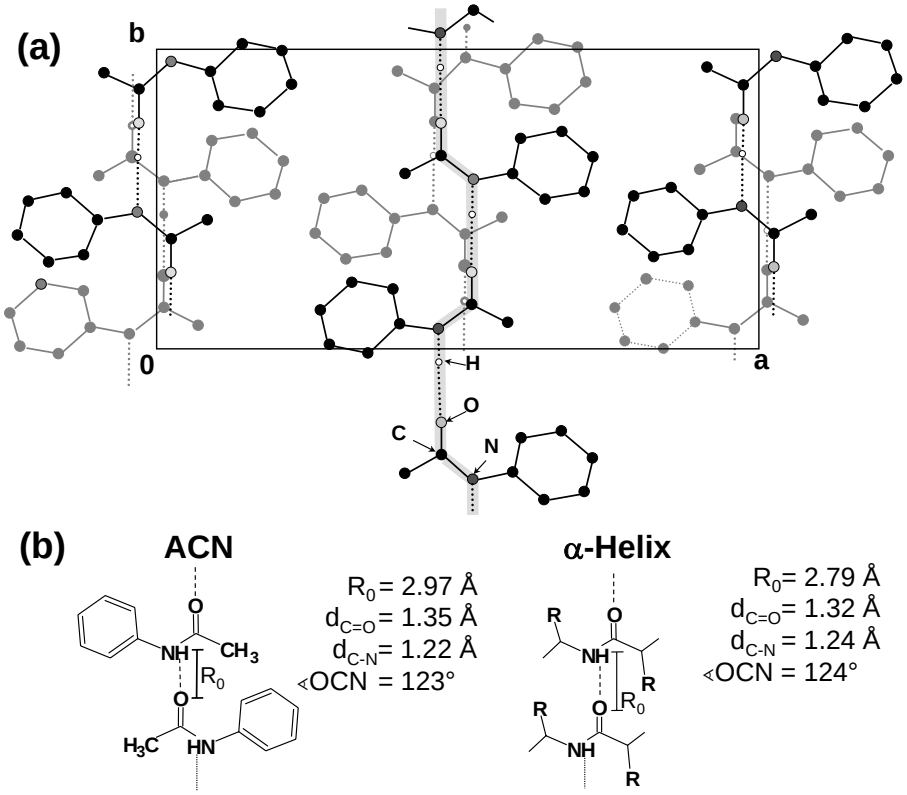

Figure 5.1: (a) Crystalline structure of acetanilide (ACN). Projection of the unit cell, which contains eight molecules in the *ab* plane. Black bonds, molecules in the plane $c/4$; grey bonds, molecules in the plane $3c/4$. The dotted lines correspond to the hydrogen bonded chain. Adapted from Sauvajol *et al.*.[131] See also Fig. 1.4 for a three dimensional illustration of the hydrogen bonded chain in the crystalline *bc* plane. (b) Comparison between the peptide units of crystalline ACN and an α-helix. Both systems contain hydrogen bonded chains with comparable structural properties.[2]

A Fermi resonance or the existence of different configurational sub-states has tentatively been discarded, based on the temperature dependent intensity ratio and energy splitting of the two bands.[2]

Vibrational self-trapping is described by the polaron-Hamiltonian Equ. 3.35, which combines two coupling mechanisms: excitonic coupling and exciton-phonon coupling. The self-trapping theory is described in detail in Chapter 3.5. In short, excitonic coupling is caused by electrostatic interactions between individual molecular oscillators, and leads to the delocalization of a vibrational excitation. This state, called vibrational exciton or vibron, is coupled to lattice phonons through a nonlinear term, which is mediated by the hydrogen bonds. As a consequence, the initially delocalized exciton collapses to form a self-trapped state. In principle the exciton can couple to an acoustic or an optical phonon. For an acoustic phonon the Franck-Condon factor, which describes the probability of a transition from the ground to the excited state, is expected to be small. Since a small

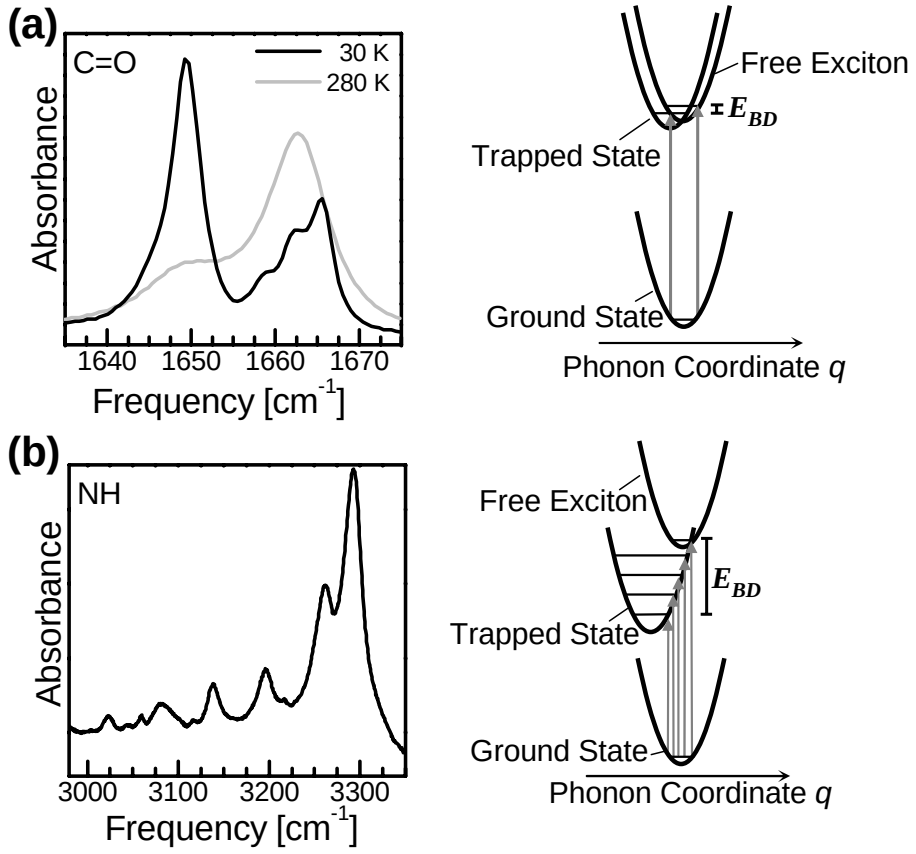

Figure 5.2: (a) Absorption spectrum of the amide I band of crystalline ACN, showing a temperature dependent doublet. According to self-trapping theory the peak at 1650 cm^{-1}, which is only observed at low temperatures, corresponds to a self-trapped state and the one at 1666 cm^{-1} to a free exciton. (b) Absorption spectrum of the NH band, consisting of a main peak at 3295 cm^{-1} (free exciton) and a sequence of satellite peaks (self-trapped states). The corresponding schemes of potential energy surfaces are depicted on the right. E_{BD} represents the binding energy of the self-trapped state.

Franck-Condon factor precludes the strong absorption that is evident from Fig. 5.2, a coupling to an optical phonon is assumed[2,3] and Hamiltonian Equ. 3.44 applies. In an adiabatic approximation the potential energy surface for each vibrational excitation level is expressed as a function of phonon coordinates, as shown in Fig 5.2. The exciton-phonon coupling gives rise to a displacement of the potential energy surfaces of the self-trapped states.

In case of the amide I mode in ACN the displacement between ground and excited state is small and at zero temperature only the zero-phonon transition (i.e. the 1650 cm^{-1} band) carries noticeable oscillator strength and all other transitions are weak. With increasing temperatures, phonons in the C=O ground state are thermally excited, and the intensity of the zero-phonon line diminishes. The temperature dependence of the anomalous band follows a $e^{-\gamma T^2}$ law at low temperatures, which can be deduced in a straightforward manner from the Hamiltonian Equ. 3.44.[2,3,87,89] The $e^{-\gamma T^2}$ temperature dependence is precisely that of a zero-phonon band of color centers[142] and is considered to be the strongest support for self-trapping theory. A further intriguing feature of self-trapping theory is that all parameters can be estimated from independent experiments.[87] This is why presently self-trapping theory is considered to be the most convincing explanation of the observed anomalous amide-I band. Thus the band at 1650 cm^{-1} has been assigned to a self-trapped state while the band at 1666 cm^{-1} corresponds to a "free" exciton, which is not affected by the interaction with the phonon system.

Nevertheless, self-trapping theory is not completely unproblematic and a controversy about the anomalous spectroscopy of ACN is still going on, which has been reviewed thoroughly in Ref. 3. Most challenging is the failure of self-trapping theory to explain the results of isotope exchange experiments. Deuteration of the amide proton of ACN[102] as well as of the methyl protons results in the disappearance of the temperature dependent amide-I band, while deuteration of the phenyl group has no effect.[103,133] Deuteration may lead to minor frequency shifts of the C=O band and the phonon modes, but the electronic coupling terms in the Hamiltonian Equ. 3.44 (the excitonic coupling β and the exciton-phonon coupling χ) and consequently, self-trapping should not be significantly affected.

The strong dependence of the appearance of the anomalous band on isotope exchange suggests a Fermi resonance mechanism, since in that case, small frequency shifts might remove an accidental resonance. Along this line, Johnston and Swanson[102] have attributed the amide I doublet to temperature tuning of a Fermi resonance between the NH-deformation band at 1553 cm^{-1} (i.e. the amide II band) and a low frequency mode at about 100 cm^{-1}. The latter shows an extraordinary strong frequency shift with temperature, which was suggested to shift the combination band into resonance with the amide I fundamental upon cooling, causing the intensity of the anomalous amide I band to increase. They showed that deuteration of the amide proton of ACN results in a strong shift of the amide-II band, destroying the Fermi resonance and hence the amide I split-

ting. Furthermore, ^{13}C substitution results in a different temperature dependence of the doublet, explained by an altered resonance condition.

Based on similar Raman and infrared studies, Barthes and coworkers have questioned the Fermi resonance model significantly.[103,134] Their experimental data showed that three modes of the amide I group (760 cm^{-1}, 1650 cm^{-1} and 3255 cm^{-1}) exhibit an anomalous temperature dependence. It seems very unlikely that an accidental degeneracy occurs for three amide modes in precisely the same way. Furthermore, methyl deuterated ACN does not exhibit any anomalous amide I band, although the two modes, which have been made responsible for the suspected Fermi resonance in Ref. 102, appear at similar frequencies as in the protonated molecule. In conclusion, these observations show that the Fermi resonance model is quite unlikely, but they are indirect and do not exclude it completely. However, one should keep in mind that self-trapping theory cannot explain the isotope effects either.

As third hypotheses it has been suggested that a conformational transition is the origin of the two bands. Picosecond-infrared pump-probe experiments on ACN, preformed by Fann *et al.*,[132,141] indicate that the transmission at the anomalous 1650 cm^{-1} band exhibits no long lived transients that might characterize self-trapped states. Therefore it has been proposed that the unusual temperature dependence can be accounted for by two slightly nondegenerate configurations of the amide-I proton. Furthermore, Blanchet and Fincher[138] have reported similar temperature dependencies of the intensities of a whole series of transitions, in particular in the low-frequency range below 100 cm^{-1}, which have been attributed to a structural transition (i.e. a "topological soliton"). However, inelastic neutron scattering experiments showed only one conformation of the proton,[135–137] questioning significantly the two-state theory. Moreover, Barthes and coworkers have recently questioned even the observation of a temperature dependent intensity of most of the bands discussed by Blanchet and Fincher[138] by carefully studying the integrated intensities of these states.[139]

In the following Chapter 5.1.2 various forms of pump-probe spectroscopy are used to show that both amide-I sub-states of ACN exhibit a distinctively different response on selective excitation:[55] A detailed analysis suggests that the anomalous band at 1650 cm^{-1} is localized, while the "normal" band at 1666 cm^{-1} is delocalized (i.e. a free exciton) at low temperatures. In Chapter 5.1.3 the alternative origins for the anomalous amide-I band are ruled out by using 2D-IR spectroscopy to distinguish between various kinds of nonlinearities.[56] To that end, the 2D-IR spectrum of ACN is compared with the 2D-IR spectra of molecular systems which are chosen as simple representatives of the two proposed alternative explanations: (i) a Fermi resonance and (ii) different configurational substates. We shall see that although the linear absorption spectra of all these systems are comparable, the nonlinear 2D-IR responses deviate significantly, albeit in a well understood way.

5.1.2 Evidence for self-trapping of the amide I band

Experimental results

In a first set of experiments short, broadband pump pulses [spectral width: 120 cm^{-1}, pulse duration: 130 fs (FWHM)] are used to impulsively excite the whole spectrum shown in Fig. 5.3(a). The excited spectrum contains both amide I bands as well as a broad, weak band at 1600 cm^{-1}, which is assigned to a ring deformation mode of the phenyl ring.[2] The present chapter focuses on the amide I bands, however the 1600 cm^{-1} band is used as a reference mode to observe relaxation of the amide I bands. The pump-probe response for the probe frequency resonant with the 1600 cm^{-1} band is shown for different temperatures in the inset of Fig. 5.4(b). These transients are highly reproducible and show pronounced oscillations which persist up to about 3 ps. A spectral analysis of the beating structure is obtained from the Fourier transformation:

$$\Delta A(\omega, \omega_{pr}) = \int_0^\infty dt_{pu,pr} e^{iwt_{pu,pr}} \Delta A(t_{pu,pr}, \omega_{pr}) \tag{5.1}$$

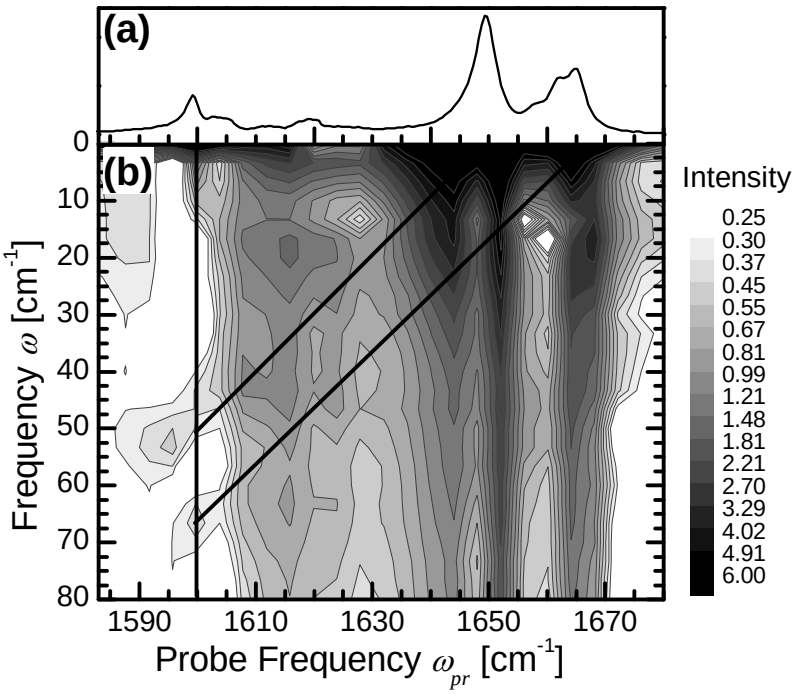

Figure 5.3: (a) Part of the absorption spectra of crystalline ACN, showing the 1600 cm^{-1} phenyl ring mode and the anomalous (1650 cm^{-1}) and normal amide-I band (1666 cm^{-1}) at 93 K. (b) Absolute value of the 2D-IR Fourier transform spectrum at 93 K. ω_{pr} is the frequency of the probe pulse and ω results from the Fourier transformation of the pump-probe data with respect to delay time $t_{pu,pr}$ between pump and probe pulse. Cross peaks appear in the spectrum where vertical lines, marking the peak position in the linear spectrum cross diagonal lines, originating from coupled bands. There are two prominent cross peaks related to the ring mode and both amide I modes (black lines).

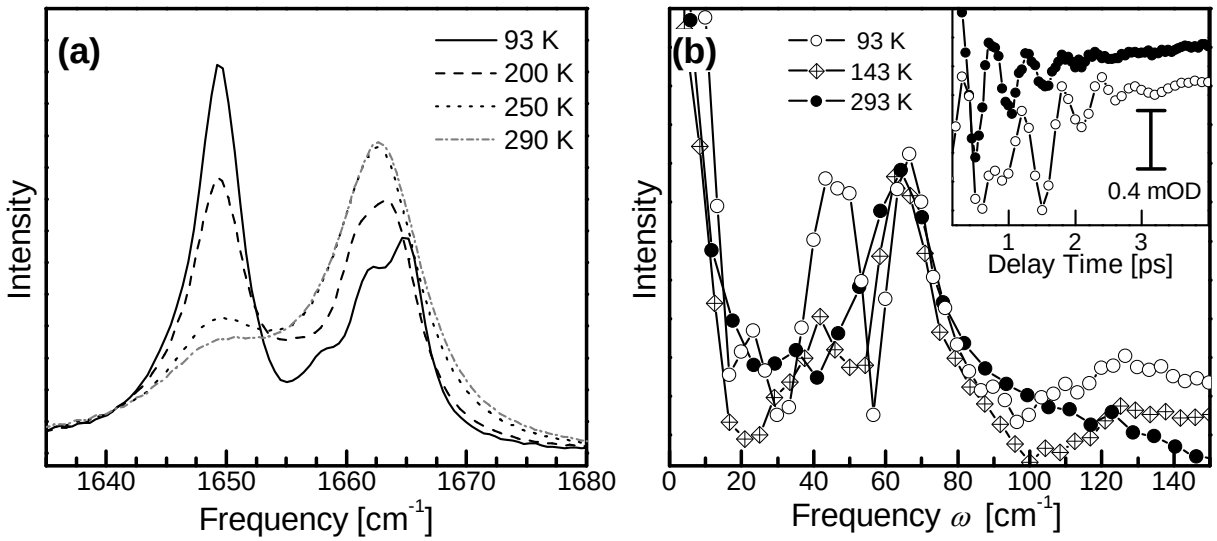

Figure 5.4: (a) Linear absorption spectra of the amide I mode of ACN for different temperatures. The intensity of the anomalous peak (1650 cm^{-1}), representing the self-trapped state, increases with decreasing temperatures. (b) Fourier transform spectra of the coherent response of the 1600 cm^{-1} mode for different temperatures. The inset shows the absorbance change signal at probe frequency corresponding to the 1600 cm^{-1} mode. At 93 K two frequencies contribute to the oscillations, at 293 K only one.

where $\Delta A(t_{pu,pr}, \omega_{pr})$ is the pump-probe signal (i.e. the transient response in the inset of Fig. 5.4) for delay times $t_{pu,pr}$ between pump and probe pulse at probe frequency ω_{pr}. The absolute value spectrum $|\Delta A(\omega, \omega_{pr})|$ is shown in Fig. 5.3(b) as a two-dimensional (2D) plot. In this representation, the x-axis corresponds to the probe frequency ω_{pr} and the y-axis to the frequency ω, which is revealed by Fourier transformation. Cross peaks are expected at positions where the vertical lines, that indicate the location of the absorption peaks in the linear spectrum cross diagonal lines, originating from coupled bands.[143] Two clear cross peaks are visible in Fig. 5.3(b), which correspond to the reference mode at 1600 cm^{-1} and the two amide I bands, respectively.

The data is analyzed in detail by inspecting different cuts through the 2D plot. Fig. 5.4(b) shows a cut along the ω-axis for a constant probe frequency ω_{pr} matching the reference mode at 1600 cm^{-1}. This Fourier transform spectrum shows a remarkable change with decreasing temperature: At 293 K, one observes only one distinct frequency component at 63 cm^{-1}. At low temperatures this component shifts slightly to 66 cm^{-1} and clearly decreases in spectral width, while an additional strong component appears at about 50 cm^{-1}. Interestingly, this temperature dependence parallels that observed for the absorption spectrum of the amide I band [see Fig. 5.4(a)]. Furthermore the frequencies of the oscillatory response match perfectly with the splitting between the reference mode at 1600 cm^{-1} and both amid I modes. Combining both observations, we conclude that the Fourier transform spectrum in Fig. 5.4(b) directly resembles the absorption spectrum of the amide I band. The important point is that one can deduce a lower limit for the

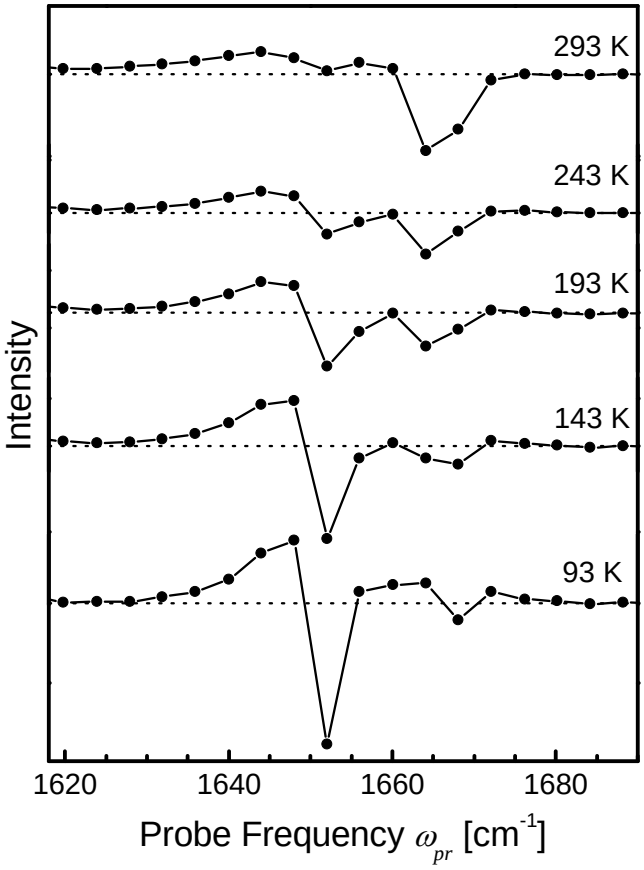

Figure 5.5: Cuts through the real part of the 2D spectrum shown in Fig. 5.3 along the probe frequency ω_{pr} axis for $\omega = 0$ for different temperatures. A bleach of the self-trapped state (1650 cm^{-1}) is only observed at low temperatures, while a bleach of the free exciton (1666 cm^{-1}) is only observed at high temperatures.

lifetime of the amide I states from the decay of the quantum beats. As we will see in the following section, one has to use this indirect approach because the direct nonlinear response of the 1666 cm^{-1} band vanishes.

Another aspect of the data is revealed by a cut along the ω_{pr}-axis for $\omega = 0$. which is plotted in Fig. 5.5 for the real part of $\Delta A(\omega, \omega_{pr})$ at various temperatures. These Fourier transform spectra single out the incoherent response of the sample and yield positive and negative peaks related to bleach, stimulated emission and excited state absorption signals of the individual absorption bands.[55] At a temperature of T=93 K, one observes a strong response of the anomalous amide-I band (1650 cm^{-1}), which is considerably larger than that of the normal amide I band (1666 cm^{-1}). With increasing temperature, however, the response of the 1666 cm^{-1} band increases and becomes the major contribution, while that of the anomalous amide I mode decreases until it has almost vanished at 293 K. This temperature dependence does not reflect that of the absorption spectrum shown in Fig. 5.4. Between 280 K and 250 K the intensity of the normal amide I mode does not change at all in the absorption spectrum, whereas the bleach signal decreases dramatically.

In a second set of experiments, narrow band, tunable pump pulses [spectral width 14 cm^{-1}, pulse duration 700 fs (FWHM)] were used to excite selectively each of the two amide I bands (see Fig. 5.6 and 5.7, measured at 93 K). When exciting exclusively the anomalous amide I band [1650 cm^{-1}, see Fig. 5.6(b)], the difference spectra show a strong instantaneous bleach and stimulated emission signal at the position of this band, which recovers on a 2 ps timescale [Fig. 5.7, crossed circles]. Essentially no response of the normal amide I band is observed. In addition, the spectrum reveals a strong positive peak at 1644 cm^{-1}, that is caused by excited state absorption of the anomalous band. Pumping the normal amide I band [1666 cm^{-1}, see Fig. 5.6(c)], on the other hand, does not lead to any significant bleach of that band. Instead, we again observe an immediate negative signal at the anomalous band. This negative peak is less intense than the bleach found when pumping the anomalous band directly. The signal decays on about the same 2 ps timescale as shown in Fig. 5.7 (black circles).

Striking feature of the experimental results is the observation that we can hardly bleach the 1666 cm^{-1} band at 93 K, while we can easily bleach the 1650 cm^{-1} band. This is evident from the impulsive excitation experiment, which excites all lines simultaneously [Fig. 5.5], as well as from the experiment with spectrally selective excitation [Fig. 5.6]. Only two effects can be responsible for the lack of an observable bleach signal after exciting a spectroscopic state: (i) the relaxation of this state back into the ground state is considerably faster than the time resolution of the experiment or (ii) all contributions to the total pump-probe signal (i.e. the negative bleach and stimulated emission signal, and the positive excited state absorption signal) cancel exactly. Possibility (ii) would be the case when the spectroscopic state is a harmonic oscillator (see Chapter 2 and 3). In the following, we will exclude possibility (i) in a first step and then discuss what can be learned from possibility (ii) in the second step. As will be discussed below, the result unambiguously proves that the 1666 cm^{-1} band is a delocalized state while the 1650 cm^{-1} band is localized, in perfect accordance with the aforementioned assignment.

Lifetime of the amide I band

A lower limit for the lifetime is obtained from the width of both amide I bands (ca. 10 cm^{-1}), which yields $T_1 \geq 500$ fs when we assume that spectral broadening is solely due to lifetime broadening. Given this limit, one concludes that the time resolution of the spectrally selective experiment [Fig. 5.6], limited by the pump pulse duration [$t_p = 700$ fs (FWHM)], should be sufficient to at least partially resolve a possible bleach.

A much more rigorous limit for the lifetime of the 1666 cm^{-1} band originates from the quantum beat experiment [Fig. 5.4(b)]. In contrast to the spectrally selective pump pulse in Fig. 5.6, this is an impulsive experiment where the pump pulse is ultrashort (150 fs). As seen in Fig. 5.4(b), the pump pulse excites inter-state coherences between the 1600 cm^{-1} band (a ring deformation of the phenyl ring, which we use as a reference state) and both the "normal" and the anomalous amide I band. The Fourier-transform of these coherences

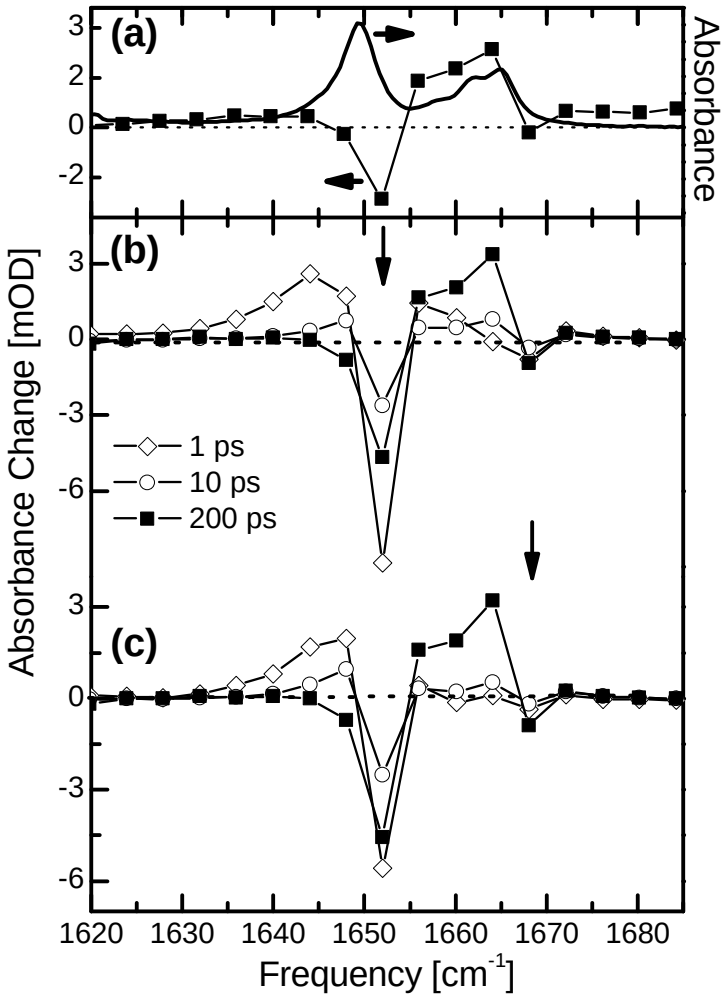

Figure 5.6: (a) Absorption spectrum of ACN (93 K) in the amide I region (black line) together with the temperature induced absorbance change upon heating the sample (■). (b) Response of the sample at 1 ps (◇), 10 ps (○) and 200 ps (■) after selective excitation of the self-trapped state (1650 cm^{-1}) and (c) the free exciton state (1666 cm^{-1}) at 93 K. The arrows mark the position of the pump pulse (spectral width 14 cm^{-1}).

directly resemble the absorption spectrum of the amide I band [Fig. 5.4(a)]. The decay of the quantum beats on a 1.5 ps timescale provides a lower limit for the T_1 lifetime of both amide I states.[a]

The cuts along the ω_{pr} axis with ω=0 shown in Fig. 5.5, on the other hand, select solely the incoherent response of the system and suppress any beating structure.[55] Thus, the spectra in Fig. 5.5 consist of a negative bleach and stimulated emission signal for each absorption band together with an excited state absorption signal shifted by the intrinsic anharmonicity. The net response of the 1666 cm^{-1} band is negligibly small at

[a]Since inter-state dephasing processes have been neglected in Ref. 143, the decay of the quantum beats should be considered a lower limit for the T_1 relaxation time, but does not necessarily reflect population relaxation directly.

low temperatures (93 K). However, in contrast to the response in Fig. 5.6, which has been measured with spectrally selective and relatively long pump pulses, the spectra in Fig. 5.5 are obtained with ultrashort pump-pulses, providing essentially unlimited time resolution (i.e. 150 fs). This time resolution is certainly sufficient to resolve a possible bleach of the 1666 cm^{-1} band, whose lifetime has been estimated to be $T_1 \geq$1.5 ps. As we do not observe such a bleach signal, the only conclusion can be that the 1666 cm^{-1} band is almost perfectly harmonic.

To summarize this paragraph, we use the 1600 cm^{-1} band, rather than the ground state, as the spectroscopic starting point to observe the lifetime of the nearby amide I bands. We have to use this indirect approach, since the direct nonlinear response of the normal amide I band (1666 cm^{-1}) vanishes.

Delocalization of the free exciton

In this paragraph, we discuss the free exciton band at 1666 cm^{-1}. For the sake of clearness, the free exciton is viewed as isolated from any other degree of freedom of the crystal. A vibrational exciton is described by the harmonic Hamiltonian equation 3.14. As is shown in Chapter 3.3.3, the anharmonicity of a delocalized state, i.e. the shift of the excited state absorption with respect to the bleach and stimulated emission, scales like the participation ratio P_k.

$$P_k = -\frac{\Delta\varepsilon_{kk}}{\Delta} = \sum_n q_{kn}^4 \tag{5.2}$$

where the q_{kn} are the expansion coefficients of the excitonic states $|k\rangle$ in the site-basis $|n\rangle$ (see Equ. 3.18).[b]

The participation ratio is a commonly used measure of delocalization of excitonic systems.[63–65] It is $P_k = 1$ for a perfectly localized state and $P_k = 1/N$ for a perfectly delocalized state, where N is the size of the aggregate. Anharmonicity of a vibrational exciton is therefore a direct measure of its degree of delocalization. This finding can be qualitatively explained in simple words: In a delocalized state, the oscillation amplitude of each individual site is reduced by a factor $1/\sqrt{N}$, where N is the delocalization length. With increasing delocalization length, each site is exploring a decreasingly smaller region of the potential energy surface, in which the harmonic approximation becomes increasingly more accurate.

At a temperature of 93 K, the 1666 cm^{-1} band can be barely bleached (as evident in Fig. 5.5 and 5.6). Since the lifetime of the excitation is long enough to make a possible bleach observable (see previous paragraph), the only conclusion then can be that the 1666 cm^{-1} band is an almost perfect harmonic state. The intrinsic anharmonicity of amide I modes, which is known from pump-probe experiments on monomeric peptide

[b] For the amide I modes the site-anharmonicity obtained from pump-probe experiments on monomeric peptide units is $\Delta \approx$16 cm^{-1},[57] while nearest neighbor coupling in ACN has been estimated to be $\beta_{n,n+1} \approx -$ 4cm^{-1}.[89] Hence the small anharmonicity limit is approximately valid for the amide I band, and Equ. 5.2 can be used to estimate the degree of delocalization.

units ($\Delta = 16$ cm^{-1}),[57] is too large to explain complete cancellation of the different contributions to the pump-probe signal. Combining both arguments, the missing bleach signal unambiguously proves that the 1666 cm^{-1} band corresponds to a delocalized state, i.e. a vibrational exciton. Only under these circumstances is the anharmonicity negligible and cancellation of the negative bleach and stimulated emission signal and that of the positive excited state absorption is essentially complete. As temperature increases, a bleach signal starts to be observed [Fig. 5.5], pointing to a non-complete cancellation of the different contributions to the total pump-probe signal. Apparently, disorder induced by thermally excited phonons starts to localize the excitation. With the onset of a bleach signal in the pump-probe experiment, we directly observe disorder-localization of the "normal" amide I mode at 1666 cm^{-1}.

The self-localized state

The anharmonicity of a self-localized vibrational state, on the other hand, has been worked out in Ref. 144.[c] Its major contribution originates from the nonlinear interaction between the amide I mode and the phonon system of the crystal ("extrinsic" anharmonicity), which is non-zero even at low temperatures. This explains why the anomalous band at 1650 cm^{-1} can be bleached even at 90 K, in contrast to the free-exciton peak. With rising temperature, the bleach of the 1650 cm^{-1} band diminishes as it disappears in the absorption spectrum. Hence, the decrease of the bleach intensity does not necessarily reflect a change of localization, but merely the intensity of the band itself.

Note that we have to distinguish carefully between two different localization effects. While the 1650 cm^{-1} band self-localizes due to interaction with phonon coordinates, a nonlinear effect that occurs even at low temperatures, the 1666 cm^{-1} band is delocalized only at low enough temperatures and localizes due to temperature induced disorder of the crystal. The second effect is a linear effect and is also known as *Anderson localization*.[145,146] Nevertheless, the onset of disorder-induced Anderson localization of the free exciton is observed at about the same temperature where the intensity of the self-trapped

[c] In Ref. 144, a band at 3250 cm^{-1} has been assigned to the first overtone of the self-trapped state at 1650 cm^{-1}. This assignment was based on the temperature dependence of the 3250 cm^{-1} band, which resembled that of the 1650 cm^{-1} band. In view of this assignment, one should expect to see an excited state absorption band at about 1600 cm^{-1} (i.e. 3250 cm^{-1} − 1650 cm^{-1}) in the pump-probe experiment after selectively exciting the 1650 cm^{-1} band. While there is a small signal at this frequency position (data not shown), the major excited state contribution emerges at 1644 cm^{-1} [Fig. 5.6b]. The reason for this discrepancy is not quite clear. However, it should be mentioned that the major contribution of anharmonicity of the self-localized state has been attributed to "extrinsic" anharmonicity in Ref. 144, i.e. to the nonlinear coupling of the amide I mode to the phonon system. Since the phonon system needs time to respond onto the amide I excitation, this is a dynamical process. The dynamical aspect of the problem has been neglected in Ref. 144, since the absorption process is instantaneous, giving the phonon system no time to relax. Therefore, it appears reasonable that the frequency of the 0-2 transition, measured in absorption, is different from the sum of the frequencies of the 0-1 and 1-2 transitions, since there is time for relaxation after population of the first excited state.

state disappears. This finding suggests that both localization mechanisms are connected. Disorder localization is due to random variation of the matrix elements of the excitonic coupling Hamiltonian Equ. 3.14. Off-diagonal disorder (i.e. a random variation of excitonic coupling elements β) would reflect displacements on the relative orientations of the various C=O groups. However, since excitonic coupling is weak ($\beta = -4$ cm^{-1}),[89] a random variation caused by small displacements of the ACN molecules in the crystal would not contribute significantly to disorder localization. On the other hand, since the amide I frequency is known to vary significantly with hydrogen bond distance (on the order of 20-30 cm^{-1}/Å),[2,147,148] diagonal disorder (i.e. a random variation of the diagonal elements ϵ_i) is expected to dominate. As shown in Chapter 5.2, there are only few phonons in ACN, which modulate the hydrogen bond distance.[d] Thermal excitation of these phonons gives rise to disorder-induced localization of the free exciton. Since these are the phonons, which also mediate self-trapping, thermal excitation at the same time diminishes the intensity of the self-localized state. This is because the Franck Condon factor for excitation from the thermally excited phonons to a self-localized state is negligible.[3,87,129,130] Hence, it is the same nonlinear interaction, namely the variation χ of the amide I excitation energy with hydrogen bond configuration, which gives rise to two effects: (i) diagonal disorder and as a consequence, disorder-induced localization of the free exciton with rising temperature and (ii) self-localization at sufficiently low temperatures.

The competition between Anderson (disorder) localization and nonlinear self-localization in the presence of disorder has been investigated in Ref. 149 for a realistic model of a globular protein. Those states that are self-localized for large enough nonlinear exciton-phonon coupling χ are quite distinct from those that are Anderson (disorder) localized. Upon reducing the nonlinear coupling, the self-trapped states become less localized and eventually reach bifurcation points, below which they do not exist. Surprisingly, the states that are Anderson localized for vanishing nonlinear coupling become rapidly delocalized and unstable as nonlinear coupling is increased just slightly.

Energy relaxation of the amide I mode

Fig. 5.7 compares the recovery of the signal from the self-trapped state (1650 cm^{-1}) after selective excitation of either the self-trapped state itself or the free exciton [Fig. 5.7, crossed circles and black circles, respectively]. The signal is larger when populating the

[d] In Chapter 5.2, it is shown that mainly two phonons with frequencies of 54 cm^{-1} and 83 cm^{-1} mediate self-trapping of the NH-stretching vibration. These phonons are excited on the NH-ground state potential surface by a stimulated impulsive Raman-like process, resonantly enhanced by the NH-vibration. The same process should also occur after excitation of the C=O band, but is not observed experimentally. This is explained by the smaller binding energy of the C=O self-trapped state, i.e. the smaller slope of the excited state potential surface, which results in a significantly weaker excitation of ground state phonons. It is nevertheless the same mechanism which modulates the C=O and NH vibrational frequency.[129] Therefore, one can assume that the same phonons, which mediate self-trapping of the NH band, also couple to the C=O band.

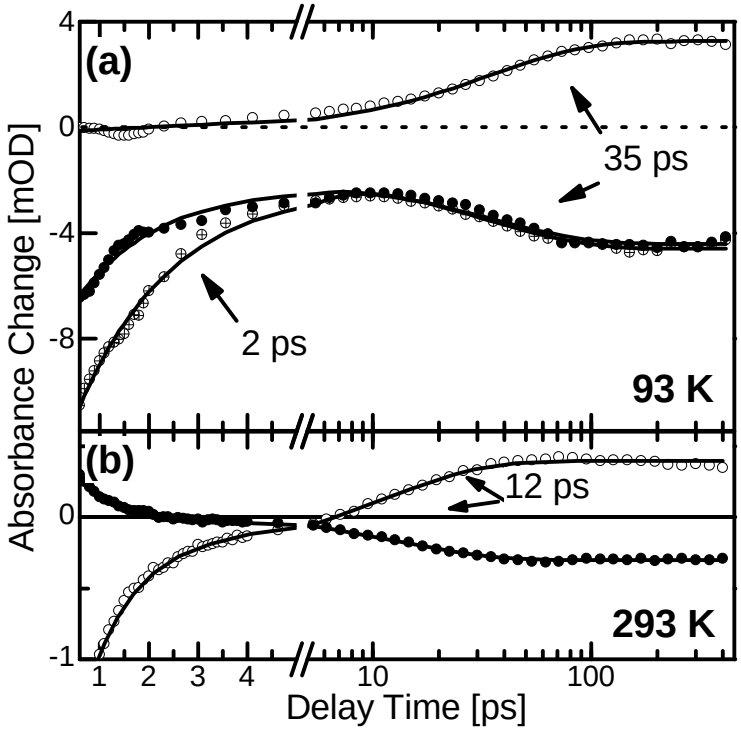

Figure 5.7: (a) Temporal evolution at 93 K of the transient signal for probe frequencies at the self-trapped state (1650 cm^{-1}) after selective excitation of this state ($\oplus$) and the free exciton state ($\bullet$). For probe frequency at the free exciton state (1666 cm^{-1}) the transients are independent of the pump pulse position ($\circ$). (b) Temporal evolution st 293 K of the signal of the free exciton ($\circ$) and the self-trapped state ($\bullet$), after excitation of the free exciton state.

self-trapped state directly since both bleach and stimulated emission signal contribute. When on the other hand populating the free exciton, only the bleach of the self-trapped state plays a role, since the common ground state is depleted, while no stimulated emission signal from the self-trapped state is expected. Both signals recover on a 2 ps timescale, reflecting relaxation of the initially excited states. Interestingly, both signals merge only after relaxation. This suggests that both the self-trapped state and the free exciton relax into the same state, however, without previous equilibration (in which case both spectra would merge previous to relaxation). However, the relaxation is not complete and a negative signal remains. This indicates that the system does not relax back into the initial ground state, but into a state, which is either spectroscopically dark or outside of our spectral window. As a consequence, a ground state depletion remains, giving rise to the observed negative signal.

The difference spectrum measured 200 ps after excitation [Figs. 5.6(b),(c)] is identical with the stationary difference spectrum induced by temperature jump [Fig. 5.6(a), black squares] and merely reflects dissipation of the pump pulse energy. Heating decreases the intensity of the self-trapped state and therefore causes a bleach of this band. The

heat signal grows in on a 35 ps timescale at 93 K [Fig. 5.7(a)]. At room temperature, reappearance of the energy is accelerated to about 12 ps [see Fig. 5.7(b)], similar to the time scale observed for the NH mode at room temperature [see following Chapter 5.2]. Thus the initially excited states relax in a few picoseconds into an intermediate state ("dark state") and the energy reappears in the form of heat only after 35 ps (12 ps). The "dark" state most likely reflects a vibrational relaxation through different intermediate states towards the bottom of the $\nu = 0$ potential. Then, at 200 ps the crystal is in thermal equilibrium at an elevated temperature.

5.1.3 Exclusion of Fermi resonances and conformational substates

In this chapter the 2D-IR spectrum of crystalline acetanilide is compared with that of two different molecular systems, which show the same doublet in the C=O stretching band: (a) benzoylchloride, which exhibits a strong symmetric Fermi resonance and (b) N-methylacetamide (NMA) dissolved in methanol which occurs in two spectroscopically distinguishable solute-solvent conformations. The corresponding 2D-IR spectra differ significantly from that of crystalline acetanilide, proving that these two alternative mechanisms cannot account for the anomalous spectroscopy of crystalline acetanilide.

Figures 5.8(a)-(c) show the linear absorption spectra (top) and the 2D-IR spectra (middle) of crystalline acetanilide (at 93 K), benzoylchloride and NMA (both at room temperature) in the spectral region of the C=O band. Benzoylchloride has been dissolved in chloroform (0.5 vol.%), in which case the intensity ratio of the two Fermi resonance bands is close to one. NMA has been measured at a concentration of 70 mM in deuterated methanol.[109] The 2D-IR spectra record the absorption change of the sample as a function of probe frequency and the center frequency of a narrow band pump pulse. Horizontal cuts through the 2D-IR spectra [Fig. 5.8(a)-(c), bottom] along pump frequencies resonant with each of the absorption lines highlight the nonlinear responses of the various molecular systems. Although the absorption spectra all exhibit a double peak structure, the 2D-IR spectra are clearly very different, emphasizing the information gain from 2D-IR spectroscopy (see Chapter 3.3.2 for an introduction to 2D-IR spectroscopy). In the following the 2D-IR spectra of the various molecular systems acetanilide, benzoylchloride, and NMA are discussed in detail.

Crystalline acetanilide

Figure 5.8(a) shows the 2D-IR spectrum of acetanilide. In a 2D-IR spectrum, one typically observes along the diagonal for each vibrator the bleach and stimulated emission of the $\nu = 0 \rightarrow 1$ transition as a negative signal (blue), and the $\nu = 1 \rightarrow 2$ excited state absorption as a positive signal (red). Connectivity between two vibrational states results in off-diagonal peaks, that are also called cross peaks. When resonantly pumping the

anomalous band (1650 cm^{-1}) of ACN, the band bleaches (negative response) and a positive band emerges at 1644 cm^{-1}. This pair of peaks constitutes a diagonal peak. When resonantly pumping the normal band (1666 cm^{-1}), on the other hand, essentially no bleach of the band itself is observed on the diagonal. Only the anomalous band responds with a signal (a cross peak) which is similar in shape, but slightly smaller than when pumping it directly. The nonlinear response is exactly the same as the one discussed in the previous Chapter (5.1.2) and the horizontal cuts through the 2D spectrum are equivalent to the narrow band excitation experiment shown in Fig. 5.6.

Figure 5.8(d) emphasizes the 2D-IR response with the help of a level scheme. When resonantly pumping the self-trapped state, one observes a bleach and stimulated emission signal at the original frequency 1650 cm^{-1} (blue arrows) and an excited state absorption signal (red arrow) that is slightly red shifted to 1644 cm^{-1} as a result of the effective anharmonicity of that state. When resonantly pumping the free exciton, on the other hand, the various signals cancel exactly since the system is perfectly harmonic and the frequency and transition strength of the excited state absorption (red arrow) matches exactly that of stimulated emission and bleach (blue arrow). Thus self-trapping theory can naturally explain the 2D-IR response of crystalline ACN at low temperatures.

Benzoylchloride

Based on isotope substitution and solvent variation methods,[150,151] it has been established that the double peak structure of the C=O band of benzoylchloride is the result of a Fermi resonance between the carbonyl stretching band and an overtone of a low frequency mode.[152] When dissolved in chloroform, the Fermi resonance is almost perfect, resulting in two peaks with about the same intensity. The 2D-IR spectrum of benzoylchloride is complex and contains in total four resolved negative and three positive peaks [Fig. 5.8(b)]. Striking is the square pattern of the four negative peaks, two on the diagonal and two at the corresponding off-diagonal positions. The diagonal peaks are about twice as intense as the corresponding off-diagonal peaks [see horizontal cuts through the spectrum in Fig 5.8(b), bottom]. In addition, two strong positive peaks at about the same probe frequency of 1710 cm^{-1} are found in the 2D-IR spectrum together with a significantly weaker positive peak on the high-frequency side.

A Fermi resonance occurs when a fundamental normal mode is accidentally resonant with an overtone or combination of lower frequency modes and when an anharmonic term of the potential energy surface couples them. While the discussion is here restricted to a Fermi resonance with an overtone, it was verified that the results are essentially the same for a Fermi resonance with a combination mode. Chapter 3.6 describes how one can calculate the 2D-IR spectrum of a Fermi resonance between two vibrational modes. If one considers only harmonic modes, the calculated 2D-IR spectrum [see Fig. 5.9(a) and Fig. 3.9] clearly fails to explain the 2D-IR spectrum of benzoylchloride [Fig. 5.8(b)]. This is since the model does not yet include the intrinsic anharmonicity of the individual vibrational oscillators.

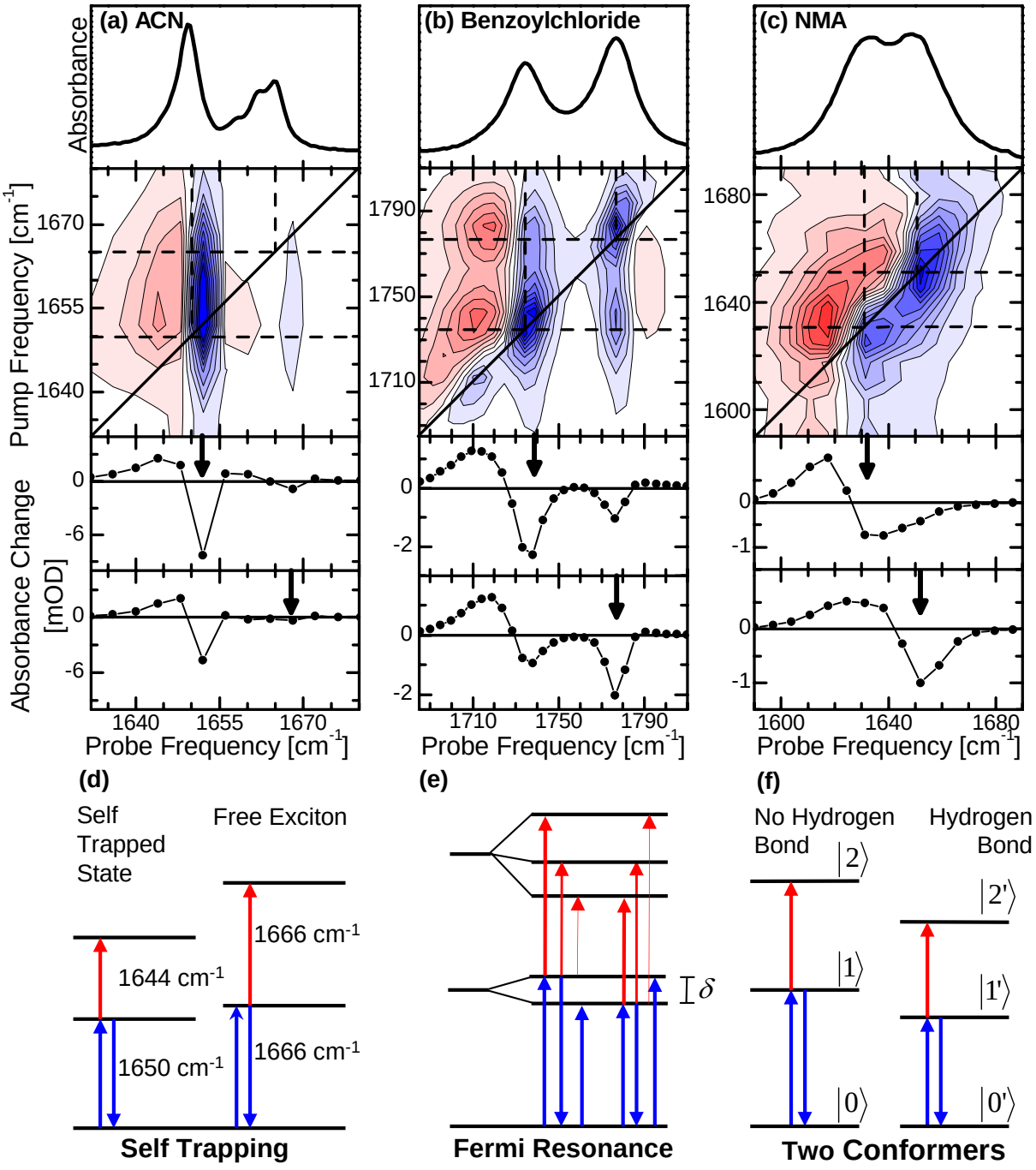

Figure 5.8: Absorption and 2D-IR spectra of the C=O mode of (a) the self-trapping mechanism in acetanilide, (b) the Fermi resonance in benzoylchloride and (c)[109] the two different conformers of the solvent-solute complex of NMA dissolved in methanol. Blue colors indicate negative, red colors positive absorption change. The contour intervals represent a linear scale. The lower panels show horizontal cuts through the 2D-IR spectrum for pump frequencies resonant with either of the two bands. The arrows mark the position of the pump pulse. (d)-(f) Corresponding vibrational energy levels. Up-going blue arrows depict bleach, down-going blue arrows stimulated emission, giving rise to negative signals. Red arrows depict excited state absorption, giving rise to positive signals. The thickness of the arrows reflects the transition strength.

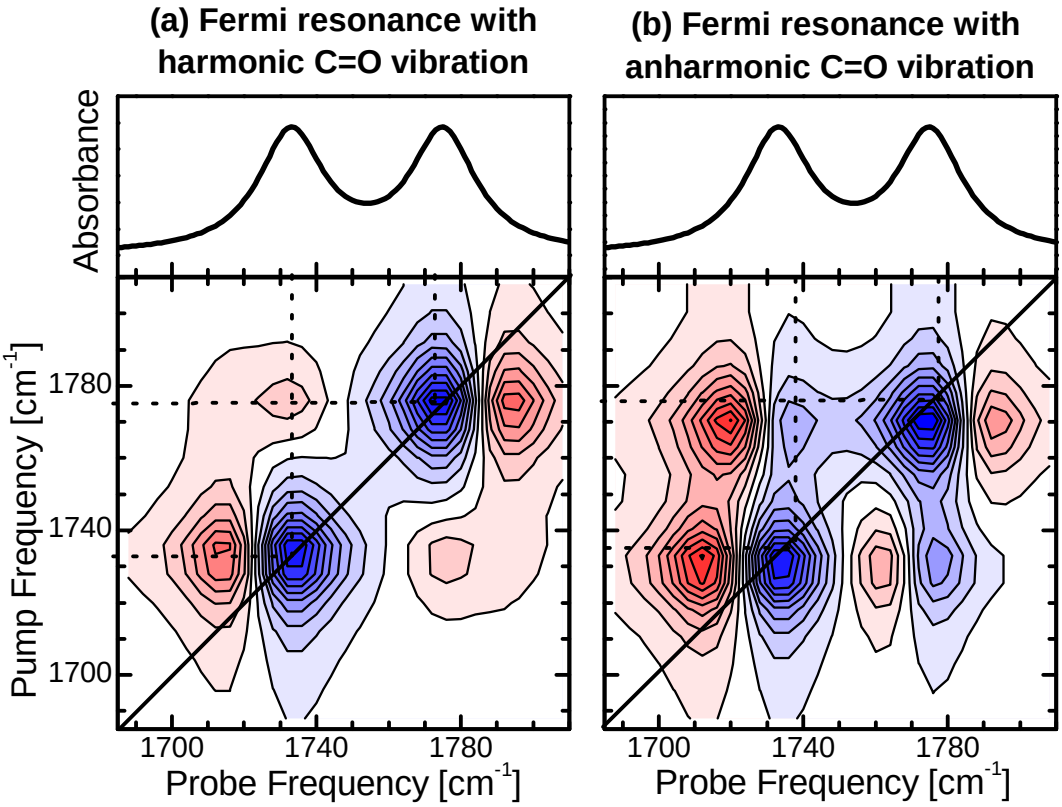

Figure 5.9: Calculated absorption spectrum and 2D-IR signal of the Fermi resonance of the C=O stretching mode in benzoylchloride assuming (a) a harmonic and (b) an anharmonic C=O vibration. The two peaks in the absorption spectra have the same intensities, since a perfect resonance is assumed. Blue colors indicate negative absorption change, red colors positive absorption change. The Fermi coupling and the unperturbed frequencies are set to account for the experimentally observed splitting

The anharmonicity of the low frequency mode is neglected, since such low frequency modes are expected to be delocalized over the whole molecule, in which case its anharmonicity is small.[153] However the anharmonicity of the C=O mode should be included. A Fermi resonance of an anharmonic mode is described by the Hamiltonian Equ. 3.57, which is diagonalized numerically, assuming a perfect Fermi resonance with $\Omega_1 - \Delta_1 = 2\Omega_2$. The Fermi coupling is set to $\delta = 40\ cm^{-1}$ to account for the experimentally observed splitting. For the intrinsic anharmonicity $2\Delta_1 = 16\ cm^{-1}$ is used, which is a typical value for C=O modes.[57] By construct the linear absorption spectrum [Fig 5.9(b), top], is the same as in the harmonic case. However, the 2D IR spectrum is different and now in good agreement with the experimental result [Fig. 5.9(b) and Fig. 5.8(b)].

The negative peaks (blue) represent bleach and stimulated emission from the one-exciton states [see Fig. 5.8(e)]. Stimulated emission signals can occur only when the corresponding state is resonantly populated (diagonal peak). The bleach signal, on the other hand, is observed for both states, since the common ground state is depleted (diagonal and off-diagonal peak). This explains the prominent square pattern in Fig. 5.8(b) and Fig. 5.9(b) with the diagonal peaks being twice as strong as the (negative) off-diagonal

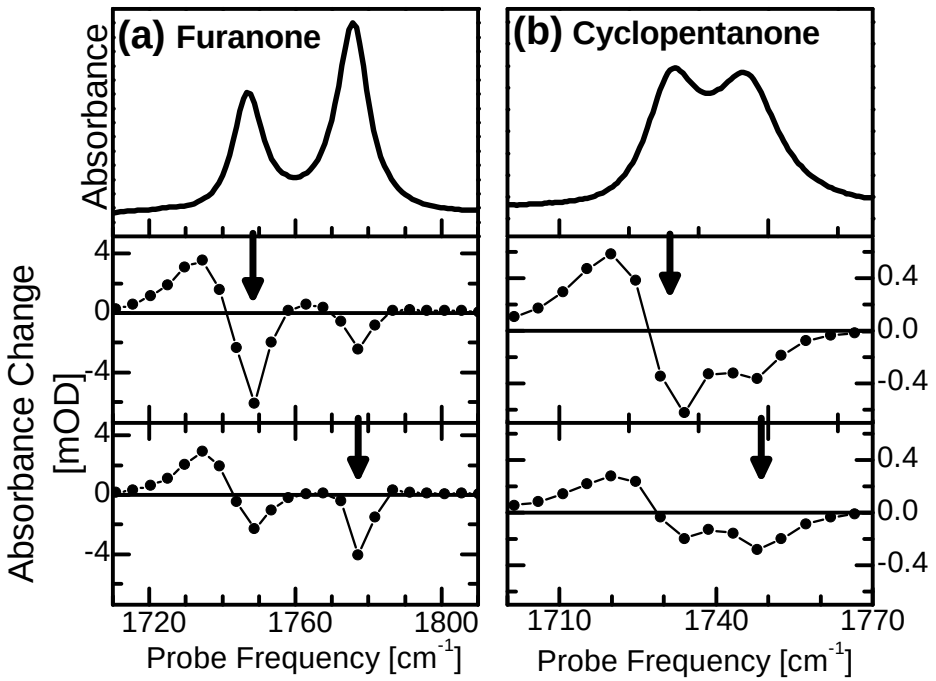

Figure 5.10: Absorption spectrum (top) of the Fermi resonances of the C=O mode in (a) furanone and (b) cyclopentanone, both dissolved in acetonitrile. The lower panels show cuts through the 2D-IR spectrum for pump frequencies resonant with the absorption bands. The arrows mark the position of the pump pulse. The 2D-IR spectra match that of benzoylchloride, shown in Fig. 5.8(b).

peaks. The excited state absorption appears as a positive (red) signal. The intensities of the transitions to the three upper states, which are in principle all allowed, are significantly different [depicted by the thickness of the arrows in Fig. 5.8(e)]. One expects to observe one strong excited state absorption band from each of the one-exciton states (intensities: $\approx 0.86|\mu|^2$), causing the two strong red peaks in the low-frequency part of the 2D-IR spectrum. Two of the weaker transitions (intensities: $\approx 0.6|\mu|^2$) can be seen as well, which however are overlaid by the stronger negative bands. The third pair of transitions carries only negligible oscillator strength, and is not seen the 2D-IR spectra.

In conclusion it has been shown that one can very well understand the 2D-IR spectrum of benzoylchloride by a simple Fermi resonance model. One observes very similar 2D-IR spectra for the C=O modes in cyclopentanone, cyclohexen-1-one and furanone, which all exhibit a well characterized Fermi resonances.[152,154–156] Compared to benzoylchloride, furanone exhibits a more asymmetric and cyclopentanone a weaker Fermi resonance [Figs. 5.10(a),(b), top panel]. Cuts through the 2D-IR spectrum, at pump frequencies resonant with the absorption bands, match the 2D-IR spectrum of benzoylchloride [Figs. 5.10(a),(b) and Fig. 5.8(b)]. Thus the observed pattern is not specific for benzoylchloride, but appears to be a general signature of a Fermi resonance of a C=O mode. If the reason for the splitting of the amide-I band in ACN were a Fermi resonance, as proposed in Ref. 102, the 2D-IR response of ACN [Fig. 5.8(a)] would look similar to Fig. 5.8(b), which clearly is not the case.

N-Methylacetamide in methanol

The absorption spectrum of NMA in methanol [Fig. 5.8(c)] exhibits a double peak, which has been explained by an equilibrium between two solute-solvent conformations. The equilibrium constant is close to unity and the peak at 1630 cm^{-1} represent NMA molecules whose C=O groups are hydrogen bonded to surrounding methanol molecules while the peak at 1650 cm^{-1} represent NMA molecules which are free at the C=O group. Hydrogen bonding leads to a red shift of the amide-I band of about 20 cm^{-1}, which explains the two different frequencies of the two sub-states. This interpretation has been verified by Woutersen *et. al.*[109] with extensive solvent dilution experiments, MD simulations, and time-dependent 2D-IR spectroscopy.

The 2D-IR spectrum of NMA in methanol, taken from Ref. 109, is shown in Fig. 5.8(c). The spectrum features two strong peaks on the diagonal, but does not show any evidence of a cross peak. This is highlighted in the horizontal cuts through the 2D-IR spectrum, each of which shows one negative and one positive peak, which is exactly the response one expects for an isolated, slightly anharmonic vibrator [see Chapter 3.2]. The negative signal corresponds to stimulated emission and bleach, while the positive signal corresponds to the excited state absorption which is slightly red shifted due to the intrinsic anharmonicity of the C=O mode. The response of both states is essentially identical. The lack of cross peaks indicates that the two states do not share any common ground state [see Fig. 5.8(f)]. In contrast to the Fermi resonance case, a bleach signal is observed only for that state which is directly excited by the pump pulse. Hence, the two peaks correspond to two completely independent oscillators which do not take any notice of each other, just as one expects for the case of two different solute-solvent configurations. In contrast, the 2D-IR spectrum of ACN [Fig. 5.8(a)] exhibits distinctively different 2D-IR signals for both amide-I sub-band as well as a coupling between both (revealed by the cross peak). This 2D-IR signature is not consistent with the existence of two conformational sub-states within the crystal.

5.1.4 Conclusion

The nature of the double peak, that one observes in the amide I band of crystalline ACN, was studied in detail at different temperatures. From the distinctively different nonlinear responses of both sub-bands, in particular their harmonicity and anharmonicity [see Fig. 5.6] the normal peak (1666 cm^{-1}) is assigned to a free exciton, while the anomalous peak (1650 cm^{-1}) is assigned to a self-trapped state. The change in anharmonicity of the free exciton shows that it is a perfectly delocalized state at low temperatures, that disorder-localizes (Anderson localization) with increasing temperatures. The self-trapped state, on the other hand, originates from a nonlinear coupling between vibrational excitons and lattice phonons, which is mediated through the hydrogen bonds and is nonzero even at low temperatures. With rising temperatures thermal disorder destroys self-trapping and the bleach of the 1650 cm^{-1} band diminishes as it simultaneously disappears in the

absorption spectrum. The assignment of the two amide I sub-bands to a self-trapped state and a free exciton confirms earlier, more indirect work, that was based solely on the temperature dependent intensities of both bands.[2,3,87,129,130]

Previously, two alternative explanations for the anomalous temperature dependence of the amide I band were proposed: Fermi resonance and conformational substates. In this thesis, the 2D-IR spectrum of ACN is compared to that of two molecular systems, which show the same splitting of the C=O band in the linear absorption spectrum as ACN, and which are chosen as simple representatives of the two alternative mechanisms. The three 2D-IR spectra differ completely, albeit in a well understood way. Based on the 2D-IR spectroscopic signature, a Fermi resonance or conformational sub-states can definitely be excluded as alternative explanations for the anomalous spectra of ACN. Self-trapping of the C=O mode, on the other hand, can naturally explain the observed 2D-IR spectrum of ACN. The work demonstrates how nonlinear 2D-IR spectroscopy can clearly distinguish between different anharmonic effects in way that is not possible with linear absorption spectroscopy. Here this capability of 2D-IR spectroscopy was applied to finally resolve the origin of the anomalous absorption spectrum of crystalline ACN.

However the self-trapping theory is not yet entirely understood. It bas been previously shown that a diagonalization of the polaron Hamiltonian, using a perturbative expansion for the excitonic term, reveals correctly the temperature dependence of the self-trapped amide I mode. However at the same time a diagonalization of the Hamiltonian fails to reproduce the existence of the free exciton state. In fact, the free exciton is introduced in a purely phenomenological way by an additional potential energy surface. Even though this approach is in full agreement with the pump-probe experiments, it is so far not justified by the polaron Hamiltonian. This failure might be due to the fact that self-trapping theory of ACN is based on a single one-dimensional hydrogen bonded chain. In case of a one-dimensional problem one expects a barrier-less self-trapping process.[157] In contrast, in three dimensions the free exciton is meta-stable and self-trapping has to overcome a barrier. Clearly ACN is not a true one-dimensional system. It is one-dimensional regarding the hydrogen bonded chains and the orientation of the amide I dipole moments that are all aligned in parallel. However there is no reason to assume that the inter-chain excitonic coupling is significantly smaller than the intra-chain excitonic coupling that causes the formation of the vibrational exciton. Including the inter-chain coupling leads to a three-dimensional theory, which would be more adequate to describe ACN. It has been shown that a numerical diagonalization of such a multidimensional polaron Hamiltonian is in principle possible.[90] In three dimensions the theory might reproduce the absorption spectrum of the free exciton.

In any case, self-trapping theory can naturally explain the observed pump-probe spectra of the amide I mode in ACN, while 2D-IR spectroscopy rules out alternative explanations, suggested in the literature. Thus the experiments prove unambiguously that vibrational self-trapping in hydrogen-bonded peptide units exists.

5.2 The NH stretching band

The NH mode of ACN is weakly temperature dependent and consists of a main peak at 3295 cm^{-1}, which is accompanied by a series of almost equally spaced satellite peaks at lower frequencies [see e.g. Fig. 5.12(a) or Fig. 6.2(a)]. This very peculiar bandshape was explained by the same self-trapping mechanism as the splitting in the amide I band of ACN [see Chapter 3.5.3]. Self-trapping is mediated by hydrogen bonds, which induce a coupling between vibrational excitations of the NH mode and low frequency phonons. According to this interpretation the main peak (the one with the highest frequency) corresponds to a free exciton, while the sidebands reflect self-trapped states.[87] Indeed, the main peak shows a small Davydov splitting [Fig. 6.2(e)] which indicates that the band corresponds to a delocalized state, i.e. a free exciton state. The nonlinearity induced by the hydrogen bonds and hence the exciton-phonon coupling and the binding energy E_{BD} of the self-trapped state are significantly larger for the NH mode than for the amide I mode [see Fig. 5.2]. As a consequence, self-trapping occurs in the NH band even at room temperatures. In fact, the binding energy E_{BD} amounts to more than three phonon quanta in case of the NH band, whereas it is smaller than one phonon quantum for the amide I mode. Therefore, one observes a "Franck-Condon-like" progression in the absorption spectrum of the NH mode, consisting of one vibrational excitation plus several quanta of phonon excitation. Previously it was assumed that all nine sidebands correspond to self-trapped states.[2,61,87,129,138] However, in Chapter 6 the absorption spectrum is analyzed in detail and it is shown that only the first four peaks correspond to self-trapped states, while the other peaks have to be attributed to different origins, such as CH modes. In the following broad-band femtosecond pulses, as well as frequency selective narrow-band pulses are used to excite the different sub-levels of the NH band in order to study the self-trapping mechanism in detail.

5.2.1 Impulsive excitation: Phonon modes mediate self-trapping

Broadband pump pulses [bandwidth: 200 cm^{-1}, pulse duration: 130 fs (FWHM)] were used to impulsively excite a section of the absorption spectrum, which includes the NH main peak and the first three satellite peaks. As a representative example, Fig. 5.11 shows the transient response for a probe frequency of 3200 cm^{-1}. At delay time zero, the signal is strongly influenced by cross phase modulation, caused by Kerr nonlinearities of the crystal and the CaF_2 windows of the sample cell. Hence, the discussion of the data is restricted to delay times >300 fs only, when temporal overlap of pump and probe pulse is essentially over. The striking feature of the data is strong oscillations, which persist at 77 K up to 14 ps. With increasing temperature, the oscillations decay faster and their amplitude decreases. A spectral analysis of the beating structure is obtained from the Fourier transformation of the transient response by Equ. 5.1. The absolute value spectrum $|\Delta A(\omega, \omega_{pr})|$ is shown in Fig. 5.12 as a 2D plot for 293 K and 77 K. The

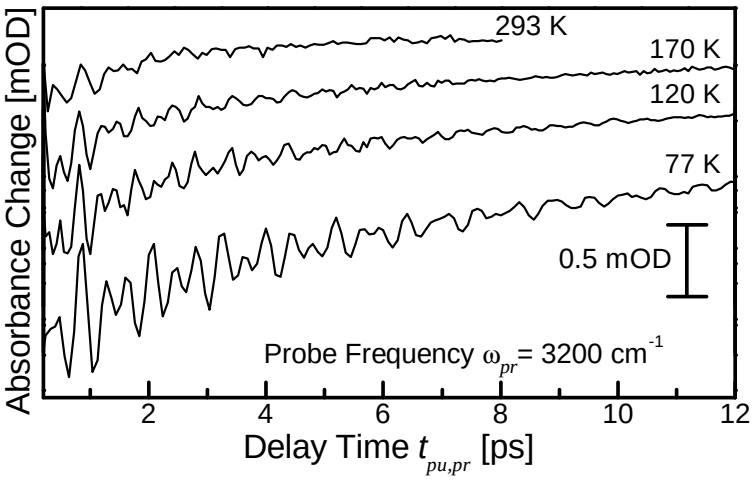

Figure 5.11: Transient response of the NH band of ACN after impulsive excitation for a probe frequency (3200 cm^{-1}) which coincides with one of the self-trapped states. The temperature is varied from 77 K to 293 K.

probe frequency ω_{pr} is plotted along the x-axis and the frequency ω, which is revealed by Fourier transformation, along the y-axis. The 2D plot for 77 K shows clearly two major frequency components at 54 cm^{-1} and 83 cm^{-1}. The oscillations reach their maxima at probe frequencies which correspond to the peaks of the NH absorption band. Vertical cuts through the spectra at the position of the satellite peaks are shown in Fig. 5.12(c),(f). Comparison between low and high temperature data reveals clearly that the frequencies of the two major oscillations decrease to 48 cm^{-1} and 76 cm^{-1} at 293K. In Fig. 5.13, the frequencies of the two major modes are plotted against temperature and compared with the frequencies of the phonon modes in the low frequency Raman spectrum (the latter taken from Johnston *et al.*[158]).

The impulsive excitation with an ultrafast laser pulse may result in the creation of vibrational wavepackets, which give rise to oscillations in the pump-probe signal. Principally speaking, two different generation mechanisms of such wavepackets are possible: (i) Impulsive absorption, yielding a wavepacket in the excited state, in which case the beating frequency should represent the energy separation between (coupled) states in the spectrum. This is the type of wavepacket discussed in Chapters 2 and 5.1.2. (ii) A Raman-like process resulting in a ground state wavepacket, giving rise to phonon excitation, in which case one expects the beating frequency to match one of the low frequency phonon modes of the molecule. Impulsive absorption and Raman-like excitation are expected to occur simultaneously with probabilities that are given by the Franck-Condon factors of the individual transitions.

Two observations are used as an argument to assign the beatings in the pump-probe signal of ACN to a ground state wavepacket. (i) The lifetime of the excited state [400 fs, see Figure 5.14(a)] is too short to support an excited state wavepacket that persists for many picoseconds. This discrepancy becomes even more pronounced at low temperatures,

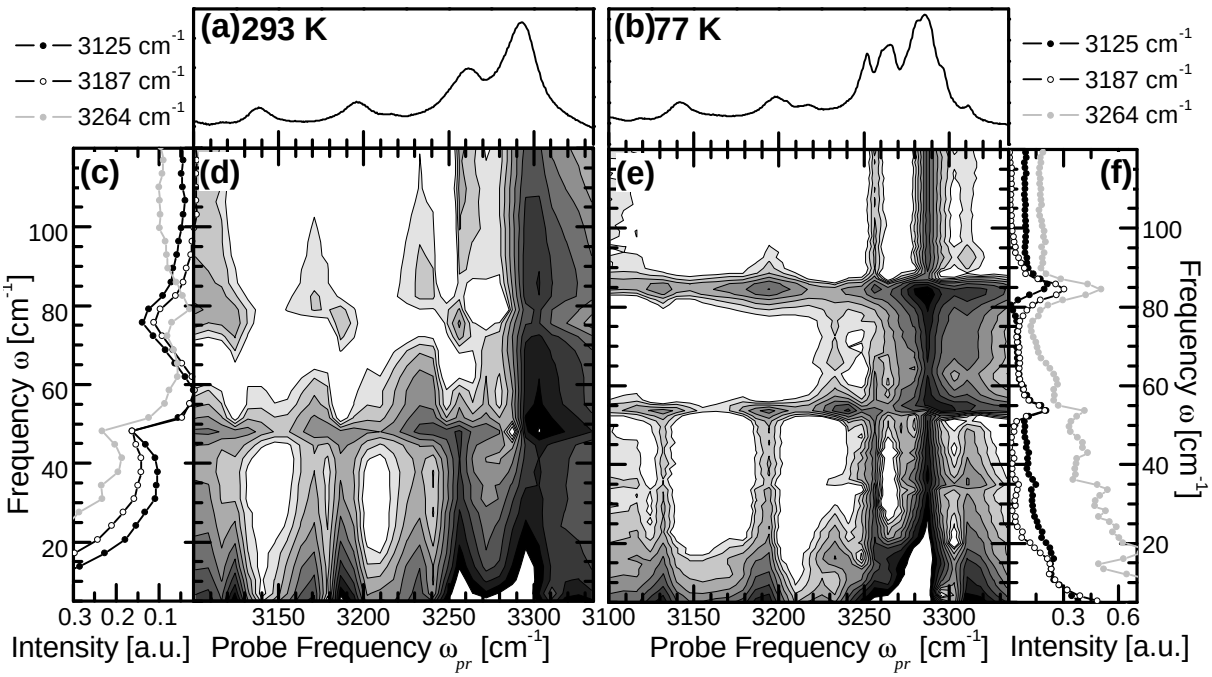

Figure 5.12: (a),(b) Absorption spectra of crystalline ACN, showing the NH band for 293 K and 77 K. (d),(e) 2D-plot of the absolute value of the Fourier transformation of the transient pump-probe signal after impulsive excitation. ω_{pr} is the frequency of the probe pulse and ω results from the Fourier transformation of the pump-probe signal with respect to delay time $t_{pu,pr}$ between pump and probe pulses. (c),(f) Vertical cuts trough the 2D spectrum at frequencies corresponding to the satellite peaks.

where the coherence decay time increases significantly [see Fig. 5.11], while the excited state lifetime stays about the same [600 fs, see Fig. 5.14(c)]. (ii) At room temperature, the frequency of the quantum beats does not fit the frequency spacings in the absorption spectrum, which would be what is expected for an excited state wave packet. To be more precise, at a probe frequency resonant with a particular sub-level, one expects to observe a beating frequency which reflects the energy splitting between this state and adjacent states which share the common ground state.[143] When taking the main peak as an example (3295 cm^{-1}), this could be a beating frequency of 35 cm^{-1}, 65 cm^{-1}, 100 cm^{-1} (i.e. 35 cm^{-1} + 65 cm^{-1}), etc. The sharp bands at 48 cm^{-1} and 76 cm^{-1} clearly do not fit into this scheme. At lower temperatures, however, the beating frequency increase slightly and the absorption spectrum becomes more structured, so that the 54 cm^{-1} beating frequency in fact matches the frequency spacing between the 3198 cm^{-1} band (the second satellite peak) and the 3252 cm^{-1} band (the first overtone of the amide I) at 77 K.

Nevertheless the interpretation of a ground state wavepacket is validated by the temperature dependence of the beating frequency of the two major components [Fig. 5.13]. In the case of a ground state wave packet, the temperature dependence of the beating frequencies should match that of certain Raman modes. The low frequency Raman spectrum of ACN has been the subject of several studies[2,158–160] and contains a total of 24 Raman

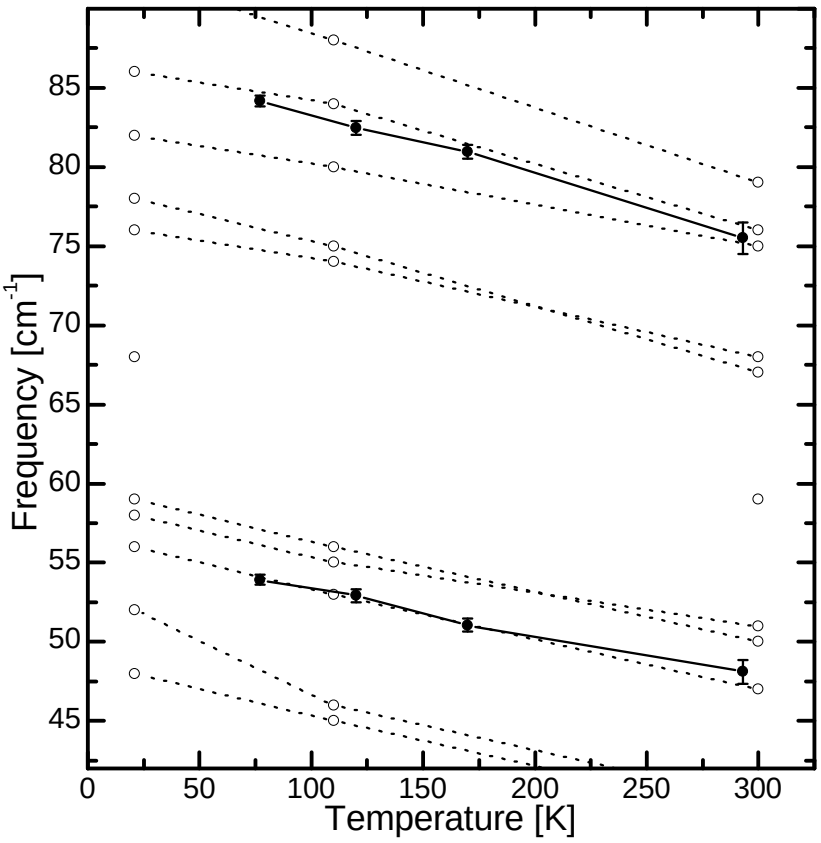

Figure 5.13: Temperature dependence of the low frequency Raman modes (○) in ACN, taken from Johnston *et al.*,[158] and of the beating frequencies observed in the pump-probe experiment (●). The temperature dependence of the beating frequencies matches perfectly that of two Raman modes.

active modes. In Fig. 5.13, the temperature dependence of the beating frequency is compared with that of the Raman-active phonons of the crystal and one finds an excellent agreement. Furthermore, the line width of the phonon modes narrows,[158] in agreement with the Fourier transform spectra in Figs. 5.12(c),(f). Hence, we conclude that the beatings in the pump-probe signal reflect a coherent excitation of two distinct phonons in the NH-ground state.

Interestingly the pump-probe experiment selectively excites just 2 out of 24 Raman-active phonons. In the present experiment, the phonons are excited by a stimulated impulsive Raman process, which is resonantly enhanced by the NH absorption band. Such a process is only possible if the respective Raman modes are coupled to the NH excitation. In the representation of Fig. 5.2, such a coupling gives rise to a shift of the potential energy surfaces, i.e. it renders the phonon to be "Franck-Condon" active. In other words, the coupling observed in the pump-probe experiment is precisely the same as the one that is responsible for self-trapping. Combining these arguments, we conclude that the phonons we observe in the pump-probe experiment are indeed the phonons that mediate self-trapping. In order to be "resonant Raman active", the lattice deformation

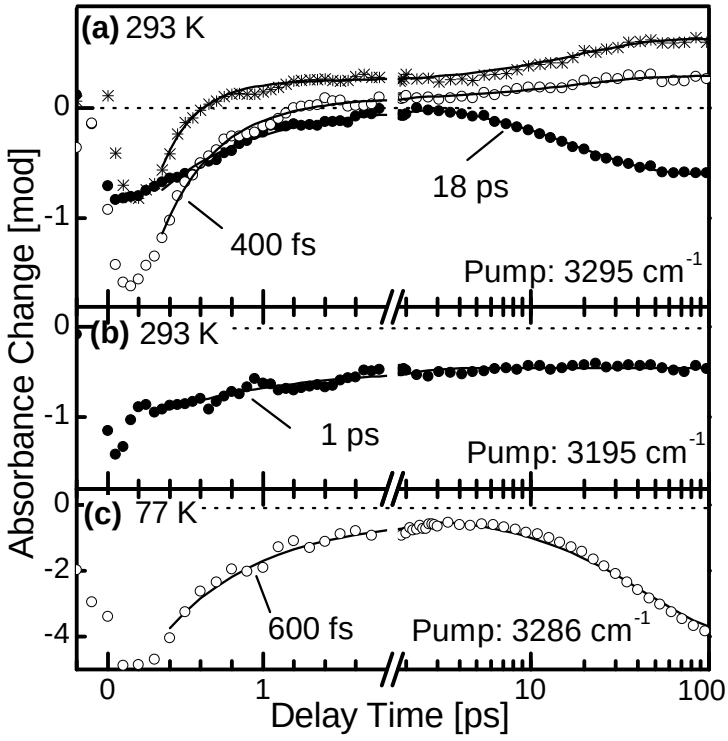

Figure 5.14: (a) Temporal evolution of the transient signal after selective excitation of the free exciton peak for probe frequencies at the red wing (3280 cm^{-1}, •), center (3295 cm^{-1}, ∘) and blue wing (3303 cm^{-1}, ∗) of the main NH band. (b) Temporal evolution of the self-trapped state at 3195 cm^{-1} after selectively pumping at the same frequency position. (c) Temporal evolution of the free exciton at 77 K after selectively pumping at the same frequency position (3286 cm^{-1}).

has to lower the total hydrogen bond energy by an overall shortening of the hydrogen bond distances. This would be, for example, a torsion of the tilted ACN molecules, straightening the hydrogen bond chain.

Deuterated ACN

Fully C-deuterated ACN (ACN-D_8) is structurally almost identical to ACN and forms the same type of hydrogen bonded crystals. Therefore ACN-D_8 should also exhibit self-trapping. The NH band of ACN-D_8 consists, just as ACN, of a main band, accompanied by a sequence of satellite peaks [see Fig. 6.2(b)]. The transient pump-probe signal of ACN-D_8 shows a striking beating pattern [Fig. 5.15], similar to ACN. The Fourier transform spectrum contains two frequency components, a sharp peak at 47 cm^{-1} and a broad peak at about 80 cm^{-1}. Since the molecular weight of ACN-D_8 is comparable to ACN one indeed expects to excite the same phonons with similar frequencies. The comparison with the splittings in the absorption spectrum rules out an excited state wavepacket. Raman spectra of fully deuterated ACN show that the spectra below 60 cm^{-1} do not change much upon deuteration and contain a distinct mode at about 50 cm^{-1} and a broad band

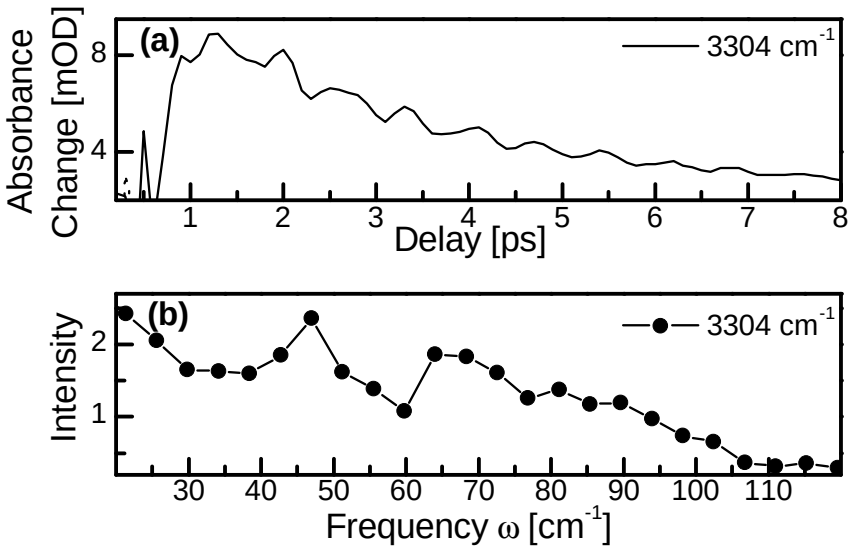

Figure 5.15: (a) Transient signal of the main peak in the NH band of ACN-D_8 after impulsive excitation for a probe frequency which coincides with the free exciton, showing pronounced oscillations. (b) The Fourier transform spectra shows a sharp band at 47 cm^{-1} and a broad band at 80 cm^{-1}.

between 60 cm^{-1} and 100 cm^{-1}.[131] Consequently the oscillations are assigned to a ground state wavepacket, using the same arguments as in the previous paragraph. This is a direct proof that the NH mode in ACN-D_8 is coupled to low frequency phonons.

5.2.2 Selective excitation: Dynamics of the self-trapped states

In a second set of experiments, narrow band, tunable pump pulses [bandwidth: 30 cm^{-1}, pulse duration: 250 fs (FWHM)] were used to selectively excite individual sub-levels of the NH band. Figure 5.16(b)-(d) shows the response of the sample after excitation of self-trapped states (at 3137 cm^{-1} and 3195 cm^{-1}, respectively) and of the free-exciton peak (3295 cm^{-1}) for delay times of 0.4 ps, 4 ps and 100 ps. The system equilibrates rapidly on a ps time scale, resulting in spectra which do not depend on pump frequency after a delay time of 4 ps [Figs. 5.16(b)-(d), white circles]. However, on the sub-picosecond time scale the free-exciton and the lower lying self-trapped states behave distinctly different [Figs. 5.16(b)-(d), black circles]. When exciting the free-exciton [Fig. 5.14(d)], a strong bleach and stimulated emission signal is observed, which recovers on a 400±100 fs time scale, representing the free-exciton lifetime [Fig. 5.14(a), white circles]. Simultaneously, population is transferred into lower lying self-trapped states, giving rise to negative peaks that are larger in the 400 fs spectrum than in the 4 ps spectrum. This can be seen after subtracting a broad positive background, reflecting anharmonically red shifted $\nu = 1 \rightarrow \nu = 2$ excited state absorption of the free exciton. On the other hand, when pumping one of the self-trapped states directly [Fig. 5.16(b),(c)], population in-between all self-trapped states equilibrates essentially instantaneously, yielding an additional neg-

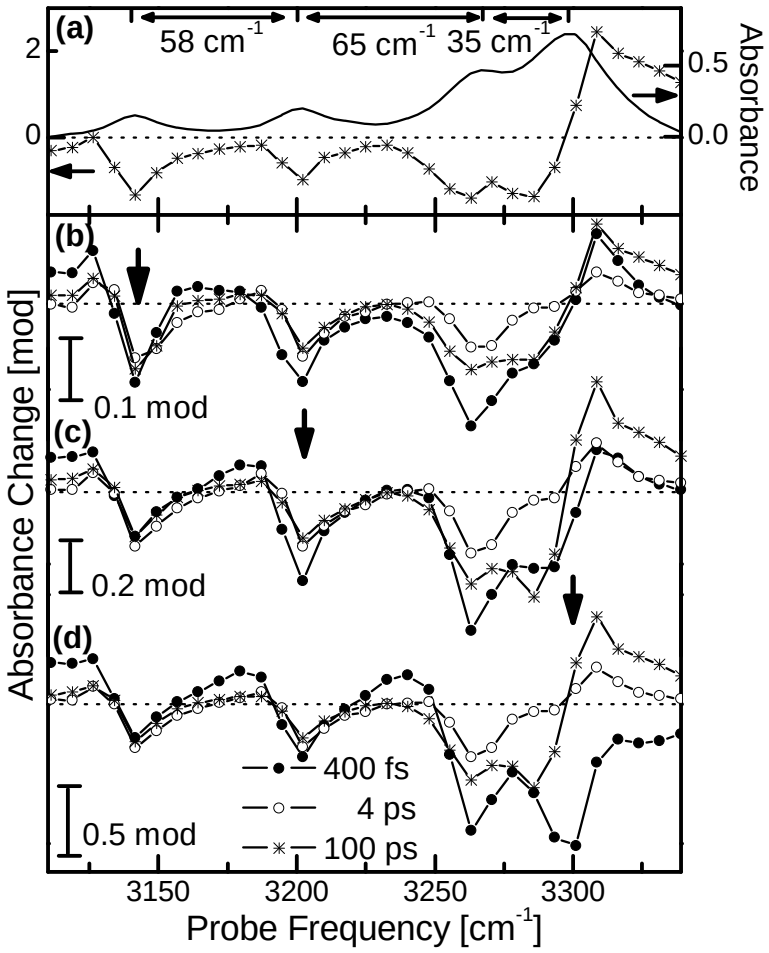

Figure 5.16: (a) Part of the NH band of crystalline ACN (black line, 293 K) together with the temperature induced absorbance change upon heating of 3 °C (∗). (b-d) Response at 293 K of the sample upon selective excitation of (b) the self-trapped states at 3137 cm^{-1} and (c) at 3195 cm^{-1} and (d) the free exciton peak for delay times of 400 fs (•), 4 ps (○) and 100 ps (∗), respectively. The position of the narrow band pump pulse [spectral width 30 cm^{-1} (FWHM)] is indicated by the arrow.

ative signal of all of these states in the 400 fs spectrum, which is almost independent on which state has been pumped. However, the free-exciton peak is not back-populated. This is a direct observation of ultrafast self-trapping: Excitation of the free-exciton leads to an irreversible population of self-trapped states. Since a back-transfer would require restoration of phonon coordinates, it does not occur even though it would be possible energetically within kT.

The subsequent, slower relaxation process is very similar to that observed for the amide I band [Chapter 5.1.2]. The difference spectra measured 100 ps after excitation [Fig. 5.16(b)-(d), stars] and that induced by a stationary temperature increase [Fig. 5.16(a), stars] are essentially identical. Hence, we conclude that the 100 ps spectra merely mirror the temperature jump induced by the intense pump pulse, and the bleach of the 3137 cm^{-1}, 3195 cm^{-1} and 3260 cm^{-1} band reflects a weakening of the self-trapping

mechanism,[87,130] rather than excitation of these states. Again, the free-exciton peak responds in a distinctively different way to such a temperature jump. Rather than a bleach, a shift towards a higher frequency is found which occurs on a relatively slow 18±3 ps time scale (i.e. a negative signal at the red side and a positive signal at the blue side of the band, see Fig. 5.14(a) black circles and stars). Such a blue shift is a well known phenomenon for hydrogen bonded systems:[161] As a consequence of the anharmonicity of the hydrogen bond potential, the average hydrogen bond distance increases with excitation of those modes, which modulate the hydrogen bond distance. Since the frequency of the NH vibration depends on the hydrogen bond distance,[66] the position of the free-exciton peak is a measure of the excitation of these modes, or, after thermalization, a measure of temperature, respectively. Furthermore, as these modes modulate the NH absorption frequency, they must be the "resonance Raman active" phonons. Owing to the large displacement of the potential surface along the phonon coordinates, corresponding to a binding energy of ≈200 cm^{-1}, the phonons are certainly excited directly upon relaxation of the system into the ground state, rather than delayed through indirect channels. Hence, combining both arguments, we conclude that the appearance of the blue shift within 18 ± 3 ps mirrors ground state recovery.

Interestingly, the lifetime of the initially excited states is much shorter than the 18±3 ps ground state recovery. This is directly evident for the free-exciton peak with a bleach recovery time of 400±100 fs [Fig. 5.14(a), white circles]. The self-trapped states equilibrate very quickly on a time scale which is in the same order as the time resolution of the experiment. These fast relaxation and equilibration times are in agreement with the absence of excited state wave packets. Besides, they are still consistent with the bandwidth of the sub-levels (i.e. $\geq (1/2\pi)\Delta\omega$) . The initially excited self-trapped states relax on a 1.0±0.3 ps time scale [Fig. 5.14(b)] into states, that are either outside of our frequency window or spectroscopically dark, and return back to the ground state with a time scale of 18±3 ps. At this point, we can only speculate on the nature of these states. However, one possibility is a relaxation through different intermediate states towards the bottom of the hot $\nu = 0$ state.

5.2.3 Conclusion

The NH band consist of a main peak and a sequence of satellite peaks, which correspond to a free exciton and a series of self-trapped states. Upon frequency selective excitation, the free-exciton and the lower lying self-trapped states behave distinctly different on a sub-picosecond time scale. When exciting the free-exciton [Fig. 5.16(d)], a strong bleach and stimulated emission signal is observed which recovers on a 400 fs time scale. Simultaneously, population is transferred into lower lying self-trapped states. On the other hand, when pumping one of the self-trapped states directly [Fig. 5.16(b)], population within all self-trapped states equilibrates essentially instantaneously, but the free exciton peak is not back-populated. This is a direct observation of ultrafast self-trapping: Excitation

of the free-exciton leads to an irreversible population of self-trapped states, but not vice versa.

The transient absorbance change signal of the NH mode in ACN shows, upon impulsive excitation, pronounced oscillations that persist up to about 14 ps. The oscillations contain two distinct frequency components whose temperature dependence and frequencies match perfectly with two phonon bands in the non-resonant electronic Raman spectrum of ACN. Therefore, the beating structure is assigned to ground state phonon wavepackets. The wavepackets are excited through a stimulated impulsive Raman effect, which is resonantly enhanced by the NH absorption band as a consequence of anharmonic coupling to lattice phonons. These phonons modulate the hydrogen bond distance and are thus the phonons that mediate self-trapping.

6 Comparison between acetanilide and N-methylacetamide*

Compelling evidence for vibrational self-trapping in hydrogen bonded systems has so far only been gathered for crystalline ACN. However, the self-trapping mechanism, described in Chapter 3.5 is expected to be generic, and should occur in any crystal with quasi-one-dimensional hydrogen bonds. In particular one expects to observe it in N-methylacetamide (CH_3–CONH–CH_3, NMA), which is often regarded to be *the* model compound for peptides and proteins. Both crystals, ACN and NMA, have an orthorhombic structure and consist of quasi-one-dimensional chains of hydrogen-bonded peptide units with structural properties that are similar to those of α-helices [Fig. 6.1 and Fig. 5.1].[76,77] Nevertheless, no convincing experimental evidence for self-trapping in NMA has been found so far. This chapter follows the strategy to transfer the knowledge gathered for ACN, for which vibrational self-trapping is clear and by now well established, to NMA. To this end one compares the infrared absorption and the pump-probe spectra of the amide I and NH mode of four different hydrogen-bonded crystals: ACN, ACN-D_8, NMA and deuterated NMA (CD_3–CONH–CD_3, NMA-D_6). It will be shown that certain nonlinear spectroscopic fingerprints appear in comparable ways for all four molecules, from which one can conclude that the mechanism giving rise to the complex band shape of the NH and CO mode of all four crystals has the same origin.

6.1 Absorption spectrum

Figures 6.2(a)-(h) shows the absorption spectra in the spectral range of the NH mode of crystalline ACN, ACN-D_8, NMA and NMA-D_6 at high (250 K and 220 K) and low temperatures (≈30 K). Since the spectra are congested we will first discuss the contributions from other but the NH stretching band. We can identify CH stretching modes by comparing the C-deuterated with the non-deuterated compounds. Figure 6.2 shows that the CH modes appear around 3000 cm^{-1} (ACN 3005 cm^{-1}, 3042 cm^{-1}, 3058 cm^{-1}, 3118 cm^{-1}; NMA 2995 cm^{-1}, 2993 cm^{-1}). Another peak, which is not part of the NH band, is labelled with "A" in the ACN spectrum [see Fig. 6.2(e)] and has been assigned

*The work presented in this chapter has been published in:
J. Edler and P. Hamm, *Spectral response of crystalline acetanilide and N-methylacetamide: Vibrational self-trapping in hydrogen-bonded crystals*, Phys. Rev. B, **69**(21), 214301, (2004).

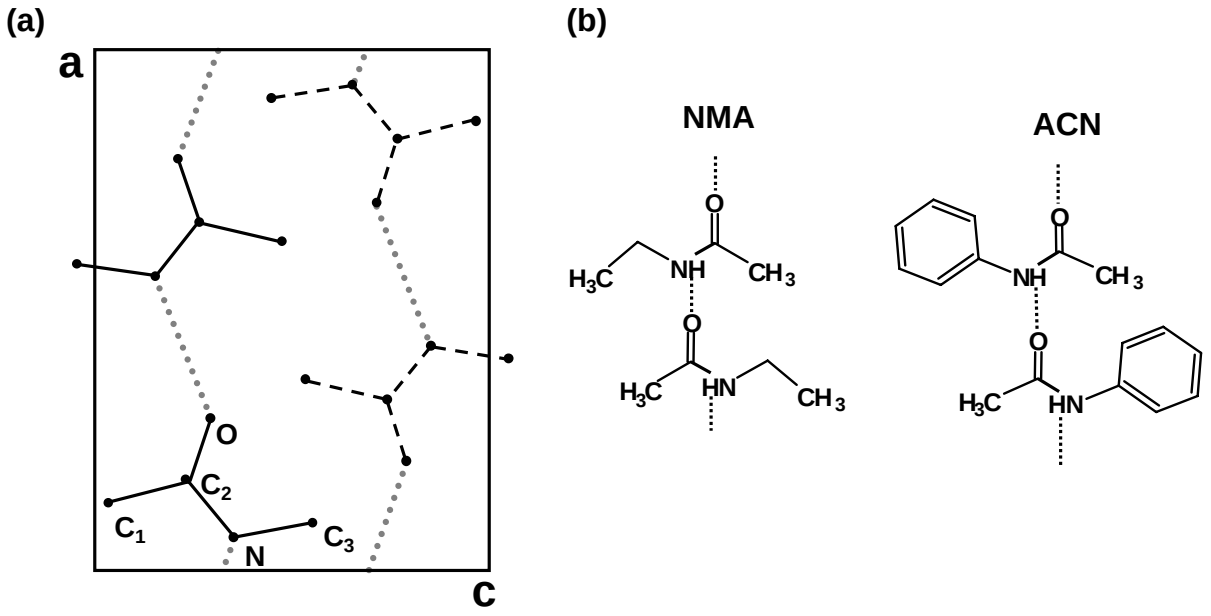

Figure 6.1: (a) Projection of the unit cell of crystalline NMA, which contains four molecules, in the *ac* plane (below phase transition, 303 K). Full bonds, molecules in the plane $b/4$; broken bonds, molecules in the plane $3b/4$. The grey lines depict the two hydrogen bonded chains, that run through a unit cell. Taken from Katz and Post.[77](b) Comparison between the structures of crystalline ACN and NMA. Both systems contain quasi-one-dimensional hydrogen bonded chains.

previously to an overtone of the amide I mode.[144] All spectra show a strong polarization dependence and most bands are only observed when the E vector is oriented parallel to the NH groups.[110,112] Only the bands B and B′ in the spectra of ACN and ACN-D_8 (ACN 2860 cm^{-1}, 2925 cm^{-1}; ACN-D_8 2860 cm^{-1}, 2913 cm^{-1}) show hardly any polarization dependence, and hence are attributed to overtone/combination modes of unknown origin.

If one combines the above observations and takes only the peaks into account that can be assigned to the NH band, one realizes that all four molecules exhibits an NH band which consists of a main band accompanied by a series of almost equidistant satellite peaks towards lower frequencies. The spacing between the satellite peaks is ≈60 cm^{-1} for ACN and ≈70 cm^{-1} for ACN-D_8. In NMA, the separation between the satellite peaks is about three times larger. The satellite peaks in NMA and NMA-D_6 further split into doublets at low temperatures [Figs. 6.2(g),(h)]. This splitting has been observed before and is of unclear origin.[162–164] In ACN the NH main peak at 3295 cm^{-1} is observed both in the parallel and in the perpendicular measurement, however, with a relative shift of 11 cm^{-1} [Fig. 6.2(a)]. The shift corresponds to the Davydov splitting, indicating that the main peak originates from a delocalized state, i.e. a free exciton state.[110]

Previous works have started from the assumption that the NH spectrum of ACN contains nine satellite peaks.[61,87,2,129,138] However, given the polarization dependence and the comparison with ACN-D_8, one must conclude that only the highest four satellite peaks

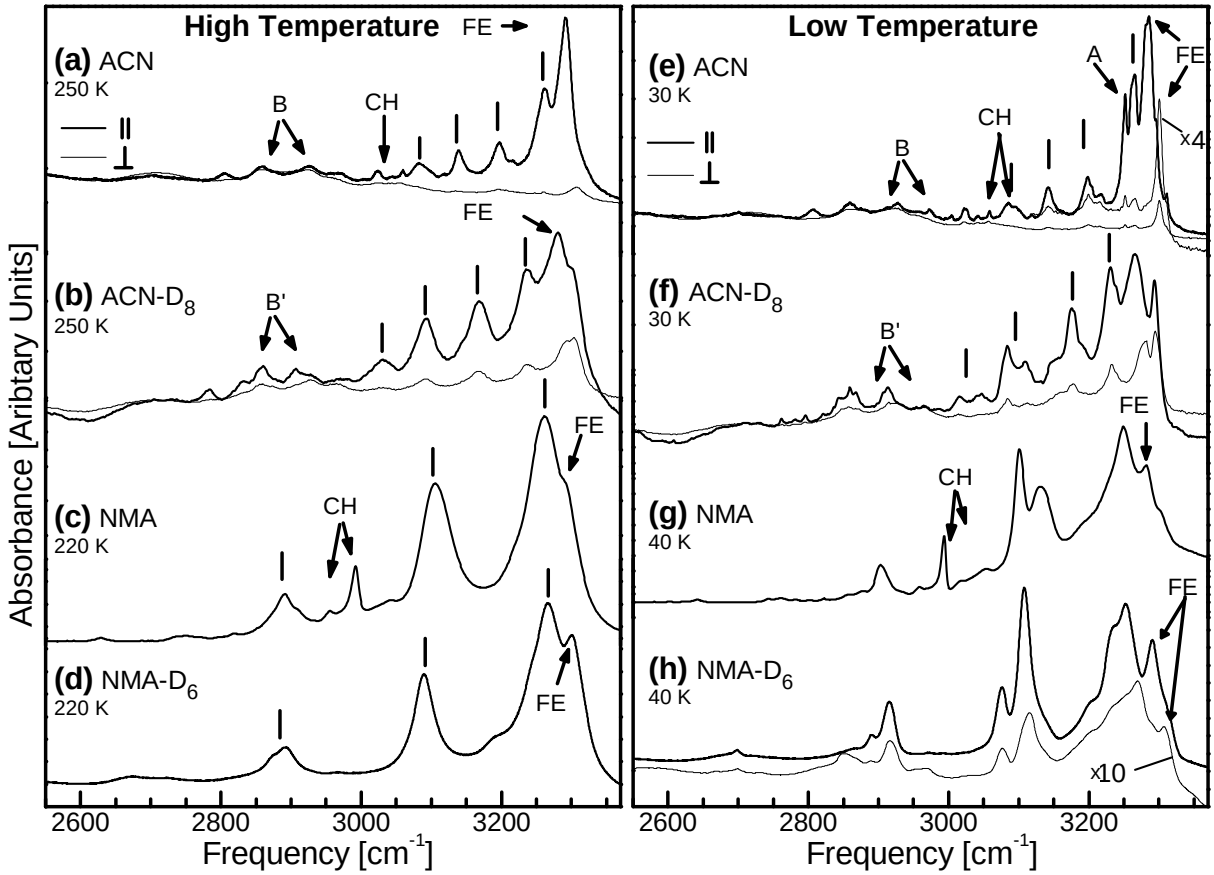

Figure 6.2: IR spectrum of the NH band of ACN, ACN-D_8, NMA and NMA-D_6 at high temperatures (a-d) and at low temperatures (e-h). All four crystals show similar band shapes, consisting of a main peak and a sequence of three to four satellite peaks. The CH modes, the amide I overtone (A) and the B modes are not part of the NH mode. The thick lines are for parallel polarization of the IR light with respect to the hydrogen bonded chain and the thin lines for perpendicular polarization (in ACN the b and c axes and in NMA the a and c axes). For NMA-D_6 the perpendicular spectra is magnified by a factor of 10. The self-trapped states are marked by black bars and the free exciton peak by FE.

are "real" (i.e. belong to the NH band), while the lower frequency part of the spectrum is perturbed by CH vibrations and weak overtones and/or combination modes.

Figures 6.3(a),(b) shows the absorption spectra of the amide I mode of ACN and NMA at different temperatures. As described before, an "anomalous" band appears at 1650 cm^{-1} in ACN with decreasing temperatures. The "normal" amide I band, on the other hand, splits into three subbands and decreases in intensity at low temperatures.[2,89,165] Interestingly, we also observe a temperature dependent side band in the amide I spectrum of NMA at 1634 cm^{-1}, whose separation from the main band, however, is about three times smaller than in ACN.

6.2 Nonlinear response

In this section we selectively excite the main peak and the satellite peaks in the NH spectrum of ACN and NMA using narrow band, tunable pump pulses [see Fig. 6.4]. For ACN we have discussed this response in detail in Chapter 5.2.2. In brief, the response of the free exciton state, which is, in case of ACN, the peak with the strongest intensity and the highest frequency, differs distinctively from that of the self-trapped states. Immediately after pumping the free exciton [Fig. 6.4(d)], a strong bleach and stimulated emission signal is observed at the position of that peak. Simultaneously negative signals appear at the position of the self-trapped states. On the other hand, when exciting one of the self-trapped states directly [Fig. 6.4(g)], we observe negative signals at the position of all self-trapped states, but not at the position of the free exciton.

Interestingly, a similar signal is also found in the pump-probe response of NMA and NMA-D_6, except that the free exciton no longer relates to the peak with the highest intensity, but to a shoulder on the high-frequency side (marked with "FE" in Figs. 6.2 and 6.4). Also this band shows a Davydov splitting between the parallel and perpendicular spectrum, an indication for a delocalized state [Fig. 6.2(h)]. Both in NMA and in NMA-D_6, a bleach of all bands is observed when the pump pulse is resonant with that shoulder, and the signal at the shoulder band decays on an ultrafast timescale comparable to the free exciton band in ACN [Fig. 6.5 and Fig. 5.14]. A direct excitation of one of the satellite peaks, on the other hand, reveals negative signals for all bands except for that shoulder, just as an excitation of a self-trapped state in ACN. In conclusion we observed also in NMA two different types of states, whose nonlinear response matches the free exciton and the self-trapped state in ACN.

In case of NMA and NMA-D_6 oscillations in the pump-probe signal are, in contrast to ACN and ACN-D_8 not observed. In ACN and ACN-D_8 such beating pattern identifies the phonons that mediate self-trapping (see Chapter 5.2.1). Since the splitting between

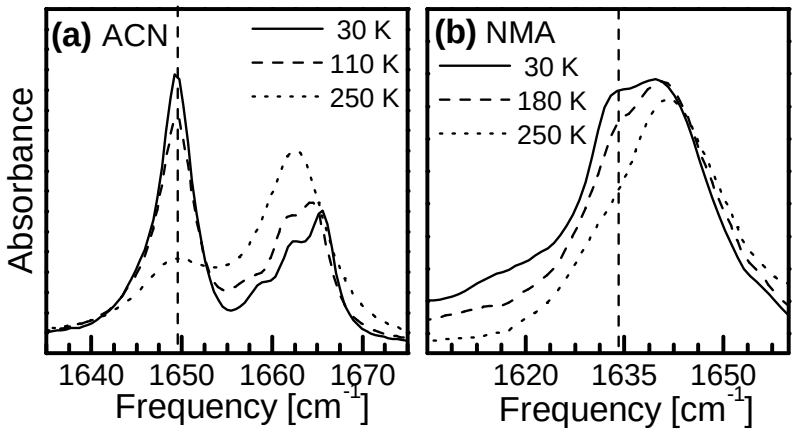

Figure 6.3: IR spectrum of the amide I band of crystalline (a) ACN and (b) NMA at three different temperatures. The vertical line marks the position of the temperature dependent sideband. The IR light was polarized parallel to the hydrogen bonded chain.

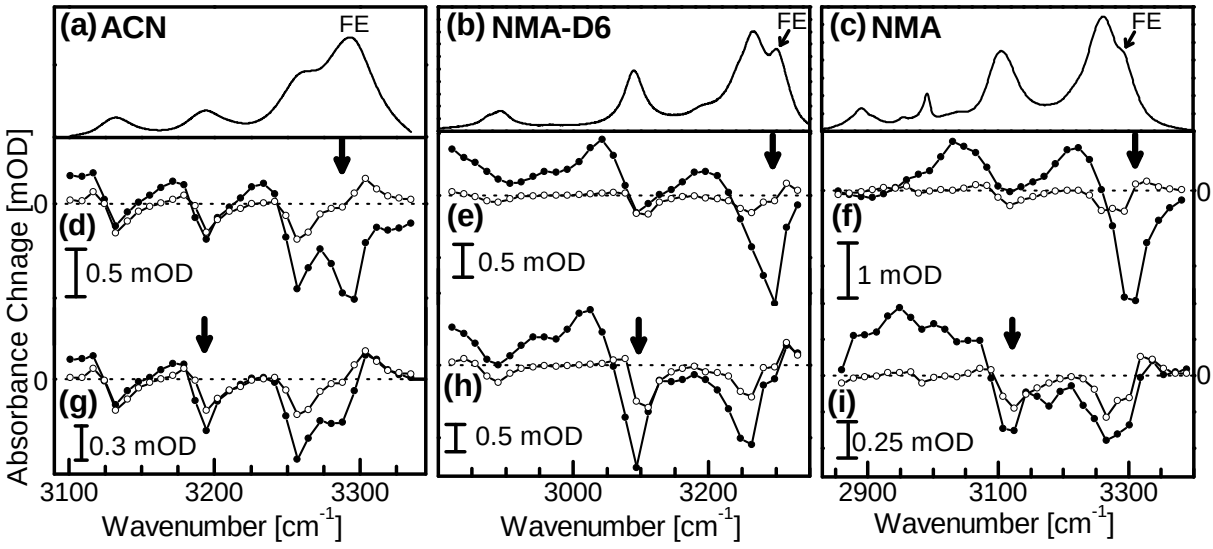

Figure 6.4: Sections of the NH band of (a) ACN, (b) NMA-D_6 and (c) NMA. Pump-probe response after selective excitation of the free exciton state (d,e,f) and of the second self-trapped states (g,h,i) for 400 fs (•) and 4 ps (○) delay times between the pump and the probe pulse. The arrows indicate the position of the narrow band pump pulse. All three molecules show qualitatively similar responses.

the satellite states is about three times larger in NMA than in ACN [Fig. 6.2(a-d)], one expects that the frequency of the corresponding phonon modes is larger by about the same factor. Part of this difference might be explained by the smaller mass of NMA. Such a high frequency mode would be at the detection limit of our setup, which is determined by the IR pulses duration. Technical improvements, i.e. pulse compression techniques, might make it possible to uncover these modes in the future. It could be also possible that the lifetime of the phonons in NMA are significantly shorter than in ACN, as suggested by the broader Raman lines,[162] and that they are thus much harder to detect.

6.3 Conclusion

In the case of crystalline ACN, it has been established in Chapter 5 that the signatures in the CO and NH spectra are an indication of vibrational self-trapping. The spectral appearance of ACN is very special, with probably the clearest manifestation of vibrational self-trapping. Nevertheless the spectral response of crystalline NMA shows striking similarities, from which one concludes that the mechanism behind the complicated band shapes is the same in both cases. For both, crystalline ACN and NMA, one observes (i) a temperature dependent amide I mode, (ii) a sequence of satellite peaks in the NH band and (iii) two different types of states in the pump-probe signal of the NH mode, reflecting a free exciton and a self-trapped state. This findings suggest that the sequence of satellite peaks in the absorption spectrum of the NH mode in NMA corresponds to self-trapped states. Hence, one can speculate that self-trapping is not a unique property of crystalline

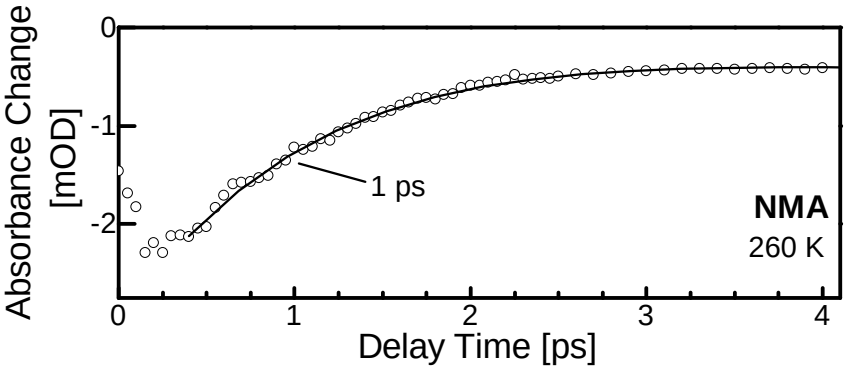

Figure 6.5: Transient signal of NMA after selective excitation of the free exciton peak of the NH band. The signal recovers on a 1 ps timescale.

ACN, but a general phenomenon in hydrogen-bonded crystals. This is indeed expected since the theory behind vibrational self-trapping is rather general. It essentially only depends on two coupling parameters, the exciton coupling and the exciton-phonon coupling, which are expected to be similar in crystals of comparable structure.

Previously the first two satellite peaks in the NH band of NMA (3100 cm^{-1} and 3250 cm^{-1}) have been assigned to a Fermi resonance with the amide II mode and were referred to as amide A and B modes.[166,167] The remaining bands in the sequence of satellite peaks (2650 cm^{-1} and 2900 cm^{-1}) have been interpreted as Fermi resonances with the overtone of the amide III band and a combination mode of amide II + amide III.[168] The Fermi resonance interpretation for the NH band in NMA has been questioned frequently in the literature.[112,162,169,170] Temperature dependent infrared and Raman studies on NMA and various isotopic species showed that a simple Fermi interpretation can not account for the two intense peaks in NMA. The present work provides strong evidence that vibrational self-trapping at least contributes to the peculiar line shape of NMA. The Fermi resonance picture completely ignores the effect of hydrogen bonding on the NH mode. It is well known that the NH mode in hydrogen-bonded systems strongly couples to low frequency vibrations of the hydrogen bond itself.[66,67] Both coupling mechanisms, Fermi resonance and coupling to low frequency modes, can coexist in a hydrogen-bonded system and hence one should consider both to understand the complex NH bandshape in polypeptides. Recent theoretical studies haven taken both coupling mechanisms into account to describe the spectra of hydrogen-bonded vibrational modes.[171,172] The simulations result in band shapes that depend strongly on the relative strength of the two couplings and range from a typical Fermi resonance doublet to complex substructures with regularly spaced sidebands.

In short, the comparison between the absorption and pump-probe spectra of ACN and NMA, both model systems for polypeptides, indicates that self-trapping is a common feature of hydrogen bonded systems. Hence one might expect that α-helices also exhibit self-trapping. This hypothesis is investigated in the following chapter.

7 Self-trapped states in α-helices *

Vibrational self-trapping in α-helices has been predicted over 30 years ago by Davydov and has since then been discussed extensively in theoretical studies [see Chapter 3.5]. An α-helix [see Fig. 1.3] consists of a helical sequence of peptides, which is stabilized by three one-dimensional (1D) chains of hydrogen bonds that run along the outside of the helix. In the previous chapters vibrational self-trapping has been investigated in detail for hydrogen bonded crystals, which are considered to be model systems for α-helices. By now, experimental evidence for vibrational self-trapping in hydrogen bonded crystals is well established. However, so far compelling experimental evidence for self-trapping in real α-helices or proteins is extremely rare. Previously only an anomalous temperature dependence in the NH-spectrum of α-helical polyalanine[47] and a lengthened lifetime of certain vibrational states in myoglobin[48,49] have been interpreted in terms of vibrational self-trapping. However, these conclusions were rather indirect and a clear connection to self-trapping theory was not shown (one can think of many other effects that modify the lifetime or intensity of a vibrational state). In the following chapter pump-probe spectroscopy is used to monitor self-trapped states in an α-helix directly directly through their anharmonicity. A quantitative comparison with polaron theory indicates that the observed nonlinear spectra are signatures of self-trapped states.

7.1 Pump-probe spectra of poly-γ-benzyl-L-glutamate

For the investigation of vibrational self-trapping in α-helices poly-γ-benzyl-L-glutamate (PBLG) was chosen as a sample, because it forms extremely stable, long α-helices in both helicogenic solvents and films grown from these solvents.[113] The monomeric unit of PBLG is a non-natural amino acid with a long side chain that stabilizes the helix. Nevertheless, the helix backbone is identical to that of natural helices [see Fig. 4.6(a)]. Because of its stability, PBLG has served as the standard model helix since the very early days of structural investigations of proteins.[113] Numerous studies, including theoretical methods,[173–176] infrared sperctroscopy,[114,120,122,166] light scattering,[113,177–179] optical rotation,[117,124,180,181] X-ray diffraction[182,183] and Nuclear Magnetic Resonance[121,126,184] have confirmed the α-helical conformation of PBLG in different solvents and films grown from these solvents.

*Parts of this chapter haven been published in:
J. Edler, R. Pfister, V. Pouthier, C. Falvo, and P. Hamm, *Direct observation of self-trapped vibrational states in α-helices*, Phys. Rev. Lett. **93**(10), 106405, (2004).

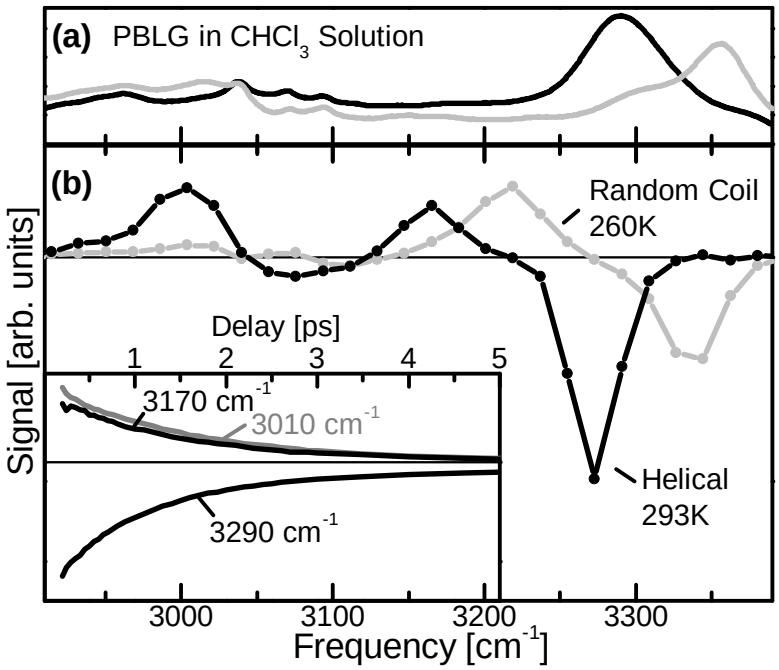

Figure 7.1: (a) Absorption spectra of PBLG in chloroform with 3% TFA at 293K (black line, helical conformation), and at 260K (grey line, random coil). (b) pump-probe spectra 600 fs after excitation under the same conditions. Insert: Decay of negative and both positive bands at 293 K.

Figure 7.1(a) (black line) shows the absorption spectrum of a PBLG helix in chloroform solution with 3% trifluoroacetic acid (TFA) at 293 K after substraction of the solvent background. The spectrum is dominated by the strong NH stretching band at 3290 cm^{-1}. Fig. 7.1(b) (black line) shows the pump-probe response of the helix 600 fs after excitation with an ultrashort broadband excitation pulse [spectral width: 200 cm^{-1}, pulse duration: 150 fs (FWHM)]. One finds a negative band at 3280 cm^{-1} and two positive bands at 3160 cm^{-1} and 3005 cm^{-1}, respectively. The two positive peaks are very characteristic for the helical state and appear under almost any condition (see below).[a]

At a concentration of 3% TFA in chloroform the PBLG helix unfolds below 268 K [see Chapter 4.2.2]. Figure 7.1(a) (grey line) shows the absorption spectrum of unfolded PBLG at 260 K, where the NH band is blue-shifted to 3355 cm^{-1}. In an intact helix, the NH-groups form *intra*molecular hydrogen-bonds with C=O groups from the next helix turn, while they form *inter*molecular hydrogen bonds with TFA molecules in a random coil configuration (which is why TFA destabilizes the helix). The latter are weaker hydrogen bonds, explaining the blue-shift of the NH band. The negative band in the pump-probe spectrum [Fig. 7.1(b), grey line] shifts accordingly. However, the important difference to the helical configuration is that only *one* positive band is observed in the random coil configuration.

[a]The systematic shift of ≈-10 cm^{-1} between absorption band and bleach signal is attributed to disorder broadening, where the more delocalized states with higher dipole strength, that are located at the low frequency side of the spectrum, contribute stronger to the nonlinear response.

If the NH stretching vibrators were isolated from other peptide units in the α-helix as well as from other normal modes within one peptide unit, one would expect the usual pump-probe response of anharmonic oscillators [see Chapter 3.2]: a negative band at the frequency of the NH fundamental associated with bleach ($\nu = 0 \rightarrow \nu = 1$) and stimulated emission ($\nu = 1 \rightarrow \nu = 0$), and a positive band associated with excited state absorption ($\nu = 1 \rightarrow \nu = 2$). The excited state absorption band is expected to be red-shifted with respect to the bleach and stimulated emission signal due to the intrinsic anharmonicity of the oscillator. This kind of pump-probe response is very characteristic and is always observed when isolated molecules are vibrationally excited (see Chapter 3.2 or Ref. 185 and many other examples). When the molecule is unfolded, the individual NH groups indeed appear to be isolated and we obtain exactly the expected response with an anharmonicity of $\omega_{01} - \omega_{12} \approx 120$ cm^{-1}, which compares well with the NH mode in isolated NMA [≈ 140 cm^{-1}, see Fig. 3.1(a)]. In contrast, the observation of *two* positive bands for the intact helix [Fig. 7.1(b), black line], rather than just one, is *exceptional*.
Numerous test experiments were performed to find the origin of the double-peak spectral signature:

- *Temperature Dependence*: In a film, the helix does not unfold even at temperatures as low as 18 K. In that case, the double peak structure stays the same over the whole temperature range from 18 K to 293 K [Fig. 7.2(b)]. This finding proofs that the spectral change in Fig. 7.1(b) is not a direct temperature effect, but indirect through a temperature induced structural change of the helix.

- *Polarization Dependence*: The anisotropies of both positive bands are identical and agree with that of the bleach/stimulated emission signal [Fig. 7.2(c)]. Hence, the transition dipoles of all signals are parallel.

- *Time Dependence*: When varying the pump-probe delay time, both the positive and the negative bands decay in parallel with a 1.5 ps time constant [Fig. 7.1(b), insert]. This indicates that all these bands originate from one state, and disappear simultaneously as this state decays.

- *Fully C-Deuterated PBLG*: The absorption spectrum of hydrogen containing PBLG exhibits small bands between 2900 and 3100 cm^{-1} [Fig. 7.2(a), black line], which are mostly due to CH stretching vibrations. They can be eliminated by C-deuterating the helix [Fig. 7.2(a), grey line]. The pump-probe response of fully C-deuterated PBLG [PBLG-D11; Fig. 7.2(d)] reveals the same double peak structure as PBLG, showing that the CH bands do not contribute.

- *Narrow Band Excitation*: When eliminating the CH stretching vibrations, a further small band (3050 cm^{-1}) remains, which is assigned to a weak overtone or combination mode. In order to assure that the overtone does not contribute, we performed frequency selective pump-probe experiments on PBLG-D11 with narrowband pump

pulse [bandwidth: 30 cm^{-1}, pulse duration: 250 fs (FWHM)]. The pump pulse spectra are shown in Fig. 7.2(e) as dashed lines. The result shows that the double peak structure appears only when pumping the NH band, while no measurable signal is obtained when pumping the overtone.

- *Intensity Dependence*: Multiphoton excitation can also result in a pump-probe spectrum with two positive absorption bands, corresponding to the $\nu = 1 \rightarrow 2$ and the $\nu = 2 \rightarrow 3$ excited state transitions. In this case the intensity ratio between the two transitions depends on the intensity of the pump pulse. In PBLG, multiphoton excitation is excluded by reducing the pump pulse intensity by a factor of 4 [Fig. 7.2(f)], still revealing the double peaks with the same intensity ratio.

Summarizing the experiments, one concludes that the two positive bands observed in the pump-probe response originate from the NH band, require an intact helix structure and represent transitions to two-quanta states. One can find two mechanisms, polaron formation and Fermi resonances, which result in excited state absorption bands that fulfill these requirements. In the following we will first discuss polaron theory and then turn to Fermi resonances to see which of these two theories can explain the pump-probe response in PBLG.

7.2 The polaron model

In an α-helix the individual NH oscillators are coupled by dipole-dipole interaction to form a delocalized state, called vibrational exciton or vibron [see Chapter 3.3]. Since the structure of the helix is translational invariant one describes the external dynamics of the peptide units as phonon modes. The strong nonlinearity of the hydrogen bonds, which stabilize the structure of the helix, couples the vibrons to these phonon modes and adds in this way a degree of freedom, that exists only in the helical state.

In this context Pouthier and co-workers have recently investigated the two-vibron dynamics in α-helices with special emphasis on the interplay between the intramolecular anharmonicity and strong vibron-phonon coupling.[97,98] The result of their work is summarized briefly in the following, for more details see Chapter 3.5. According to Davydov's theory,[1] the system can be described as a 1D chain formed by N periodically distributed peptide groups. Each group in this lattice contains a NH stretching vibration, which behaves as a high frequency anharmonic oscillator coupled to acoustic phonons.[b] The vibrational excitations reduce to anharmonic vibrons dressed by a virtual cloud of phonons, i.e. to small polarons. Both the intrinsic anharmonicity and the dressing effect favor the formation of two-polaron bound states. A two-polaron bound state corresponds to the trapping of two quanta of vibrational energy over a few neighboring peptide sites with an

[b]The absence of optical phonons in an α-helix may explain the absence of side peaks in the NH absorption spectrum[3] that are typically observed in molecular crystals such as ACN.

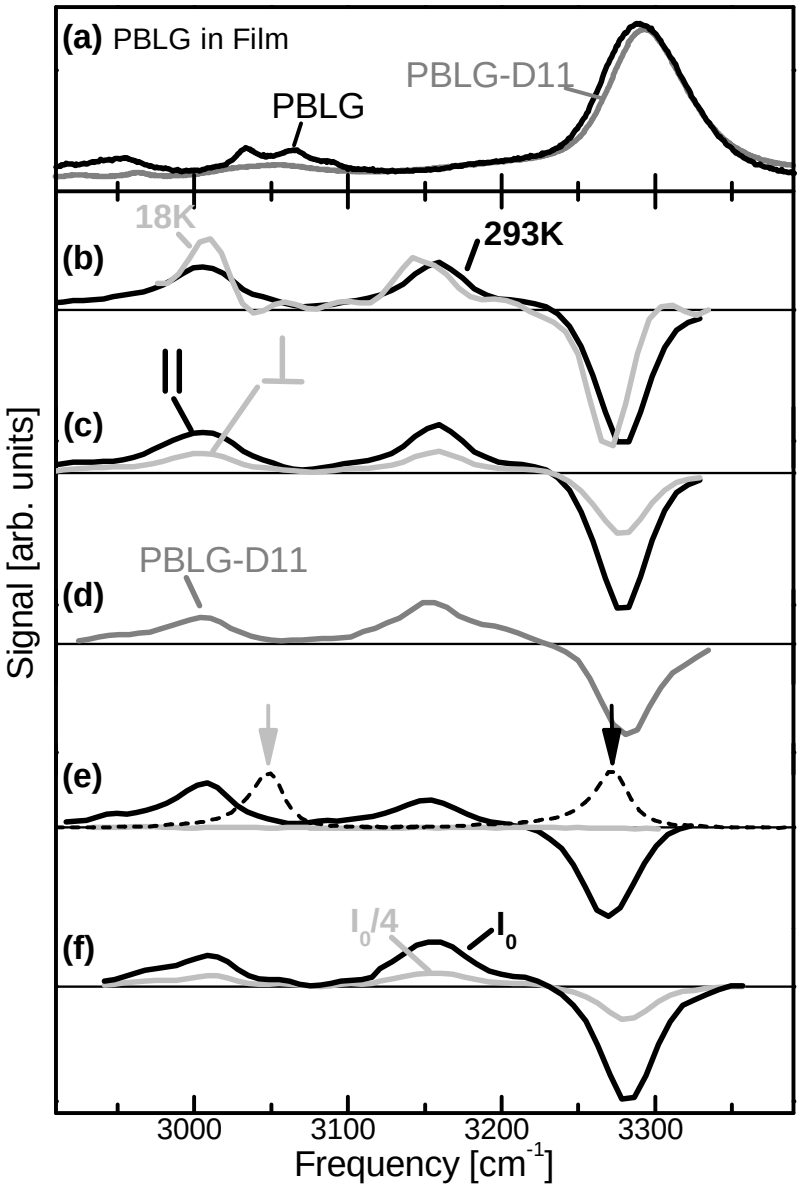

Figure 7.2: (a) Absorption spectra of PBLG (black) and fully C-deuterated PBLG (grey) in films grown from chloroform solution. (b) pump-probe response at 293 K (black) and 18 K (grey). (c) Polarization dependence of pump-probe response. (d) pump-probe response of fully C-deuterated PBLG (PBLG-D11). (e) Pump-probe response of PBLG-D11 upon narrow band excitation at 3272 cm^{-1} (black) and 3047 cm^{-1} (grey). The pump pulse spectra are shown as dashed black lines. (f) pump-probe response with the pump pulse intensity varied by a factor of 4.

energy that is lower than the energy of two quanta lying far apart. The insert in Fig. 7.3 shows the corresponding energy spectrum. Here the energy is plotted versus the wave vector k, which belongs to the first Brillouin zone and is associated with the motion of the center of mass of the two bound states. The two-polaron energy spectrum exhibits then three types of states [see Fig. 7.3, insert]: (i) two-polaron free states (TPFS) be-

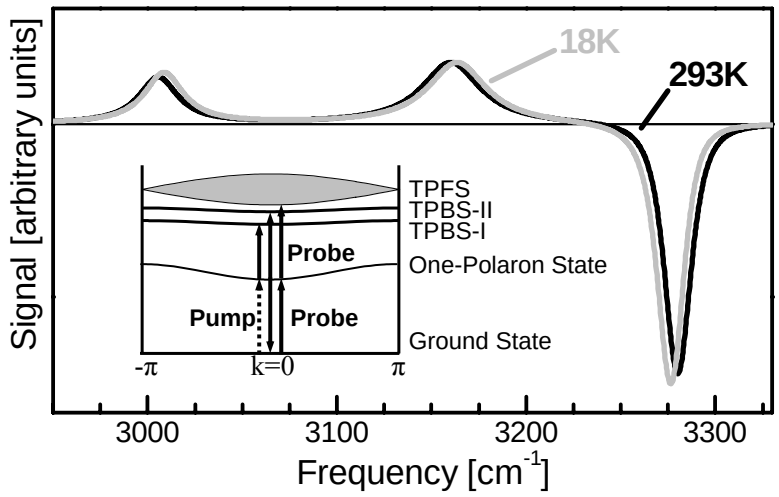

Figure 7.3: Simulated pump-probe spectrum for 293 K (black line) and 18 K (grey line) using the theory of Pouthier.[97]; for parameters see text. Insert: Schematic of the energy levels (not on scale). The arrows illustrate the interactions with the pump and probe pulses.

longing to an energy continuum which corresponds to two non-interacting polarons and consists of all possible combinations of one-polaron states, (ii) two-polaron bound states I (TPBS-I) which refer to the trapping of the polarons at the same site, and (iii) two-polaron bound states II (TPBS-II) which characterize polarons trapped at nearest neighbor sites. The TPBS-II appear as a signature of the acoustic nature of the phonons, that correlate adjacent sites.

Compared with a previous work,[97,98] which was devoted to the amide-I vibrations, Pouthier and Falvo made some modifications to account for the stronger nonlinearity of the NH modes.[186] First, the NH polaron hopping constant almost vanishes due to the dressing effect so that the polaron mass becomes infinite. Therefore, the TPFS bandwidth, as well as the dispersion of both bound state bands, are negligible. Second, in addition to the Davydov coupling (see Equ. 3.39), $\hat{H}_{int} = \sum_n \chi(\hat{u}_{n+1} - \hat{u}_{n-1})\hat{B}_n^\dagger \hat{B}_n$ (where $\hat{u}_n$ refers to the phonon displacement and $\hat{B}_n$ and $\hat{B}_n^\dagger$ stand for the vibron operators), a state-dependent coupling is introduced via an additional term $\hat{H}'_{int} = -\sum_n \chi'(\hat{u}_{n+1} - \hat{u}_{n-1})\hat{B}_n^{\dagger 2}\hat{B}_n^2$.

With these modifications Pouthier and Falvo used the theory detailed in Refs. 97 and 98 to compute the pump-probe signal of PBLG, using the following parameters: harmonic NH frequency $\omega_0 = 3520$ cm^{-1}, phonon cutoff frequency $\Omega_c = 100$ cm^{-1},[87] intramolecular anharmonicity $A = 60.0$ cm^{-1} (i.e. the anharmonicity of isolated NH groups in the unfolded helix), undressed hopping constant $J = 5$ cm^{-1}, i.e. a typical value for vibron hopping in proteins (see for instance Ref. 3), and small polaron binding energy $E_B = 84$ cm^{-1} (see for instance Ref. 87). The ratio χ'/χ is fitted to 0.22. Finally, an arbitrary linewidth is used which takes into account that the dephasing rate of TPBS-I is 1.5 times smaller than that of TPBS-II.[98]

Figure 7.3 clearly shows that the model reproduces the experimental pump-probe spectra [Figs. 7.1 and 7.2] very well. At $T = 293$ K, it reveals a single negative peak

located at 3280 cm^{-1} and two positive peaks located at 3005 cm^{-1} and 3160 cm^{-1}. The negative peak refers to the bleach and stimulated emission between the ground state and the zero wave vector one-polaron state.[c] This process overcompensates the absorption from the one-polaron state to the zero wave vector TPFS, which takes place at the same frequency. In contrast, the positive peaks located at 3005 cm^{-1} and 3160 cm^{-1} correspond to the excited state absorption from the zero wave vector one-polaron state to the zero wave vector TPBS-I and TPBS-II, respectively. From the theory one expects for the integrated intensities $I_{TPBS-I}/I_{TPBS-II}/I_{TPFS} \approx 1/2/-3$, in good agreement with the experiment [e.g Fig. 7.2(d)]. Note that these intensities are inherent to the model, and do not contain explicit fit parameters. Furthermore, the theoretical spectrum is almost temperature independent as a result of the infinite polaron mass due to the strong dressing effect [Fig. 7.3], again reproducing the experimental finding [Fig. 7.2(b)].

It should be noted that the self-trapped states in PBLG do not correspond to soliton-like excitations (e.g. "Davydov's soliton"), but instead to small polaron states. These polaron states (TPBS-I and TPBS-II) are not localized on a specific site in the α-helix, but correspond instead to a superposition of pairs of localized polarons (Equ. 3.47). The center of mass of such a superposition is fully delocalized over the α-helix.[97] Nevertheless, there is a localization of the separation distance between the two polarons, which is either zero sites for the TPBS-I or one site for the TPBS-II. Hence the TPBS are self-trapped with respect to the separation distance, but not with respect to a specific lattice site.

[c] In optical spectroscopy we are only able to observe $k = 0$ transitions, since the wavelength is much longer than a unit cell.

7.3 Fermi resonance

It has been argued that the NH band of proteins, peptides and peptide model systems is complicated by a Fermi resonance with the amide II mode (q_{AII}) at 1550 cm^{-1}.[147] In absorption spectroscopy the Fermi resonance is usually weak because of the large frequency mismatch ($2\Omega_{AII} - \Omega_{NH} \approx -200$ cm^{-1}). However, owing to the much larger intrinsic anharmonicity of the NH band, the resonance condition improves for the excited-state absorption bands. Quantum chemistry calculations show that the Fermi coupling between the NH and the amide II mode is very strong (100-200 cm^{-1}, see following paragraph). If the two states are nearly resonant and strongly coupled they mix and both can be excited in a pump-probe experiment. In this case, the double peak in the pump-probe spectra of PBLG could reflect a Fermi resonance between the first overtone of the NH mode ($2q_{NH}$) and the $q_{NH} + 2q_{AII}$ combination mode.

However, if the Fermi coupling is so strong that it causes a splitting of 160 cm^{-1} in the double excited NH state, it should also perturb the single excited NH state. In particular one would expect that the normally dark amide II overtone gains some oscillator strength due to the Fermi coupling and is hence observed as a weak band in the absorption spectrum. With a pump-probe experiment on the amide II band one can excite this overtone directly and thus determine exactly the frequency of the overtone band. In the following sections the Fermi resonance problem is analyzed in detail to see whether it can explain the nonlinear response of PBLG. First the strength of the Fermi coupling is estimated based on theoretical calculations and subsequently the expected absorption and pump-probe spectra are calculated and compared to the experimental data.

Quantum chemical calculation of the Fermi Coupling

The strength of a Fermi resonance between the NH mode and the amide II overtone is determined by the Fermi coupling δ, which is proportional to the term $\frac{\partial^3 V}{\partial q_{NH} \partial^2 q_{AII}}$ in the potential energy surface [see Chapter 3.6]. One can derive δ from a projection of the potential energy surface V onto the NH mode q_{NH} and the amide II mode q_{AII}. To that end hybrid density functional calculation were performed to obtain single points of the potential energy surface V for different displacements along the q_{NH} and q_{AII} mode. Since the PBLG helix or even just a PBLG monomer is a very large molecular system, a single NMA molecule was used as a model, as it contains the same peptide group as PBLG. The calculations were performed with the program *Gaussian 98*,[187] using the *B3LYP* functional[188] with a *6-311++G*** basis set and the *tight* option for the SCF convergence. After a geometry optimization with *very tight* convergence criteria, the normal modes were determined. Subsequently a two dimensional grid of at least 121 points of the potential energy surface was obtained by single point energy calculations. In order to estimate the Fermi coupling the function

$$f(q_{NH}, q_{AII}) = \frac{k_{NH}}{2} q_{NH}^2 + \Delta_{NH}^{(3)} q_{NH}^3 + \Delta_{NH}^{(4)} q_{NH}^4 + \frac{k_{AII}}{2} q_{AII}^2 + \Delta_{AII}^{(3)} q_{AII}^3 + \Delta_{AII}^{(4)} q_{AII}^4 + \delta q_{NH} q_{AII}^2 \quad (7.1)$$

was fitted to the potential energy surface grid. The coefficients k_{NH}, $\Delta^{(3)}_{NH}$, $\Delta^{(4)}_{NH}$, k_{AII}, $\Delta^{(3)}_{AII}$ and $\Delta^{(4)}_{AII}$ were obtained by two independent one dimensional fits along the q_{NH} and q_{AII} axes. The Fermi coupling δ was subsequently obtained from a two dimensional fit over the entire grid. The procedure was repeated for different maximal displacements along the q_{NH} and q_{AII} modes. The fits resulted in a Fermi coupling in the order of 140 cm^{-1}. Additional q^5_{NH}, $q^2_{NH}q_{AII}$ or $q^2_{NH}q^2_{AII}$ terms did not result in substantially different values for δ. Based on these calculations, the corresponding Fermi coupling in PBLG is estimated to be in the order of $100 - 200$ cm^{-1}.

Fermi resonance parameters

In the potential energy surface a Fermi resonance between the q_{NH} and the $2q_{AII}$ mode is described by the term $\delta q_{NH}q^2_{AII}$ [see Chapter 3.6]. If one considers only resonant terms one can write the Hamiltonian, using creation and annihilation operators, as

$$\begin{aligned}\hat{H} =&\hbar\Omega_{NH}\hat{B}^\dagger_{NH}\hat{B}_{NH} + \Delta_{NH}\hat{B}^{\dagger 2}_{NH}\hat{B}^2_{NH} + \hbar\Omega_{AII}\hat{B}^\dagger_{AII}\hat{B}_{AII}\\ &+ \Delta_{AII}\hat{B}^{\dagger 2}_{AII}\hat{B}^2_{AII} + \frac{\delta}{\sqrt{8}}\left(\hat{B}_{NH}\hat{B}^{\dagger 2}_{AII} + \hat{B}^\dagger_{NH}\hat{B}^2_{AII}\right),\end{aligned} \tag{7.2}$$

where Ω_{NH} and Ω_{AII} are the unperturbed frequencies of the NH and the amide II mode, Δ_{NH} and Δ_{AII} the respective intrinsic anharmonicities and δ is the Fermi coupling parameter. One can use the method outlined in Chapter 3.6 to calculate the corresponding pump-probe and absorption spectra. To that end one expands the Hamiltonian Equ. 7.2 in the basis

$$\{|0,0\rangle, |0,1\rangle, |0,2\rangle, |1,0\rangle, |2,0\rangle, |1,2\rangle, |0,4\rangle\}, \tag{7.3}$$

where the first digit labels the excitation of the NH mode and the second digit that of the amide II mode. Subsequently one solves the eigenvalue problem and calculates the transition dipole moments, which one needs in order to construct the absorption and pump-probe spectra. A scheme of the vibrational energy levels and transitions is sketched in Fig. 7.4, where the new states $|n_m\rangle$ correspond to the eigenstates of the Fermi resonance Hamiltonian 7.2. In such a picture the $|2_2\rangle \rightarrow |4_3\rangle$ and the $|2_2\rangle \rightarrow |4_2\rangle$ transitions would correspond to the two positive peaks in the NH pump-probe spectrum. The splitting between $|4_3\rangle$ and $|4_2\rangle$, and hence between the two positive peaks in the spectrum, is mostly determined by the Fermi coupling δ. The parameter Δ_{NH} shifts the $|2,0\rangle$ state into resonance with the $|1,2\rangle$ state, which is slightly perturbed by Δ_{AII}. Thus Δ_{NH} determines the intensity ratio of the two positive bands as well as the shift between the two positive peaks and the negative peak. Finally the effective anharmonicity of the amide II mode, which causes a signal in the amide II pump-probe spectrum, originates from both anharmonic contributions, Δ_{AII} and δ. Consequently the frequencies and intensities of the different transition in the system depend strongly on the interplay between the unperturbed frequencies, the intrinsic anharmonicities and the Fermi coupling. Hence one has to analyze

the Fermi resonance in detail to see whether it can indeed explain the nonlinear response of PBLG.

The energies of the states $|n_m\rangle$, that one excites in spectroscopy, depend on the five parameters of Hamiltonian 7.2 (Ω_{AII}, Ω_{NH}, Δ_{AII}, Δ_{NH} and δ). Since the $|0\rangle \rightarrow |1_1\rangle$ transition is not perturbed by the Fermi resonance one can determine the corresponding frequency Ω_{AII}, directly from the absorption spectrum. However, all other spectroscopic transitions are perturbed by the Fermi resonance and thus the remaining parameters cannot be measured directly. Nevertheless, the anharmonicities Δ_{AII} and Δ_{NH} can be estimated from pump-probe experiments on comparable NH or amide II modes ($\Delta_{NH} \approx 70$ cm^{-1} and $\Delta_{AII} \leq 16$ cm^{-1}, see Ref. 189 and Fig. 3.1), while the Fermi coupling δ is approximately known from the quantum chemistry calculation (100-200 cm^{-1}). In the following, different values are used for these parameters to calculate the absorption and pump-probe spectra of the NH and amide II modes. The comparison with the data shows that one can not simultaneously explain all four spectra by a Fermi resonance.

The calculations show in particular that a large Fermi coupling of about 100 cm^{-1} would result in an intense amide II overtone band in the absorption spectrum. This calculation, which is based on the parameters P1 in Table 7.3, is illustrated by the red line in Fig. 7.5(b). Experimentally one can exactly measure the frequency of the expected amide II overtone band, since it corresponds directly to the sum of the excited state absorption and bleach in the amide II pump-probe signal. As these two contribution clearly overlap in the spectrum [Fig. 7.5(a), black circles], one can only determine lower and upper limits for the excited state absorption (1542 cm^{-1} and 1552 cm^{-1}), which implies that the amide II overtone has a frequency between 3090 cm^{-1} and 3100 cm^{-1}. Figure 7.5(b) shows clearly that no absorption band exists in this spectral region except

	Parameters					*Observables*					
	δ	Ω_{NH}	Δ_{NH}	Ω_{AII}	Δ_{AII}	I	D	ν_1	ν_2	Ω_{NH}	Δ'_{AII}
	cm^{-1}					-	cm^{-1}				
Exp.				1550			155	3160	3005	3293	≤ 10
P1 (red)	90	3284	110	1550	0	0.50	142	3170	3028	3297	10
P2 (blue)	62	3283	114	1550	2	0.45	101	3138	3037	3296	9
P3 (green)	112	3283	106	1550	14	1.01	156	3162	3006	3294	42

Table 7.1: The table shows the different parameter sets used to calculate the spectra shown in Fig. 7.5. Only the amide II frequency Ω_{AII} can be determined from experiments. The parameters are defined by the Hamiltonian Equ. 7.2. The spectra are described by the splitting D and the intensity ratio I between the two positive peaks which emerge at ν_1 and ν_2 in the NH pump-probe spectra, by the NH absorption band at Ω_{NH} and by the effective anharmonicity Δ'_{AII} of the amide II mode.

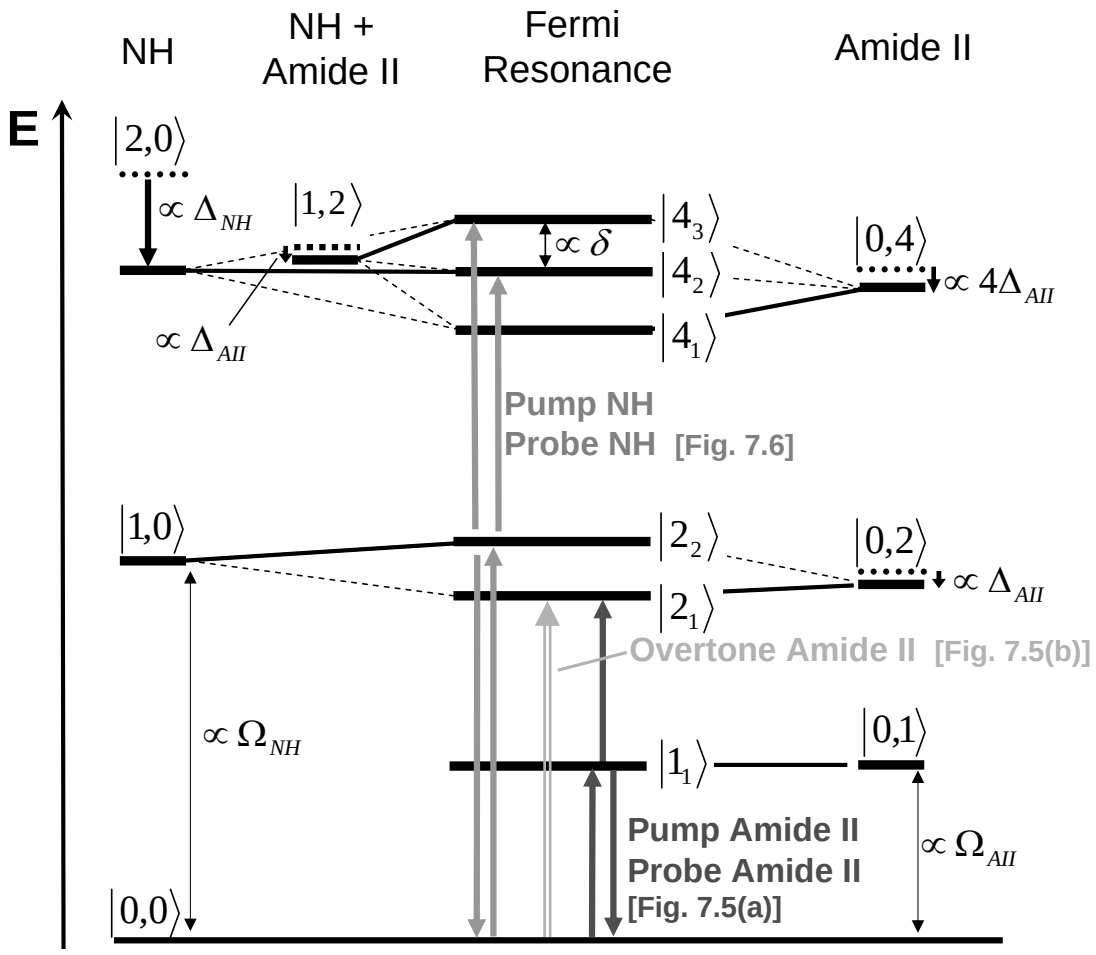

Figure 7.4: Vibrational energy levels in case of a Fermi resonance between the NH and the amide II mode. The $|n,m\rangle$ correspond to the unperturbed states, where n signifies an excitation of the NH mode and m one of the amide mode. The eigenstates of the Fermi resonance problem $|n_m\rangle$ are combinations of the unperturbed sates. The arrows illustrate the transitions observed in pump-probe and absorption spectroscopy. The dark grey arrows correspond to a pump-probe measurement on the NH mode [Fig. 7.6] and the black arrows to one on the amide II mode [Fig. 7.5(a)]. The light grey arrow depicts the transition to the amide II overtone, that one would observe in absorption spectroscopy [Fig. 7.5b].

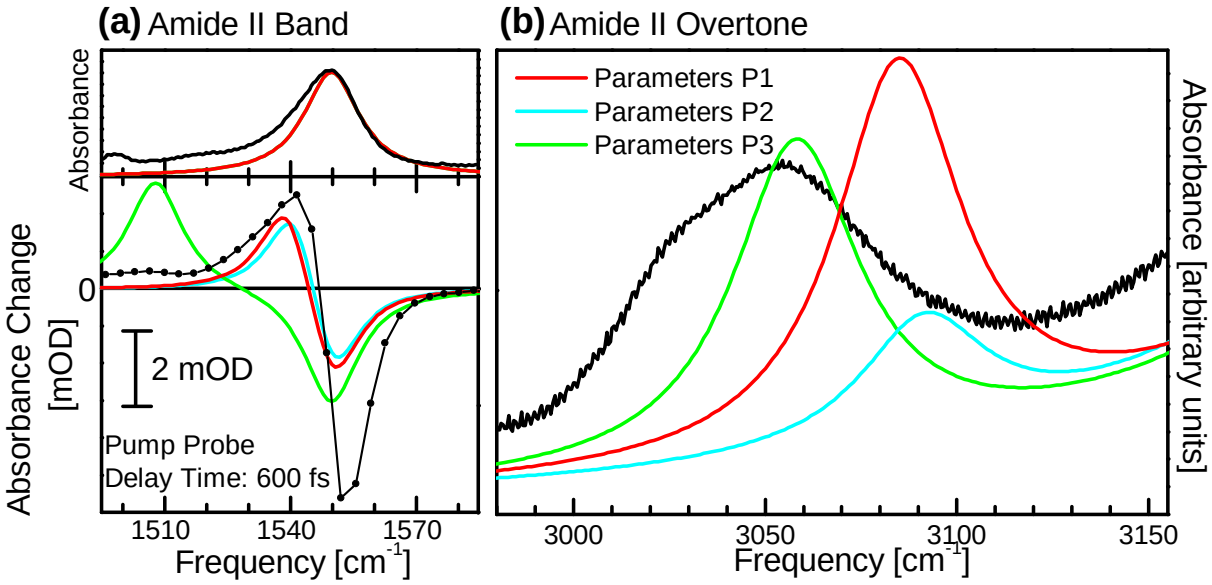

Figure 7.5: (a) Absorption and pump-probe spectrum of the amide II mode in a PBLG film (black lines). The colored lines illustrate the calculated response for the different parameters shown in Table 7.3; red: P1, green: P2 and blue: P3. The line widths (8 cm^{-1}) was chosen to match the experimental values. (b) Absorption spectrum of a deuterated PBLG Film in the spectral region of the amide II overtone. One expects, based on the amide II pump-probe spectrum to observe the Fermi resonant amide II overtone at about 3100 cm^{-1} (red line). Clearly there is no indication of an absorption band at 3100 cm^{-1}. The line width of the overtone (20 cm^{-1}) can be regarded as an upper limit for this band.

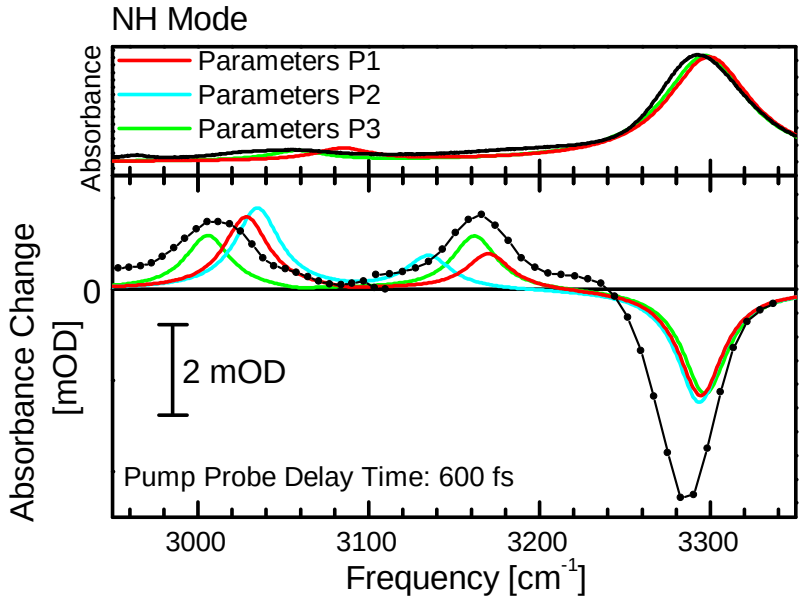

Figure 7.6: Absorption and pump-probe spectrum of the NH mode in a PBLG film. The colored lines illustrate the calculated response for the different parameters. The line widths were chosen to match the experimental values. Only the green line, which is completely inconsistent with the amide II pump-probe spectrum, can explain the NH response perfectly.

the broad band at 3050 cm^{-1}. However, if the band at about 3050 cm^{-1}, which seems to consist of two sub bands, were the overtone the excited state absorption would have to appear at ≈1510 cm^{-1} in the pump-probe spectrum [green line in Fig. 7.5], which is clearly in disagreement with the experimental observations. In conclusion the observed pump-probe and overtone spectra of the amide II mode do not allow a strong Fermi coupling.

Nevertheless, one could argue that a Fermi coupling which is smaller than the one predicted by the quantum chemical calculations, could explain the spectra, since such a coupling would result in an overtone that is so weak, that one can not observe it in the absorption spectrum. However, such a small Fermi coupling would result in a Fermi splitting in the NH pump-probe spectrum, that is too small and too asymmetric to be consistent with the NH pump-probe experiments (see blue lines in Fig. 7.5 and 7.6 and parameters P2 in Table 7.3). Of course one can find parameters that reproduce the splitting and the intensity ratio of the NH pump-probe spectrum exactly, e.g. the green lines in Fig. 7.6 and parameters P3 in Table 7.3. However, since such parameters require a large Fermi coupling δ and a large intrinsic anharmonicity Δ_{AII} they result in a huge effective anharmonicity Δ'_{AII} of the amide II mode (≈40 cm^{-1}) and can thus not at all describe the amide II pump-probe spectrum [Fig. 7.5, green line]. Hence one has to conclude that a Fermi resonance between the NH mode and the amide II overtone can not simultaneously explain the corresponding NH and amide II pump-probe and absorption spectra of PBLG, which is however what one expects from such a model. Nevertheless, as shown in Fig. 7.5(b) and Table 7.3, the Fermi resonance can describe the main feature of the data, i.e. the appearance of two intense positive peaks.

Pump-probe measurements on unfolded PBLG

Finally we want to see whether a Fermi resonance could explain the disappearance of the second positive peak in the NH pump-probe spectrum of unfolded PBLG. As described in Section 7.1 the NH mode shifts to 3355 cm^{-1} upon unfolding and one observes just one positive band. In contrast to the experiments, the Fermi resonance model yields for unfolded PBLG a nonlinear response consisting of two positive bands at 3200 cm^{-1} and 3070 cm^{-1} with an intensity ratio of almost 1 [light grey line in Fig. 7.7], if one assumes the same intrinsic anharmonicity Δ_{NH} for the folded state as for the unfolded state (parameters P1 with Ω_{NH}=3345 cm^{-1}). However, since the hydrogen bonds, which strongly alter the intrinsic anharmonicity of the NH mode, are weakened upon unfolding one can expect a decrease of Δ_{NH}. When one assumes that the intrinsic anharmonicity decreases to $\Delta_{NH} = 74$ cm^{-1}, the NH overtone ($2q_{NH}$) and the combination mode ($q_{NH} + 2q_{AII}$) are moved out of resonance and the calculated spectra fit perfectly to the experimental data [dark grey line in Fig. 7.7]. In short, when one assumes different anharmonicities Δ_{NH} for the folded and unfolded state, a huge Fermi coupling of δ=100 cm^{-1} can qualitatively explain the NH pump-probe spectrum for both conformations.

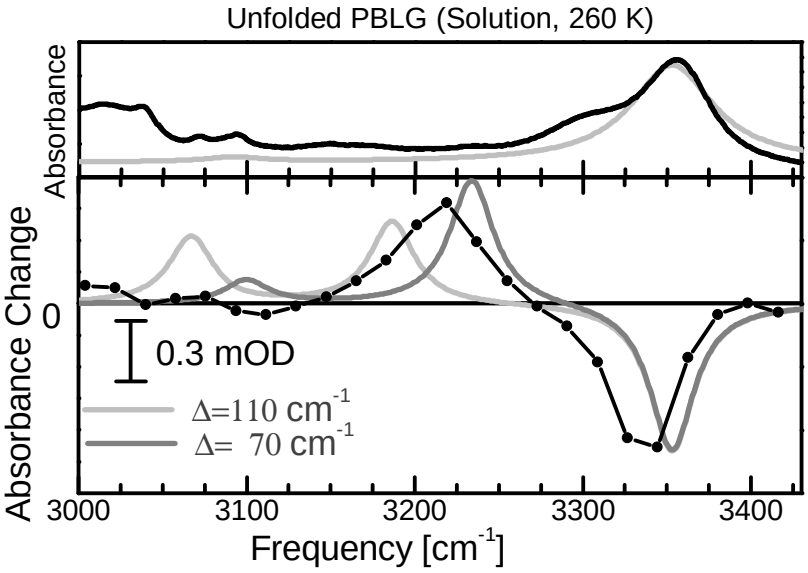

Figure 7.7: Absorption and pump-probe spectrum (pump-probe delay time: 700 fs) of unfolded PBLG in chloroform solution (with 3% TFA). The grey lines show the calculated response for two different NH anharmonicities. In order to explain the experimental data one has to assume that the NH anharmonicity decreases by 40 cm^{-1} upon unfolding.

Summary of the Fermi resonance hypothesis

The Fermi resonance model explains qualitatively the appearance of two positive peaks in the NH pump-probe spectrum of PBLG. In this picture the two positive peaks correspond to an excitation of the NH overtone ($2q_{NH}$) and of the combination band between NH mode and amide II overtone ($q_{NH} + 2q_{AII}$). Theoretical calculations show that such a Fermi resonance requires, besides a large intrinsic NH anharmonicity, a very strong (≈100 cm^{-1}) Fermi coupling. Quantum chemical studies prove that the Fermi coupling between the amide II overtone and the NH mode in a peptide group is in principle strong enough to cause such a resonance. However a Fermi resonance effects besides the double excited NH mode, also the single excited NH mode and the amide II overtone. Hence the Fermi resonance model has to explain simultaneously the NH and amide II pump-probe and absorption spectra. Figures. 7.5 and 7.6 show that it is impossible to explain all these signals with the same parameter set. In particular the amide II overtone, whose spectral position is exactly determined by the pump-probe experiments, is not found in the PBLG absorption spectrum, even though it should gain, due to the Fermi coupling, enough oscillator strength to be observable. The discrepancies could indicate that the two positive bands in the NH pump-probe spectra are either not caused by a Fermi resonance or that the chosen Fermi resonance model is too simple. The model considers the most elementary resonance: an overtone and a fundamental mode. More complicated Fermi resonances, such as combination modes instead of overtones or three level Fermi resonances might explain all features of the data. There are many modes below 1550 cm^{-1} in PBLG and hence many possible combinations, which could be resonant with the NH overtone.

In Ref. 186 we suggested that two-color pump-probe experiments, where the NH band is excited and the spectral range of the amide II mode is probed, could be used to test for Fermi resonances. However, in the context of new experiments, an in-depth analysis of the two-color data and the corresponding Hamiltonian showed that such measurements can, in case of PBLG, neither exclude nor confirm the Fermi resonance explanation. The experiments on the amide I mode in ACN show how 2D-IR spectroscopy can be used to differ Fermi resonances from self-trapping [Chapter 5.1.3]. In case of the NH mode in PBLG this approach is not possible, since the Fermi resonant overtone mode (the $|0\rangle \rightarrow |2_1\rangle$) has almost no intensity. Thus one expects in the 2D-IR spectrum just the response of the NH mode, instead of the striking square pattern, observed for Fermi resonant carbonyl modes.

7.4 Conclusion

The pump-probe spectrum of PBLG shows two positive peaks that appear only in the helical conformation. In the helical conformation the individual NH vibrations are correlated by acoustic phonons, which can enable the formation of polaron states, i.e. localized bound states. When the helical structure breaks down, the correlation vanishes and thus the bound states disappear. Polaron theory assigns the two positive peaks to the existence of two types of two-polaron bound states corresponding to the trapping of two polarons at the same peptide site and at nearest neighbor sites, respectively. The latter state originate from the overlap between a virtual cloud of acoustic phonons with each vibron.

Alternative explanations, such as multi photon excitation and CH and CH_2 vibrations have been successfully excluded based on pump-probe experiments. However one can suspect that a Fermi resonance between the NH and the amide II mode might be the origin of the two positive peaks. In the helical conformation the NH overtone and an amide II combination mode are in resonance, which could result in two positive bands in the NH pump-probe spectrum. When the helical structure breaks down the modes are moved out of resonance and thus the second positive band disappears. However, a Fermi resonance with the amide II mode can not explain consistently the absorption and pump-probe spectra of the NH and the amide II modes, indicating that this Fermi resonance interpretation is incorrect or at least incomplete. Still, as one could propose more complicated Fermi resonances, that might result in similar pump-probe spectra, one can not completely exclude a Fermi resonance as the origin of the two positive peaks.

Nevertheless, the most obvious Fermi resonance, the one with the amide II overtone, can clearly not explain the pump-probe spectra of PBLG. In contrast polaron theory can reproduce the spectra and assigns the two positive peaks to two kinds of bound states. In conclusion, femtosecond pump-probe experiments on the NH mode of a stable α-helix reveal a spectroscopic signature, which can be attributed to vibrational self-trapping.

8 Summary and outlook

The formation of localized states in solids originates from the interaction between (quasi)-particles, e.g. electrons or excitons, and lattice phonons. Such localized states have been observed or speculated upon in various materials and are generally known as polarons while the occurrence is commonly called self-trapping or self-localization. In the present study nonlinear spectroscopy has been used to identify and characterize vibrational self-trapped states in molecular crystals and α-helices. α-Helices represent one of the most common secondary structures in proteins, while molecular crystals serve as natural model systems for polypeptides. Both systems consist of quasi-one-dimensional hydrogen bonded peptide chains and are thus ideally suited to study self-trapping. Vibrational self-trapping in hydrogen bonded peptide chains is caused by combination of two coupling mechanisms: Excitonic coupling and exciton-phonon coupling.[3] Excitonic coupling arises from the electrostatic interactions between the individual vibrational oscillators of each peptide unit (i.e. the NH or C=O stretching modes), yielding a delocalized vibrational excitation. This so-called vibrational exciton couples through a nonlinear interaction, which is mediated by the hydrogen bonds, to lattice phonons. As a consequence, the initially delocalized vibrational exciton collapses to form a self-localized state. Even though originally self-trapping was suggested to occur in real α-helices, so far most experimental work has been performed on model systems, such as crystalline acetanilide (CH_3-CONH-C_6H_5, ACN). The strategy of this thesis is to first establish the nonlinear spectroscopic signatures of model systems and then to extend the study to real α-helices.

ACN, a molecular crystal that consists of hydrogen bonded peptide units, has been regarded since the early 1970s as a model system to study vibrational excitations in polypeptides and proteins. It is well established that the vibrational spectrum of ACN exhibits anomalies in the region of the amide I (i.e the C=O stretching) and the NH stretching band.[2] The amide I mode exhibits an anomalous sideband at low temperatures, while the temperature independent NH mode consists of a main peak, which is accompanied by an almost-regular sequence of satellite peaks. Both anomalies have been previously explained by self-trapping theory,[2,3] according to which the main peak represents a free exciton and the side bands represent self-trapped states.

In previous works self-trapping in ACN was observed through an indirect effect, namely the temperature dependence of the linear absorption spectrum.[2,3] The work presented here uses a more direct approach, namely nonlinear vibrational spectroscopy, to investigate self-trapping. The nonlinear vibrational response is exclusively sensitive to the

anharmonic part of the potential energy surface, since the response of a harmonic system vanishes exactly. Anharmonicity at the same time gives rise to nonlinear dynamics. Hence, nonlinear spectroscopy is extremely valuable to study nonlinear phenomena such as vibrational self-trapping.

One aim of this thesis is to confirm the self-trapping theory of the amide I mode in ACN. To that end pump-probe experiments are used to reveal the distinctively different anharmonicities of the two amide I sub-bands. Due to their nonlinear responses the "anomalous" band is attributed to a self-trapped state and the "normal" band to a delocalized, free exciton. In addition to this assignment, which agrees with previous studies, the pump-probe experiments show how thermal disorder localizes the free exciton (Anderson localization) at room temperature while it simultaneously destroys the self-trapping mechanism. Even though self-trapping is the most plausible explanation for the anomalous amide I band, alternative explanations such as Fermi resonances or conformational substates have been also discussed in the literature.[3] In the present work the two-dimensional infrared (2D-IR) spectrum of ACN is compared to those of molecular systems, which represent Fermi resonances and conformational substates and which show the same doublet in the C=O absorption spectrum as ACN. Based on the various 2D-IR spectra the two alternatives can be definitely excluded, while self-trapping of the C=O mode explains naturally the 2D-IR signature. Thus the study shows explicitly how nonlinear spectroscopy can distinguish between different anharmonic contributions in a way that is not possible with linear absorption spectroscopy. Here this capability is used to ultimately resolve the origin of the anomalous amide I band in crystalline ACN.

In contrast to the amide I band the NH band has been studied to a much lesser extent. This is surprising since one expects a significantly stronger anharmonicity for the NH mode with respect to the amide I mode, since the exciton-phonon coupling is about 5-10 times larger. In this thesis the first extensive experimental study on vibrational self-trapping of the NH mode in ACN is presented. The pump-probe experiments reveal a distinctively different nonlinear response for the free exciton with respect to the self-trapped states. On observes in particular an ultrafast irreversible energy transfer from the free exciton to the lower lying self-trapped states, which is interpreted as a signature of vibrational self-trapping. Yet, the strongest evidence for self-trapping is found upon impulsive excitation of the NH band. The response exhibits a pattern of pronounced oscillations that persist up to 14 ps and contain two frequency components. Since their temperature dependence matches perfectly that of two phonon bands in the Raman spectrum of ACN, the beating structure is attributed to a ground state phonon wavepacket. The phonons are excited due to the nonlinear exciton-phonon coupling, which also induces self-trapping. In this way the phonons which mediate self-trapping in ACN have been identified for the first time.

So far convincing evidence for vibrational self-trapping was only found in ACN. This is surprising since the self-trapping mechanism should be generic and one thus expects to observe self-trapping in any system with a comparable structure, that is a system that con-

sists of quasi-one-dimensional hydrogen bonded peptide chains. In this thesis self-trapping is studied in four hydrogen bonded crystals, namely ACN, NMA (N-methylacetamide, CH_3-CONH-CH_3) and carbon deuterated ACN and NMA. The NH absorption and pump-probe spectra of all these compounds show striking similarities, from which one concludes that the mechanism behind the band shapes is the same in all cases. Since the oscillations in the nonlinear response of ACN clearly demonstrate that the NH mode in ACN is coupled to low frequency phonons, the experiments suggest that the ones in NMA and in the deuterated derivatives are coupled to phonons as well. However, typically the NH band shape in NMA is attributed to Fermi resonances with amide modes.[166–168] Even though the previous Fermi resonance interpretation of NMA is based on theoretical calculations and agrees very well with experiments it has been controversially discussed in the literature. The presented work suggests that the usual assignment of the NH band in NMA solely to a Fermi resonance is not sufficient and that phonon coupling plays an important additional role. Thus the experiments indicate that future theoretical studies should consider the interplay between Fermi resonances and polarons to describe self-trapping and nonlinear spectroscopy on hydrogen bonded systems.

The previous paragraphs show how nonlinear spectroscopy can be used to verify self-trapping in molecular crystals. However these systems serve, in this respect, merely as model systems for real α-helices. Naturally the final goal is to see whether self-trapping can exist in real α-helical polypeptides. To that end an extremely stable and long α-helix, poly-γ-benzyl-L-glutamate (PBLG), has been studied. The pump-probe experiments on the NH mode reveal two excited state absorption signals (i.e. two positive bands), which appear only in the helical conformation. The observation of two excited state absorption signals, rather than just one, is exceptional for a vibrational oscillator. Extensive experiments allow only two plausible explanations: Fermi resonances or vibrational self-trapping. It is in general assumed that the NH band of polypeptides is complicated by a Fermi resonance with the amide II overtone.[147,166,167] However, an extensive analysis of the PBLG absorption and pump-probe spectra shows that such a Fermi resonance with the amide II mode is not the origin of the two positive peaks. On the other hand, self-trapping theory can clearly explain the appearance of the two bands. In this case the two states correspond to the trapping of two polarons at the same site in the helix or, respectively, at nearest neighbor sites. However, three points should be noted: (i) Only the most prominent Fermi resonance was excluded, that is the Fermi resonance between the NH mode and the overtone of the amide II mode. Clearly one can not rule out that more complicated Fermi resonances, e.g. three level Fermi resonances, can explain the pump-probe signal in PBLG. (ii) The self-trapped states in PBLG do not correspond to soliton-like pulses of vibrational energy, as originally suggested by Davydov, but instead to a superposition of pairs of localized polarons, so-called bound states. These states are self-trapped with respect to their separation distance, but not with respect to a specific lattice site on the helix. Evidence for an energy transport along a hydrogen bonded chain, as initially anticipated by Davydov,[1] has not been found. In future experiments

one could try to deposit energy at one end of an α-helix and then monitor the amide I or NH modes of individual peptides to examine the energy propagation. However, such an experiment would require isotopic labelling at specific sites, which might hinder or even destroy the self-trapping mechanism. (iii) The polaron theory, which explains the PBLG spectrum,[97,98] does not include the influence of the helical structure, as it is only based on a one-dimensional chain. In contrast to this, real helices are three-dimensional and the different hydrogen bonded chains, that run along the outside of the helix are coupled to each other. Future theoretical works should emphasize the structure of the helix and its effect on polaron formation and on spectroscopy.

In summary this thesis establishes the nonlinear spectroscopic signatures of vibrational self-trapping in the molecular crystals ACN and NMA. The experiments on ACN unambiguously prove that both, the amide I and the NH mode, exhibit self-trapping. Previous alternative explanations for the "anomalous" amide I mode are finally excluded and the phonons that mediate self-trapping are identified. Furthermore the thesis clearly demonstrates how self-trapping can explain the nonlinear response of the NH band in an α-helical polypeptide. As alternative explanations are successfully excluded one can conclude that this study presents the first convincing evidence of vibrational self-trapped states in α-helices, some 30 years after their prediction by Davydov.

Abbreviations

2D	two dimensional
2D-IR	two dimensional infrared
ACN	acetanilide (CH_3-CONH-C_6H_5)
ACN-D_8	fully C-deuterated acetanilide (CD_3-CONH-C_6D_5)
BBO	β-barium borate (β-BaB_2O_4)
DM	dichroic mirror
FWHM	full-width-half-maximum
IR	infrared
NMA	N-methylacetamide (CH_3–CONH–CH_3)
NMA-D_6	fully C-deuterated N-methylacetamide (CD_3–CONH–CD_3)
OPA	optical parametric amplifyer
PBLG	Poly-γ-benzyl-L-glutamate
PBLG-D11	fully C-deuterated poly-γ-benzyl-L-glutamate
rms	root-mean-square
TFA	trifluoro acetic acid
TPFS	two-polaron free state
TPBS-I	two-polaron bound state I
TPBS-II	two-polaron bound state II

References

[1] A. S. Davydov, *Solitons and energy-transfer along protein molecules*, J. Theor. Biol. **66**, 379 (1977).

[2] G. Careri, U. Buontempo, F. Galluzzi, A. C. Scott, E. Gratton, and E. Shyamsunder, *Spectroscopic evidence for Davydov-like solitons in acetanilide*, Phys. Rev. B **30**, 4689 (1984).

[3] A. C. Scott, *Davydov's soliton*, Phys. Rep. **217**, 1 (1992).

[4] P. S. Lomdahl, *What is a soliton ?*, Los Alamos Science **10**, 27 (1984).

[5] J. S. Russell, *Report on waves*, in *Rep. 14th Meet. British Assoc. Adv. Sci.*, edited by J. Murray, page 311, 1844.

[6] D. J. Kortweg and G. de Vries, *On the change of form of long waves advancing in rectangular channel, and on a new type of long stationary waves*, Phil. Mag. **39**, 442 (1895).

[7] E. Fermi, J. Pasta, and R. Ulam, *Studies of nonlinear problems*, Los Alamos Science Laboratory Report No. LA-1940 (1955), unpublished; reprinted in *Collected Papers of Enrico Fermi*, edited by E. Segre (University of Chicago Press, Chicago, 1965), Vol. 2, p. 978. Also in *The Many-Body Problem*, C. C. Mattis (Ed.), World Scientific, Singapore, 1993.

[8] M. Remoissenet, *Waves called solitons*, Springer-Verlag, Berlin, 2003.

[9] A. Scott, *Nonlinear science: Emergence and dynamics of coherent structures*, Oxford University Press, New York, 2nd edition, 2003.

[10] N. J. Zabusky and M. D. Kruskal, *Interaction of solitons in a collisionless plasma and recurrence of initial states*, Phys. Rev. Lett. **15**, 240 (1965).

[11] S. Flach, *Computational studies of discrete breathers*, in *Energy Localisation and Transfer*, edited by T. Dauxois, A. Litvak-Hinenzon, R. MacKay, and A. Spanoudaki, volume 22 of *Advanced Series in Nonlinear Dynamics*, World Scientific, Singapore, 2004.

[12] A. S. Davydov, *Solitons in molecular systems*, volume 61 of *Mathematics and its applications*, Kluwer Academic Publishers, Dordrecht, 1991.

[13] L. V. Yakushevich, *Nonlinear physics of dna*, Wiley-VCH Verlag-GmbH & Co KGaA, Weinheim, 2004.

[14] S. Aubry, *Breathers in nonlinear lattices: Existence, linear stability and quantization*, Physica D **103**, 201 (1997).

[15] Y. S. Kivshar and S. Flach, *Introduction: Nonlinear localized modes*, Chaos **13**, 586 (2003).

[16] S. Flach and C. R. Willis, *Discrete breathers*, Phys. Rep. **295**, 181 (1998).

[17] D. K. Campbell, S. Flach, and Y. S. Kivshar, *Localizing energy through nonlinearity and discreteness*, Phys. Today **57**, 43 (2004).

[18] A. A. Ovchinnikov, *Localized long-lived vibrational states in molecular crystals*, Zh. Eksp. Teor. Fiz. **57**, 263 (1969), [Sov. Phys. JETP, **30**, 147 (1970).].

[19] A. M. Kosevich and A. S. Kovalev, *Selflocalization of vibrations in a onedimensional anharmonic chain*, Zh. Eksp. Teor. Fiz. **67**, 1793 (1974), [Sov. Phys. JETP **40**,891 (1974)].

[20] A. S. Dolgov, *The localization of vibrations in a nonlinear crystal-structure*, Fiz. Tverd. Tela **28**, 1641 (1986), [Sov. Phys. Solid State, **28**, 907 (1986)].

[21] A. J. Sievers and S. Takeno, *Intrinsic localized modes in anharmonic crystals*, Phys. Rev. Lett. **61**, 970 (1988).

[22] J. B. Page, *Asymptotic solution of localized vibrational modes in strongly anharmonic periodic systems*, Phys. Rev. B **41**, 7835 (1990).

[23] Y. S. Kivshar, A. R. Champneys, D. Cai, and A. R. Bishop, *Multiple states of intrinsic localized modes*, Phys. Rev. B **58**, 5423 (1998).

[24] D. Cai, A. R. Bishop, and N. Grønbech-Jensen, *Localized states in discrete nonlinear SchrÖdinger-equations*, Phys. Rev. Lett. **72**, 591 (1994).

[25] Y. S. Kivshar, *Nonlinear localized modes in inhomogeneous chains*, Phys. Lett. A **161**, 80 (1991).

[26] G. Kopidakis and S. Aubry, *Localization and targeted energy transfer of atomic-scale nonlinear excitations: persepective for applications*, in *Energy Localisation and Transfer*, edited by T. Dauxois, A. Litvak-Hinenzon, R. MacKay, and A. Spanoudaki, volume 22 of *Advanced Series in Nonlinear Dynamics*, World Scientific, Singapore, 2004.

[27] E. Trías, J. J. Mazo, and T. P. Orlando, *Discrete breathers in nonlinear lattices: Experimental detection in Josephson array*, Phys. Rev. Lett. **84**, 741 (2000).

[28] P. Binder, D. Abraimov, A. V. Ustinov, S. Flach, and Y. Z. Y, *Observation of breathers in josephson ladders*, Phys. Rev. Lett. **84**, 745 (2000).

[29] M. Sato, B. E. Hubbard, A. J. Sievers, B. Ilic, D. A. Czaplewski, and H. G. Craighead, *Observation of locked intrinsic localized vibrational modes in micromechanical oscillator arrays*, Phys. Rev. Lett. **90**, 044102 (2003).

[30] H. S. Eisenberg, Y. Silberberg, R. Morandotti, A. R. Boyd, and J. S. Aitchison, *Discrete spatial optical solitons in waveguide arrays*, Phys. Rev. Lett. **81**, 3383 (1998).

[31] J. W. Fleischer, M. Segev, N. K. Efremidis, and D. N. Christodoulides, *Observation of two discrete solitons in optically induced nonlinear photonic lattices*, Nature **422**, 147 (2003).

[32] M. Sato and A. J. Sievers, *Direct observation of the discrete character of intrinsic localized modes in an antiferromagnet*, Nature **432**, 486 (2004).

[33] U. T. Schwarz, L. Q. English, and A. J. Sievers, *Experimental generation and observation of intrinsic localized spin wave modes in an antiferromagnet*, Phys. Rev. Lett. **83**, 223 (1999).

[34] V. Fleurov, *Discrete quantum breathers: What do we know about them?*, Chaos **12**, 676 (2003).

[35] F. Fillaux, C. J. Carlile, and G. J. Kearley, *Inelastic-neutron-scattering study at low-temperature of the quantum sine-Gordon breather in 4-methyl-pyridine with partially deuterated methyl-groups*, Phys. Rev. B **44**, 12280 (1991).

[36] F. Fillaux, C. J. Carlile, and G. J. Kearley, *Inelastic-neutron-scattering study of the sine-Gordon breather interactions in isotopic mixtures of 4-methyl-pyridine*, Phys. Rev. B **58**, 11416 (1998).

[37] T. Asano, H. Nojiri, Y. Inagaki, J. P. Boucher, T. Sakon, Y. Ajiro, and M. Motokawa, *ESR investigation on the breather mode and the spinon-breather dynamical crossover in Cu benzoate*, Phys. Rev. Lett. **84**, 5880 (2000).

[38] B. I. Swanson, J. A. Brozik, S. P. Love, G. F. Strouse, and A. P. Shreve, *Observation of intrinsically localized modes in a discrete low-dimensional material*, Phys. Rev. Lett. **82**, 3288 (1999).

[39] N. K. Voulgarakis, G. Kalosakas, A. R. Bishop, and G. P. Tsironis, *Multiquanta breather model for PtCl*, Phys. Rev. B **64**, 020301 (2001).

[40] J. W. Ellis, *Heats of linkage of C-H and N-H bonds from vibration spectra*, Phys. Rev. **33**, 27 (1929).

[41] R. Mecke, *Absorption investigations on hydrocarbons in the near infrared. IV. Calculation of anharmonic valency vibrations of polyatomic molecules*, Z. Phys. **99**, 217 (1936).

[42] R. Mecke, *The measurement of the electrical conductivity of associated substances*, Z. Elektrochem. **54**, 38 (1950).

[43] M. Quack, *Spectra and dynamics of coupled vibrations in polyatomic-molecules*, Annu. Rev. Phys. Chem. **41**, 839 (1990).

[44] R. Koradi, M. Billeter, and K. Wüthrich, *MOLMOL: a program for display and analysis of macromolecular structures*, J. Mol. Graphics **14**, 51 (1996).

[45] L. D. Landau, *The motion of electrons in a crystal lattice*, Phys. Zeit. Sowjetunion **3**, 664 (1933).

[46] P. L. Christiansen and A. C. Scott, editors, *Davydov's soliton revisited: Self trapping of vibrational energy in protein*, volume 243 of *NATO ASI Series*, Plenum Press, New York, 1990.

[47] V. Helenius, J. Korppi-Tommola, S. Kotila, J. Nieminen, R. Lohikoski, and J. Timonen, *Anomalous temperature dependence of the IR spectrum of polyalanine*, Chem. Phys. Lett. **280**, 325 (1997).

[48] R. H. Austin, A. Xie, L. van der Meer, M. Shinn, and G. Neil, *Self-trapped states in proteins ?*, J. Phys.: Condens. Matter **15**, S1693 (2003).

[49] A. Xie, L. van der Meer, and R. H. Austin, *Long-lived amide I vibrational modes in myoglobin*, Phys. Rev. Lett. **84**, 5439 (2000).

[50] G. Careri, *Cooperative phenomena*, Springer, Berlin, 1973.

[51] S. Mukamel, *Principles of nonlinear optical spectroscopy*, Oxford University Press, Oxford, 1995.

[52] P. Hamm, *Principles of non-linear spectroscopy – A lecture series based on Shaul Mukamel's book*, Lecture Notes, Max-Born Institute, Berlin, 2001.

[53] J. Stenger, *Ultrafast response of inter- and intramolecular hydrogen bonds in liquids: vibrational quantum beats and dephasing*, Logos Verlag, Berlin, 2002, PhD thesis.

[54] P. Hamm and J. Edler, *Nonlinear vibrational spectroscopy: a method to study vibrational self-trapping*, in *Energy Localisation and Transfer*, edited by T. Dauxois, A. Litvak-Hinenzon, R. MacKay, and A. Spanoudaki, volume 22 of *Advanced Series in Nonlinear Dynamics*, World Scientific, Singapore, 2004.

[55] J. Edler and P. Hamm, *Self-trapping of the amide I band in a peptide model crystal*, J. Chem. Phys. **117**, 2415 (2002).

[56] J. Edler and P. Hamm, *Two-dimensional vibrational spectroscopy of the amide I band of crystalline acetanilide: Fermi resonance, conformational substates or vibrational self-trapping ?*, J. Chem. Phys. **119**, 2709 (2003).

[57] P. Hamm, M. Lim, and R. M. Hochstrasser, *Structure of the amide I band of peptides measured by femtosecond nonlinear-infrared spectroscopy*, J. Phys. Chem. B **102**, 6123 (1998).

[58] A. S. Davydov, *Theory of molecular excitons*, Plenum Press, New York, 1971.

[59] S. Woutersen and P. Hamm, *Nonlinear two-dimensional vibrational spectroscopy of peptides*, J. Phys.: Condens. Matter **14**, R1035 (2002).

[60] P. Hamm and R. M. Hochstrasser, *Structure and dynamics of proteins and peptides: femtosecond two-dimensional infrared spectroscopy*, in *Ultrafast Infrared and Raman Spectroscopy*, edited by M. D. Fayer, page 273, Marcel Dekker, New York, 2001.

[61] J. Edler, P. Hamm, and A. C. Scott, *Femtosecond study of self-trapped excitons in crystalline acetanilide*, Phys. Rev. Lett. **88**, 067403 (2002).

[62] P. Hamm, M. Lim, W. F. DeGrado, and R. M. Hochstrasser, *The two-dimensional IR nonlinear spectroscopy of a cyclic penta-peptide in relation to its three-dimensional structure*, Proc. Natl. Acad. Sci. **96**, 2036 (1999).

[63] T. Meier, Y. Zhao, V. Chernyak, and S. Mukamel, *Polarons, localization, and excitonic coherence in superradiance of biological antenna complexes*, J. Chem. Phys. **107**, 3876 (1997).

[64] D. Thouless, *Electrons in disordered systems and the theory of localization*, Phys. Rev. **13**, 93 (1974).

[65] M. Schreiber and Y. Toyozawa, *Numerical experiments on the absorption lineshape of the exciton under lattice-vibrations. II. The average oscillator strength per state*, J. Phys. Soc. Jpn. **51**, 1537 (1982).

[66] O. Henri-Rousseau and P. Blaise, *The infrared spectral density of weak hydrogen bonds within the linear response theory*, **103**, 1 (1998).

[67] D. Hadži and S. Bratos, *Vibrational spectroscopy of the hydrogen bond*, in *The Hydrogen Bond: Recent Developments in Theory and Experiment*, edited by P. Schuster, G. Zundel, and C. Sandorfy, Elsevier, Amsterdam, 1976.

[68] G. C. Pimentel and A. McClellan, *The hydrogen bond*, W.H. Freemann, San Francisco, 1960.

[69] E. T. J. Nibbering and T. Elsaesser, *Ultrafast vibrational dynamics of hydrogen bonds in the condensed phase*, Chem. Rev. **104**, 1887 (2004).

[70] D. Madsen, J. Stenger, J. Dreyer, E. T. J. Nibbering, P. Hamm, and T. Elsaesser, *Coherent vibrational ground-state dynamics of an intramolecular hydrogen bond*, Chem. Phys. Lett. **341**, 56 (2001).

[71] B. I. Stepanov, *Interpretation of the regularities in the spectra of molecules forming the intermolecular hydrogen bond by the predissociation effect*, Nature **157**, 808 (1946).

[72] J. Stenger, D. Madsen, J. Dreyer, E. T. J. Nibbering, P. Hamm, and T. Elsaesser, *Coherent response of hydrogen bonds in liquids probed by ultrafast vibrational spectroscopy*, J. Phys. Chem. A **105**, 2929 (2001).

[73] K. Heyne, N. Huse, E. T. J. Nibbering, and T. Elsaesser, *Ultrafast coherent nuclear motions of hydrogen bonded carboxylic acid dimers*, Chem. Phys. Lett. **369**, 591 (2003).

[74] N. W. Ashcroft and N. D. Mermin, *Solid state physics*, Saunders College Publishing, Fort Worth, 1976.

[75] M. P. Marder, *Condensed matter physics*, John Wiley & Sons, New York, 2000.

[76] C. J. Brown and D. E. C. Corbridge, *The crystal structure of acetanilide*, Acta Crystallogr. **7**, 711 (1954).

[77] J. L. Katz and B. Post, *The crystal structure and polymorphism of N-methyl acetamide*, Acta Crystallogr. **13**, 624 (1960).

[78] H. Fröhlich, *Electrons in lattice fields*, Adv. Phys. **3**, 325 (1954).

[79] Z. Ivić and D. W. Brown, *Soliton excitations of a small polaron band*, Phys. Rev. Lett. **63**, 426 (1989).

[80] D. W. Brown, K. Lindenberg, and X. Wang, *When is a soliton ?*, in *Davydov's Soliton Revisited: Self-Trapping of Vibrational Energy in Protein*, edited by P. L. Christiansen and A. C. Scott, volume 243 of *NATO ASI Series B, Physics*, page 63, Plenum Press, New York, 1990.

[81] Z. Ivić, Ž. Prźulj, D. Kostić, D. Kapor, and M. Škrinjar, *Effects of quantum fluctuations on vibron pairing in two-sites system*, Phys. Rev. B **54**, 2992 (1996).

[82] J. Tekić, Z. Ivić, S. Zeković, and Željko Pržulj, *Kinetic properties of multiquanta Davydov-like solitons in molecular chains*, Phys. Rev. E **60**, 821 (1999).

[83] C. Kittel, *Quantum theory of solids*, John Wiley & Sons, New York, 1963.

[84] H. Haken, *Quantum field theory of solids*, North-Holland, Amsterdam, 1976.

[85] D. W. Brown, B. J. West, and K. Lindenberg, *Davydov solitons - New results at variance with standard derivations*, Phys. Rev. A **33**, 4110 (1986).

[86] V. Zakharov and A. Shabat, *Exact theory of 2-dimensional self-focusing and one-dimensional self-modulation of waves in nonlinear media*, Zh. Eksp. Theor. Fiz. **61**, 118 (1971), [Sov. Phys. JETP **34**,62 (1972)].

[87] D. M. Alexander and J. A. Krumhansel, *Localized excitations in hydrogen-bonded molecular crystals*, Phys. Rev. B **33**, 7172 (1986).

[88] T. Holstein, *Studies of polaron motion*, Ann. Phys. (N.Y.) **8**, 325 (1959), [reprinted in Ann. Phys. (N.Y.) **281**, 706 (2000)].

[89] C. B. Eilbeck, P. S. Lomdahl, and A. C. Scott, *Soliton structure in crystalline acetanilide*, Phys. Rev. B **30**, 4703 (1984).

[90] J. Bonča, S. Trugman, and I. Batistić, *Holstein polaron*, Phys. Rev. B **60**, 1633 (1999).

[91] D. W. Brown and Z. Ivić, *Unification of polaron and soliton theories of exciton transport*, Phys. Rev. B **40**, 9876 (1989).

[92] Z. Ivić, D. Kapor, M. Škrinjar, and Z. Popović, *Self-trapping in quasi-one-dimensional electron- and exciton-phonon systems*, Phys. Rev. B **48**, 3721 (1993).

[93] M. Ueta, H. Kanzaki, K. Kobayashi, Y. Toyozawa, and E. Hanamura, *Excitonic processes in solids*, volume 60 of *Springer Series in Solid-State Sciences*, Springer-Verlag, Berlin, 1986.

[94] I. Pekar, *Untersuchungen über die Elelektronentheorie der Kristalle*, Akademie Verlag, Berlin, 1954.

[95] Z. Ivić, D. Kostić, Željko Pržulj, and D. Kapor, *Effects of quantum lattice fluctuations on multiquanta Davydov-like solitons in a molecular chain*, J. Phys.: Condens. Matter **9**, 413 (1997).

[96] A. C. Scott, J. C. Eilbeck, and H. Gilhøj, *Quantum-lattice solitons*, Physica D **78**, 194 (1994).

[97] V. Pouthier, *Two-vibron bound states in α-helix proteins: The interplay between the intramolecular anharmonicity and the strong vibron-phonon coupling*, Phys. Rev. E **68**, 021909 (2003).

[98] V. Pouthier and C. Falvo, *Relaxation channels of two-vibron bound states in α-helix proteins*, Phys. Rev. E **69**, 041906 (2004).

[99] S. Takeno, *Vibron solitons in one-dimensional molecular-crystals*, Prog. Theor. Phys. **71**, 395 (1984).

[100] V. Pouthier, *Two-vibron bound states lifetime in a one-dimensional molecular lattice coupled to acoustic phonons*, J. Chem. Phys. **118**, 3736 (2003).

[101] G. Herzberg, *Infrared and Raman spectra*, Van Nostrand, New York, 1945.

[102] C. T. Johnston and B. I. Swanson, *Temperature dependence of the vibrational spectra of acetanilide: Davydov solitons or Fermi resonance*, Chem. Phys. Lett. **114**, 547 (1985).

[103] J. Sauvajol, G. D. Nunzio, R. Almairac, J. Moret, and M. Barthés, *Anomalous excitations in hydrogen-bonded molecular crystals – A Raman scattering study of specifically deuterated acetanilide (C_6D_5)–CONH–CD_3*, Solid State Commun. **77**, 199 (1991).

[104] C. Rullière, *Femtosecond laser pulses*, Springer-Verlag, Berlin, 1998.

[105] N. H. Rizvi, P. M. W. French, and J. R. Taylor, *Continuously self-mode-locked Ti-sapphire laser that produces sub-50-fs pulses*, Opt. Lett. **17**, 279 (1992).

[106] D. E. Spence, P. N. Kean, and W. Sibbett, *60-fsec pulse generation from a self-mode-locked Ti-sapphire laser*, Opt. Lett. **16**, 42 (1991).

[107] D. Strickland and G. Mourou, *Compression of amplified chirped optical pulses*, Opt. Commun. **55**, 447 (1985).

[108] P. Hamm, R. A. Kaindel, and J. Stenger, *Noise supression in femtosecond mid-infrared light sources*, Opt. Lett **25**, 1798 (2000).

[109] S. Woutersen, Y. Mu, G. Stock, and P. Hamm, *Hydrogen-bond lifetime measured by time-resolved 2D-IR spectroscopy: N-methylacetamide in methanol*, Chem. Phys. **266**, 137 (2001).

[110] N. B. Abbott and A. Elliott, *Infra-red spectrum and dichroism of crystalline acetanilide*, Proc. R. Soc. London, Ser. A **234A**, 247 (1956).

[111] J. Eckert, M. Barthes, W. T. Klooster, A. Albinati, R. Aznar, and T. F. Koetzle, *No evidence for proton transfer along the N-H$\cdots$O hydrogen bond in N-methylacetamide: Neutron single crystal structure at 250 and 276 K*, J. Phys. Chem. B **105**, 19 (2001).

[112] E. M. Bradbury and A. Elliott, *The infra-red spectrum of crystalline N-methyl acetamide*, Spec. Acta **19**, 995 (1963).

[113] P. Doty, J. H. Bradbury, and A. M. Holtzer, *Polypeptides. IV. The molecular weight, configuration and association of poly-γ-benzyl-L-glutamate in various solvents*, J. Am. Chem. Soc. **78**, 947 (1956).

[114] E. R. Blout and R. H. Karlson, *Polypeptides. III. The synthesis of high molecular weight poly-γ-benzyl-L-glutamates*, J. Am. Chem. Soc. **78**, 941 (1956).

[115] E. R. Civitello and H. Rapoport, *Synthesis of the enantiomeric fuorobenzofurans, late precursors for the synthesis of (+)-aflatoxins and (-)-aflatoxins B_1, B_2, G_1, and G_2*, J. Org. Chem. **59**, 3775 (1994), Page 3779.

[116] W. H. Daly and D. Poché, *The preparation of N-carboxyanhydrides of α-amino-acids using bis(trichloromethyl)carbonate*, Tetrahedron Lett. **29**, 5859 (1988).

[117] P. Doty, A. M. Holtzer, J. H. Bradbury, and E. R. Blout, *Polypeptides. II. The configuration of polymers of γ-benzyl-L-glutamate in solution*, J. Am. Chem. Soc. **76**, 4493 (1954).

[118] E. R. Blout and A. Asadourian, *Polypeptides. V. The infrared spectra of polypeptides derived from γ-benzyl-L-glutamate*, J. Am. Chem. Soc. **78**, 955 (1956).

[119] S. Ikeda and T. Imae, *β-Conformation and association of low-molecular-weight poly-γ-benzyl-L-glutamate in solutions*, Biopolymers **11**, 493 (1972).

[120] T. Imae and S. Ikeda, *Viscosity behavior and conformations of low-molecular-weight poly-γ-benzyl-L-glutamate in various solvents*, Biopolymers **12**, 1203 (1973).

[121] J. A. Ferretti and B. W. Ninham, *Nuclear magnetic resonance investigation of helix to random coil transformation in poly(α-amino acids). II. Poly(γ-benzyl L-glutamate)*, Macromolecules **3**, 30 (1970).

[122] E. J. Ambrose and A. Elliott, *The structure of synthetic polypeptides. II. Investigation with polarized infra-red spectroscopy*, Proc. Roy. Soc. A **205**, 47 (1951).

[123] A. Elliott and E. J. Ambrose, *Evidence of chain folding in polypeptides and proteins*, Discuss. Faraday Soc. **9**, 246 (1950).

[124] P. Doty and J. T.Yang, *Polypeptides. VII. Poly-γ-benzyl-L-glutamate – the helix-coil transition in solution*, J. Am. Chem. Soc. **78**, 498 (1956).

[125] A. Teramoto, K. Nakagawa, and H. Fujita, *Solution properties of synthetic polypeptides. III. Viscosity behavior of poly-γ-benzyl-L-glutamate in helix-coil transition region*, J. Chem. Phys. **46**, 4197 (1967).

[126] K. Liu, J. Lignowski, and R. Ullmann, *NMR and optical activity observations on helix-coil transition in poly(γ-benzyl L-glutamate) solutions*, Biopolymers **5**, 375 (1967).

[127] J. Bredenbeck and P. Hamm, *Versatile small volume closed-cycle flow cell system for transient spectroscopy at high repetition rates*, Rev. Sci. Instrum. **74**, 3188 (2003).

[128] G. Careri, U. Buontempo, F. Carta, E. Gratton, and A. C. Scott, *Infrared-absorption in acetanilide by solitons*, Phys. Rev. Lett. **51**, 304 (1983).

[129] D. M. Alexander, *Analog of small Holstein polaron in hydrogen-bonded amide systems*, Phys. Rev. Lett. **54**, 138 (1985).

[130] A. C. Scott, I. J. Bigio, and C. T. Johnston, *Polarons in acetanilide*, Phys. Rev. B **39**, 12883 (1989).

[131] J. Sauvajol, R. Almairac, J. Moret, M. Barthes, and J. Ribet, *Temperature dependence of the Raman spectrum of fully deuterated acetanilide*, J. Raman Spectrosc. **20**, 517 (1989).

[132] W. Fann, L. Rothberg, M. Roberson, S. Benson, J. Madey, S. Etemad, and R. Austin, *Dynamical test of Davydov-type solitons in acetanilide using a picosecond free-electron laser*, Phys. Rev. Lett. **64**, 607 (1990).

[133] H. Kellouai, PhD thesis, Univerity of Montpellier, 1993.

[134] M. Barthes, *Optical anomalies in acetanilide: Davydov soliton, localised modes, or Fermi resonance ?*, J. of Mol. Liqu. **41**, 143 (1989).

[135] S. W. Johnson, M. Barthes, J. Eckert, R. K. McMullan, and M. Muller, *Dynamical test of Davydov-type solitons in acetanilide using a picosecond free-electron laser – Comment*, Phys. Rev. Lett. **74**, 2844 (1995).

[136] M. Barthes, R. Almairac, J. L. Sauvajol, R. Currat, J. Moret, and J. L. Ribet, *Neutron-scattering investigation of deuterated crystalline acetanilide*, Europhys. Lett. **7**, 55 (1988).

[137] M. Barthes, R. Almairac, J. L. Sauvajol, J. Moret, R. Currat, and J. Dinanoux, *Incoherent neutron-scattering in acetanilide and 3 deuterated derivatives*, Phys. Rev. B **43**, 5223 (1991).

[138] G. B. Blanchet and C. R. Fincher Jr., *Defects in a nonlinear pseudo one-dimensional solid*, Phys. Rev. Lett. **54**, 1310 (1985).

[139] A. Spire, M. Barthes, H. Kellouai, and G. D. Nunzio, *Far-infrared spectra of acetanilide revisited*, Physica D **137**, 392 (2000).

[140] G. Araki, K. Suzuki, H. Nakayama, and K. Ishii, *Polaronlike vibrational bands of molecular crystals with one-dimensional hydrogen-bonded chains: N-methylacetamide*, Phys. Rev. B **43**, 12662 (1991).

[141] R. H. Austin, *Dynamical test of Davydov-type solitons in acetanilide using a picosecond free-electron laser - Reply*, Phys. Rev. Lett. **74**, 2845 (1995).

[142] D. B. Fitchen, in *Physics of Color Centers*, edited by W. B. Fowler, Academic Press, New York, 1968.

[143] P. Hamm, M. Lim, W. F. DeGrado, and R. M. Hochstrasser, *Pump/probe self heterodyned 2D spectroscopy of vibrational transitions of a small globular peptide*, J. Chem. Phys. **112**, 1907 (2000).

[144] A. Scott, E. Gratton, E. Shyamsunder, and G. Careri, *IR overtone spectrum of the vibrational soliton in crystalline acetanilide*, Phys. Rev. B **32**, 5551 (1985).

[145] P. Anderson, *Absence of diffusion in certain random lattices*, Phys. Rev. **109**, 1492 (1958).

[146] P. Anderson, *Local moments and localized states*, Rev. Mod. Phys. **50**, 191 (1978).

[147] S. Krimm and J. Bandekar, *Vibrational spectroscopy of peptides and proteins*, Adv. Protein Chem. **38**, 181 (1986).

[148] H. Torii, T. Tatsumi, and M. Tasumi, *Effects of hydrogen bonding and solvation in dielectric media on the amide I frequencies: Ab initio molecular orbital study*, Mikrochim. Acta **Suppl. 14**, 531 (1997).

[149] H. Feddersen, *Localization of vibrational-energy in globular protein*, Phys. Lett. A **154**, 391 (1991).

[150] E. Ortiz, J. F. Bertran, and L. Balleste, *Substituent effect on Fermi resonance in p-substituted benzoyl chlorides*, Spectrochim. Acta, Part A **27A**, 1713 (1971).

[151] C. N. R. Rao and R. Venkataraghavan, *Infrared spectra of substituted benzoyl chlorides and benzoyl bromides - explanation of the anomalous carbonyl band-splittings*, Spectrochim. Acta **18**, 273 (1962).

[152] J. F. Bertran, L. Ballester, L. Dobrihalova, N. Sánchez, and R. Arrieta, *Study of Fermi resonance by method of solvent variation*, Spectrochim. Acta, Part A **24A**, 1765 (1968).

[153] P. E. Maslen, N. C. Handy, R. D. Amos, and D. Jayatilaka, *Higher analytic derivatives. IV. Anharmonic effects in the benzene spectrum*, J. Chem. Phys. **97**, 4233 (1992).

[154] C. L. Angell, P. J. Krueger, R. Lauzon, L. C. Leitch, K. Noack, R. J. D. Smith, and R. N. Jones, *The carbonyl stretching frequency of cyclopentanone*, Spectrochim. Acta **15**, 926 (1959).

[155] S. I. Nam, E. S. Min, Y. M. Jung, and M. S. Lee, *Fermi resonance and solvent dependence of the ν C=O frequency shifts of Raman spectra: Cyclohexanone and 2-cyclohexen-1-one*, Bull. Korean Chem. Soc **22**, 989 (2001).

[156] R. N. Jones, C. L. Angell, T. Ito, and R. J. D. Smith, *The carbonyl stretching bands in the infrared spectra of unsaturated lactones*, Can. J. Chem. **37**, 2007 (1959).

[157] K. S. Song and R. T. Williams, *Self-trapped excitons*, Springer, Berlin, 1996.

[158] C. T. Johnston, S. F. Agnew, J. Eckert, L. H. Jones, B. I. Swanson, and C. J. Unkefer, *Low-frequency single-crystal Raman, far-infrared, and inalestic neutron scattering studies of acetanilde at low temperatures*, J. Phys. Chem. **95**, 5281 (1991).

[159] V. P. Gerasimov, *Low-frequency polarized Raman spectra of some complex molecular crystals*, Opt. Spektrosk. **43**, 705 (1977), [Opt. Spectrosc. (USSR) **43**, 417 (1977)].

[160] M. Sakai, N. Kuroda, and Y. Nishina, *High-pressure Raman study of vibrational spectra in crystalline acetanilide*, Phys. Rev. B **47**, 150 (1993).

[161] H. Nienhuys, S. Woutersen, R. van Santen, and H. Bakker, *Mechanism for vibrational relaxation in water investigated by femtosecond infrared spectroscopy*, J. Chem. Phys. **111**, 1494 (1999).

[162] W. A. Herrebout, K. Clou, and H. O. Desseyn, *Vibrational spectroscopy of N-methylacetamide revisited*, J. Phys. Chem. A **105**, 4865 (2001).

[163] F. Fillaux, *Vibrational-spectra and dynamics of conformation and hydrogen-bonding of N-methylacetamide. II. Dynamics of the NH=O hydrogen-bond and NH (ND) stretching band-structure*, Chem. Phys. **62**, 287 (1981).

[164] M. Barthes, H. N. Bordallo, J. Eckert, O. Maurus, G. de Nunzio, , and J. Léon, *Dynamice of crystalline N-methylacetamide: Temperature dependence of infrared and inelastic neutron scattering spectra*, J. Phys. Chem. B **102**, 6177 (1998).

[165] G. Careri, E. Gratton, and E. Shyamsunder, *Fine structure of the amide I band in acetanilide*, Phys. Rev. A **37**, 4048 (1988).

[166] T. Miyazawa, *The characteristic band of secondary amides at 3100 cm^{-1}*, J. Mol. Spectrosc. **4**, 168 (1960).

[167] M. Beer, H. B. Kessler, and G. B. B. Sutherland, *Spectra of homologous series of monosubstituted amides*, J. Chem. Phys. **29**, 1097 (1958).

[168] H. Pivcová, B. Schneider, and J. Ŝtokr, *On the structure and properties of polyamides. XX. Fermi resonance effects in vibrational spectra of N-methylacetamide*, Collect. Czech. Chem. Commun. **30**, 2215 (1965).

[169] G. Dellepiane, S. Abbate, P. Bosi, and G. Zerbi, *Fermi resonances in solid N-methyl-acetamide*, J. Chem. Phys. **73**, 1040 (1980).

[170] F. Fillaux and M. Baron, *Vibrational-spectra and dynamics of conformation and hydrogen-bonding of N-methylacetamide. I. Conformational dynamics of the $CH_3CONHCH_3$ molecule and NH out of plane band splitting*, Chem. Phys. **62**, 275 (1981).

[171] K. Belhayara, D. Chamma, and O. Henri-Rousseau, *Infrared spectra of weak H-bonds: Fermi resonances and intrinsic anharmonicity of the H-bond bridge*, J. Mol. Struct. **648**, 93 (2003).

[172] H. Ratajczak and A. M. Yaremko, *Theory of the profiles of hydrogen stretching infrared bands of hydrogen-bonded solids: Fermi resonance effect and strong coupling between the high-frequency hydrogen stretching vibration and low-frequency phonons*, Chem. Phys. Lett. **314**, 122 (1999).

[173] B. H. Zimm, P. Doty, and K. Iso, *Determination of the parameters for helix formation in poly-γ-benzyl-L-glutamate*, Proc. Natl. Acad. Sci. **45**, 1601 (1959).

[174] J. R. Kim and T. Ree, *Molecular dimensions of polypeptides in helicogenic solvents*, J. Polym. Sci. **23**, 215 (1985).

[175] J. Helfrich, R. Hentschke, and U. M. Apel, *Molecular-dynamics simulation study of poly(γ-benzyl L-glutamate) in dimethylformamide*, Macromolecules **27**, 472 (1994).

[176] Y. Muroga and M. Nagasawa, *On the flexibility of poly(γ-benzyl L-glutamate) in helicogenic solvents*, Biopolymers **45**, 281 (1998).

[177] M. L. Wallach and H. Benoit, *Light scattering by poly-L-benzyl glutamate solutions subjected to an electrical field*, J. Polym. Sci. **57**, 41 (1962).

[178] B. R. Jennings and H. G. Jerrard, *Light scattering by poly-γ-benzyl-L-glutamate solutions subjected to electric fields*, J. Phys. Chem. **69**, 2817 (1965).

[179] H. Fujita, A. Teramoto, K. Okita, T. Yamashita, and S. Ikeda, *Solution properties of synthetic polypeptides. I. Light scattering and osmometry of poly-γ-benzyl-L-glutamate in helicogenic solvents*, Biopolymers **4**, 769 (1966).

[180] T. Norisuye, A. Teramoto, and H. Fujita, *Solution properties of synthetic polypeptides. XIII. Dimensions of interrupted helices of poly(γ-benzyl L-glutamate)*, Polym. J. **4**, 323 (1973).

[181] K. Weir and B. R. Jennings, *Experimental-study of electrooptical rotation of helical polypeptides*, Polymer **33**, 2287 (1992).

[182] D. A. D. Parry and A. Elliott, *X-ray diffraction patterns of liquid crystalline solutions of poly-γ-benzyl-L-glutamate*, Nature **206**, 616 (1965).

[183] D. A. D. Parry and A. Elliott, *Structure of a paracrystalline phase of poly-γ-benzyl-L-glutamate in dimethylformamide*, J. Mol. Biol. **25**, 1 (1967).

[184] J. A. Ferretti and R. L. Jernigan, *Conformational lifetimes in helix-random-coil transition region by nuclear magnetic-resonance with application to poly(γ-benzyl L-glutamate)*, Macromolecules **6**, 687 (1973).

[185] P. Hamm, M. Lim, and R. M. Hochstrasser, *Vibrational energy relaxation of the cyanide ion in water*, J. Chem. Phys. **107**, 10523 (1997).

[186] J. Edler, R. Pfister, V. Pouthier, C. Falvo, and P. Hamm, *Direct observation of self-trapped vibrational states in α-helices*, Phys. Rev. Lett. **93**, 106405 (2004).

[187] M. J. Frisch, and G. W. Trucks, and H. B. Schlegel, and G. E. Scuseria, and M. A. Robb, and J. R. Cheeseman and V. G. Zakrzewski, and J. A. Montgomery, Jr. and R. E. Stratmann, and J. C. Burant and S. Dapprich, and J. M. Millam and A. D. Daniels, and K. N. Kudin and M. C. Strain, and O. Farkas, and J. Tomasi and V. Barone, and M. Cossi, and R. Cammi, and B. Mennucci and C. Pomelli, and C. Adamo, and S. Clifford, and J. Ochterski and G. A. Petersson, and P. Y. Ayala, and Q. Cui and K. Morokuma, and D. K. Malick, and A. D. Rabuck and K. Raghavachari, and J. B. Foresman, and J. Cioslowski and J. V. Ortiz, and B. B. Stefanov, and G. Liu and A. Liashenko, and P. Piskorz, and I. Komaromi, and R. Gomperts and R. L. Martin, and D. J. Fox, and T. Keith and M. A. Al-Laham, and C. Y. Peng, and A. Nanayakkara and C. Gonzalez, and M. Challacombe, and P. M. W. Gill and B. Johnson, and W. Chen, and M. W. Wong, and J. L. Andres and C. Gonzalez, and M. Head-Gordon, and E. S. Replogle and J. A. Pople, *Gaussian 98*, Revision A.5, Gaussian, Inc., Pittsburgh, PA, 1998.

[188] A. D. Becke, *Density-functional thermochemistry. III. The role of exact exchange*, J. Chem. Phys. **98**, 5648 (1993).

[189] I. V. Rubtsov, J. P. Wang, and R. M. Hochstrasser, *Dual-frequency 2D-IR spectroscopy heterodyned photon echo of the peptide bond*, Proc. Natl. Acad. Sci. **100**, 5601 (2003).

Acknowledgements

Many individuals supported me during the completion of this thesis and I would like to take this opportunity to express my gratitude to them.

The research described in this thesis was carried out in the group of Prof. Dr. Peter Hamm, first at the *Max-Born-Institute for Nonlinear Optics and Short Pulse Spectroscopy* in Berlin and then at the *Institute of Physical Chemistry* at the *University of Zürich*. I thank Peter for the excellent guidance of this project. His continuous support and the confidence he granted me have been very motivating. I benefited immensely from his broad knowledge and learned from him much of what I know today about spectroscopy, physical chemistry, scientific presentations and proper writing in English. In addition Peter gave me the opportunity to extend my scientific education at numerous international conferences and graduate schools, for which I am very grateful.

Further, I wish to express my gratitude to Prof. Dr. Thomas Elsässer for giving me the opportunity to work at the *Max-Born-Institute* and for providing excellent research conditions in a fascinating field of science.

I thank Prof. Dr. George Tsironis for his continuous interest in our work and for agreeing to referee this thesis. I further wish to express my appreciation to Prof. Dr. Jürg Hutter and Prof. Dr. Stefan Seeger for serving on the Promotionskomitee.

I thank Dr. Vincent Pouthier and Cyril Falvo from the University in Besançon for the fruitful collaboration on the α-helix project. They explained to us the concept of two-vibron bound states and calculated the pump-probe spectra of the NH mode of PBLG.

Special thanks go to Jens Bredenbeck for the companionship on our venture towards a PhD. We spent more than three years in the same office and I appreciate greatly our many stimulating and instructive discussions, which often clarified my ideas. I further wish to offer my thanks and appreciation to Dr. Jan Helbing for contributing his talent and skills, sharing his point of view on all aspects of spectroscopy and physics, as well as trying to teach me skiing. I have been very fortunate to have the support of Rolf Pfister, who synthesized the deuterated poly-γ-benzyl-L-glutamate and offered his general advice on all chemical problems. I further appreciate a lot that Dr. Viktor Volkov and Dr. Hiroyuki Katasuki built a two color pump-probe setup and generously helped me on those experiments. All beginnings are difficult. I thank Dr. J. Stenger, Dr. D. Madsen and Dr. S. Woutersen for the valuable introduction to the femtosecond lab as well as their companionship.

Many thanks go to the staff of the *PCI Institute* for providing an excellent infrastructure. I am particularly grateful to our technicians, Armin Küne, Horst Blasi, Roland Zehnder, Hermann Schwarz and Andreas Knecht. I was often surprised how quickly and efficiently all types of technical problems were solved. I further owe thanks to Ueli Feusi for his first class computer management. It was a big help that I never had to experience any serious software, hardware or network problems. Also the staff at the *Max-Born-Institute* supported me and I want to thank in particular Frau R. Goleschny, Frau B. Steinert and Herr P. Scholze.

Furthermore I want to thank Dr. F. Eickemeyer, Dr. T. Günther, Dr. F. Intonti, Dr. V. Malyarchuk, Dr. E. T. J. Nibbering, Dr. M. Rini, V. Boţan, V. Cervetto, H. Bregy, R. Herger, P. Kocian, Dr. C. Kolano and Dr. R. H. Schanz for inspiring discussions, helpful support, valuable advice and friendship.

I am in particular thankful to my parents as well as my sister who have been generous with their support and encouragement throughout my entire studies. Finally, I thank especially Estrella. Her constant support, patience and love enabled me to complete this work.

Curriculum Vitae

Name: Edler

First name: Julian

Date of birth: August 6th, 1974

Citizenship: German

Education:

2001 – pres. *PhD Program*
Universität Zürich, Zürich, Switzerland

2000 – 2001 *Research Assistant*
Max-Born-Institute, Berlin, Germany

1994 – 2000 *Studies in Physics*
Universität Heidelberg, Heidelberg, Germany
Diploma in Physics

Diploma Thesis Titel:
Immobilisation of antibodies in oligo(ethylen)-glykolthiolmonolayers on gold for biosensors with acoustic plate modes

1997 – 1998 *Fulbright Exchange Program*
University of Illinois, Urbana Champaign, USA
Master of Science

1985 – 1994 *Abitur*
Friedrich-Magnus-Schwerd-Gymnasium, Speyer, Germany